UNIVERSITÀ
DEGLI STUDI
DI PADOVA

Sede Amministrativa: Università degli Studi di Padova

Dipartimento di *Biologia*

SCUOLA DI DOTTORATO DI RICERCA IN: BIOSCIENZE E BIOTECNOLOGIE

INDIRIZZO: GENETICA E BIOLOGIA MOLECOLARE DELLO SVILUPPO

CICLO XXVII

Extracellular collagen type VI has prosurvival and autophagy instructive properties in mouse embryonic fibroblasts

Direttore della Scuola: Ch.mo Prof. Giuseppe Zanotti

Coordinatore d'indirizzo: Ch.mo Prof. Rodolfo Costa

Supervisore: Ch.mo Prof. Paolo Bonaldo

Dottoranda: Silvia Castagnaro

Abstract

Collagen VI is a major protein of the extracellular matrix with a broad distribution in many tissues, including skeletal muscle and connective tissues. It is composed of three distinct alpha chains, α1, α2 and α3(VI), encoded by separate genes. Mutations of collagen VI genes in humans cause several muscle diseases, such as Bethlem myopathy and Ullrich congenital muscular dystrophy. Collagen VI null (*Col6a1*$^{-/-}$) mice display a myopathic phenotype characterized by mitochondrial dysfunction, spontaneous apoptosis and autophagic impairments in myofibers. These findings indicate that collagen VI has a key role for skeletal muscle homeostasis.

Before starting my PhD, I participated to a project aimed at investigating the effects of physical exercise on wild type and *Col6a1*$^{-/-}$ skeletal muscle. This work demonstrated for the first time that exercise is able to activate the autophagic response in muscle. Moreover, this study revealed that physical exercise is detrimental for *Col6a1*$^{-/-}$ muscles.

I decided to focus my main PhD work on investigating the role of collagen VI in fibroblasts, which are the major cell type responsible for the secretion and extracellular deposition of this protein, and elucidating the consequences on fibroblasts due to ablation of collagen VI. In patients affected by Bethlem myopathy and Ullrich congenital muscular dystrophy, the mutated forms of collagen VI are produced and retained by fibroblasts, suggesting a potential contribution for this cell type in the onset and progression of muscle defects.

To assess how lack of collagen VI impacts on fibroblast functions, I generated stable mouse embryonic fibroblast (MEF) lines from wild type and *Col6a1*$^{-/-}$ mice and showed that collagen VI is necessary for autophagy regulation and has prosurvival properties in fibroblasts. *Col6a1*$^{-/-}$ MEFs displayed accumulation of LC3 both basally and following autophagy induction. To dissect the autophagic response of these cells, I studied the autophagy flux and the activity of the nutrient sensor kinase mTOR. I found that in *Col6a1*$^{-/-}$ MEFs the mTORC1 downstream targets, such as 4E-BP1 and S6, are persistently activated under nutrient depletion stimuli, leading to autophagy inhibition in starving

activation of the AMP-activated protein kinase. These signaling defects lead to massive accumulation of autophagosomes inside *Col6a1*$^{-/-}$ fibroblasts, due to a compromised autophagosome-lysosome fusion in association with the presence of enlarged lysosomes and LAMP-2 protein depletion. These lysosomal defects are also associated with aberrant localization and activity of TFEB, a master transcription factor for lysosome biogenesis and autophagy regulation.

In addition, *Col6a1*$^{-/-}$ MEFs showed increased susceptibility to cell death, especially under nutrient stress, that ended with activation of the intrinsic pathway of apoptosis. This phenotype was specifically rescued by culturing cells onto purified collagen VI provided as an adhesive substrate. Lack of collagen VI also influenced the organization of the mitochondrial network, which has a key role in cell survival. Mitochondria of *Col6a1*$^{-/-}$ MEFs exhibited increased fragmented morphology, associated with Parkin translocation and defective mitophagy.

These findings show that fibroblasts play a relevant role in the development of the pathophysiological defects of collagen VI null mice, a finding that provide a thus far undisclosed and valuable information for the diagnosis and therapy of inherited diseases associated with collagen VI gene mutations. Moreover, they reveal for the first time a direct effect of collagen VI on the regulation of autophagy and associated mechanisms in this cell type.

Riassunto

Il collagene VI è una proteina della matrice extracellulare con caratteristiche uniche, presente ed abbondante in numerosi tessuti, come nel muscolo scheletrico e i tessuti connettivi. Si compone di tre diverse catene, chiamate α1, α2 e α3(VI), codificate da geni distinti. Mutazioni a carico dei geni per il collagene VI nell'uomo sono causa di diverse patologie muscolari, quali la miopatia di Bethlem e la distrofia muscolare congenita di Ullrich. Il modello murino privo di collagene VI (*Col6a1*$^{-/-}$), generato nel nostro laboratorio, sviluppa un fenotipo miopatico caratterizzato da disfunzione mitocondriale, insorgenza di apoptosi e difetti di autofagia nelle miofibre muscolari. Il collagene VI risulta in sostanza fondamentale per l'omeostasi generale del muscolo scheletrico.

Al termine della laurea specialistica, ho partecipato ad un primo progetto volto a studiare gli effetti dell'esercizio fisico sul muscolo scheletrico di topi wild type e *Col6a1*$^{-/-}$. Questo lavoro ha dimostrato per la prima volta che l'esercizio fisico è in grado di attivare l'autofagia nel muscolo; in secondo luogo che l'esercizio fisico è dannoso per il muscolo dei topi *Col6a1*$^{-/-}$, già soggetti a problemi di attivazione dell'autofagia, escludendone un possibile utilizzo come strategia terapeutica.

In seguito ho deciso di focalizzare il mio lavoro di dottorato sullo studio delle alterazioni insorgenti in fibroblasti privi di collagene VI e sugli effetti diretti di questa proteina sulla regolazione dell'autofagia. Il fibroblasto è il principale tipo cellulare che produce collagene VI. Inoltre, in pazienti distrofici con patologie correlate a mutazioni del collagene VI, le varianti mutate di collagene VI vengono prodotte proprio dai fibroblasti e ritenute all'interno del loro citoplasma, suggerendo così un contributo primario dei fibroblasti nella patogenesi muscolare.

Per indagare più a fondo il contributo di queste cellule, ho generato delle linee cellulari di fibroblasti embrionali murini (MEF) da topi wild type e *Col6a1*$^{-/-}$ e ho dimostrato come il collagene VI sia necessario per una corretta attivazione di autofagia e per la sopravvivenza dei fibroblasti. Per analizzare la risposta autofagica di queste cellule, ho studiato il flusso autofagico e l'attività della protein chinasi mTOR, uno dei principali

sensori cellulari di risposta ai nutrienti. Nei MEF *Col6a1*$^{-/-}$, i target a valle di mTORC1, 4E-BP1 ed S6, risultano costantemente attivati anche in seguito a stimoli di induzione di autofagia, ad indicare un'inibizione a valle della via autofagica. Tuttavia, nei MEF *Col6a1*$^{-/-}$ è presente uno squilibrio energetico generale, che porta all'iper-attivazione della protein chinasi attivata da AMP (AMPK), che a sua volta è implicata nell'induzione di autofagia. Le analisi relative al fattore di trascrizione TFEB, che svolge un ruolo chiave nella biogenesi e funzionalità lisosomiale, dimostrano inoltre un'alterata localizzazione e attività di questo fattore, ad indicare un'alterata risposta trascrizionale del programma autofagico dei fibroblasti *Col6a1*$^{-/-}$. Questa complessa situazione porta infine ad un accumulo intracellulare di autofagosomi nei MEF *Col6a1*$^{-/-}$, dovuto alla mancata fusione di autofagosomi e lisosomi, ed è inoltre associato alla presenza di lisosomi dilatati ed alla diminuzione dei livelli proteici di LAMP-2.

Inoltre i MEF *Col6a1*$^{-/-}$ hanno dimostrato una maggiore suscettibilità a morte cellulare indotta da stress o induzione di autofagia, tramite attivazione della via intrinseca di apoptosi. È importante evidenziare che questo difetto viene specificatamente recuperato quando i fibroblasti sono coltivati su collagene VI purificato, fornito come substrato. L'assenza del collagene VI nei MEF *Col6a1*$^{-/-}$ influenza infine l'organizzazione della rete mitocondriale, la quale è nota svolgere un ruolo chiave nella sopravvivenza cellulare. I mitocondri dei MEF *Col6a1*$^{-/-}$ risultano infatti più frequentemente frammentati rispetto ai wild type, e questa alterazione potrebbe facilmente essere correlata ad una disfunzione mitocondriale. In questo contesto, i mitocondri *Col6a1*$^{-/-}$ inducono la traslocazione di Parkin e vengono sottoposti ad un'alterata risposta del processo selettivo di mitofagia.

In conclusione, questi risultati dimostrano per la prima volta che i fibroblasti contribuiscono in modo rilevante all'insorgenza e alla progressione dei difetti patofisiologici nei topi *Col6a1*$^{-/-}$, fornendo così informazioni preziose e finora ignote per la diagnosi e la terapia delle patologie legate a mutazioni nei geni codificanti per il collagene VI. Inoltre, essi dimostrano che il collagene VI svolge un effetto diretto sulla regolazione dell'autofagia e sui meccanismi ad essa associati in questo tipo cellulare.

Part I: main project

1. Introduction

1.1. Extracellular matrix

The extracellular matrix (ECM) is the dynamic and multifaceted space in which cells are layered and anchored to form specialized tissues and organs. This microenvironment plays a crucial role for tissue homeostasis and ensures proper functionality through physical cell-matrix interactions and structural support. Moreover, ECM proteins are involved in several key cellular processes such as binding, activation and presentation of soluble factors, modulation of morphogen gradients, maintenance of the stem cell niche, and signal transduction into cells (Hynes, 2009; Tsang, Cheung, Chan, and Cheah, 2010; Gattazzo, Urciuolo, and Bonaldo, 2014).

The ECM displays a fine tissue-specific composition, but in general terms it is composed by major groups of secreted macromolecules. Mechanical strength and flexibility are allowed by fibrous proteins (typically collagens, fibronectin, elastin, and fibrillins). ECM components also include enzymes able to modify these molecules ,such as lysyl oxidase, and proteinases, such as the matrix metalloproteinases. Proteoglycans consist of different core proteins covalently linked to sulfated glycosaminoglycan side chains. These macromolecular complexes are important to assure the ECM hydration, thus providing tissue turgidity and facilitating molecular transport. Another category of molecules is able to connect cells to matrix and to modulate interactions with plasma membrane receptors. These are termed matricellular proteins or multifunctional adhesive proteins, such as thrombospondins and tenascins (Tsang *et al.*, 2010; Hubmacher and Apte, 2013).

Among ECM proteins, collagens are the most abundant components of connective tissues, mainly produced by fibroblasts. There are different subgroups of collagen types that differ to their structure and functions: fibril-forming collagens (such as types I, II, III, V), fibril-associated collagens with interrupted triple helix (such as types IX, XII, XIV),

beaded microfilaments (collagen type VI), multiplexin (such as types VII, XV and XVIII) and network-forming collagens (types IV, typical of the basement membrane, VI, VIII, and X) (Ricard-Blum, 2011). They are made of three polypeptide α chains that are enriched in regions with a repeated Gly-X-Y pattern, which is also known as the collage domain. The α chains assemble in homo- or hetero-trimeric fashions to form triple helical structures (Ricard-Blum, 2011; Brodsky and Persikov, 2005).

ECM protein networking has a crucial role in modulate cell behavior and homeostasis. In parallel, different ECM defects have been linked to an increasing number of human pathologies, such as inflammation processes, muscle and neurodegenerative diseases (Tsang *et al.*, 2010; Hubmacher and Apte, 2013). Mutant and knockout animal models for ECM molecules provide a valuable tool for translational studies and for the mechanistic understanding of human disease pathogenesis associated with ECM defects.

1.2. Collagen VI

Collagen VI is a protein with a broad and dynamic distribution in the ECM of several tissues, such as skeletal muscle, tendons, intervertebral disks, peripheral nerves, lungs, heart, adipose tissue, skin and cartilages (Kuo *et al.*, 1997). Collagen VI is encoded by three different genes and is tipically composed of the three distinct polypeptides, called α1(VI) (140 kDa), α2(VI) (130 kDa) and α3(VI) (250-350 kDa) chains (Colombatti and Bonaldo, 1987; Colombatti *et al.*, 1995).

The α1 and α2(VI) chains are encoded by *Col6a1* and *Col6a2* genes, mapping to chromosome 21q22.39, while α3(VI) is encoded by *Col6a3*, that is located on 2q37 chromosome (Lampe and Bushby, 2005). The three α chains contain a triple helical domain of 335-336 amino acids, flanked by large N- and C-terminal globular regions made of repeated modules of about 200 amino acid residues sharing similarity with the von Willebrand factor type A (vWF-A)-like domain. The α1 and α2(VI) polypeptides contain one N-terminal- and two C-terminal vWF-A globular domains (namely N1, C1 and C2). The α3(VI) chain displays ten N-terminal and two C-terminal vWF-A domains (N1-N10 and C1-C2), followed by three additional C-terminal modules (C3-C5): a proline-rich domain, a

fibronectin type III domain and a Kunitz-like domain (Bonaldo *et al.*, 1990) (Fig. 1). *Col6a3* transcripts can undergo multiple alternative splicing, therefore generating different α3(VI) variants characterized by a variable number of vWF-A modules (Saitta *et al.*, 1990; Doliana *et al.*, 1998).

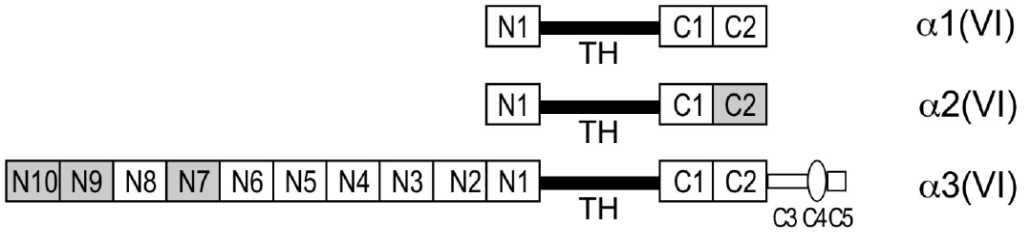

Figure 1. Schematic structure of collagen VI. The alpha chains, α(VI), are divided into domains. N1-N10, N-terminal vWF-A globular domains; C1-C5, C-terminal vWF-A globular domains; TH, triple helix.

Collagen VI biosynthesis is a complex process involving multiple steps. Following translation and entry of the three α(VI) chains within the endoplasmic reticulum, the three chains associate in equimolar ratios giving rise to a triple helical monomer (≈500 kDa), stabilized by disulfide bonds. Before secretion, monomers associate into disulfide-bonded antiparallel dimers (=1,0000 kDa), which align to form tetramers (≈2,000 kDa) that are finally secreted in the extracellular space. Outside the cell, collagen VI tetramers associate laterally by non-covalent bonds, forming a network of beaded microfilaments in the ECM meshwork (Bernardi and Bonaldo, 2008).

Collagen VI structure and networking not only favour cell embedding in the connective tissue. Thanks to its modularity, collagen VI is able to bind different components of the ECM and is involved in intracellular signaling. It was shown that collagen VI binds collagen IV and decorin at the basal lamina, creating a physical connection between muscle cells and ECM (Kuo *et al.*, 1997). Furthermore, it can bind collagen I, collagen II, fibronectin, decorin and other ECM components (Bonaldo *et al.*, 1990; Sabatelli *et al.*, 2001; Neill *et al.*, 2012). Integrin α1β1 and α2β1 and the CSPG4/NG2 proteoglycan are known membrane receptors able to bind collagen VI and transduce intracellular signals by acting on the cytoskeleton (Burg *et al.*, 1996; Stallcup, 2002).

Several mutations of human *COL6* genes were reported, and they are mainly linked to inherited muscular disorders, indicating a critical role of this protein for skeletal muscle maintenance. Indeed, Bethlem myopathy (BM), Ullrich congenital muscular dystrophy (UCMD) and myosclerosis myopathy were found to be caused by mutations of collagen VI genes (Lampe and Bushby, 2005; Bönnemann, 2011). BM is characterized by axial and proximal muscle wasting and weakness, associated with finger flexion contractures. BM is usually mild, with slow progression of the symptoms (Pepe *et al.*, 2002; Lampe and Bushby, 2005). The more severe UCMD is characterized by an early-onset muscle weakness and wasting, generalized and rapidly progressive, with proximal limb contractures, distal hyperlaxity, rigid spine and rare ability to walk. The rapid progression of UCMD clinical symptoms usually leads to early death, due to respiratory failure (Mercuri and Longman, 2005; Brinas *et al.*, 2010). The third phenotype, myosclerosis myopathy, displays early and diffuse contractures resulting in severe limitation of movement of axial, proximal, and distal joints, and in a "woody" consistence of muscles (Merlini *et al.*, 2008).

1.2.1. Collagen VI null mouse model

Several years ago, a collagen VI knockout mouse model (*Col6a1*$^{-/-}$) was produced by targeted inactivation of *Col6a1* gene. Despite the fact that α2(VI) and α3(VI) chains are normally translated, lack of the α1(VI) chain completely abolishes the assembly and secretion of collagen VI in the homozygous *Col6a1*$^{-/-}$ mice (Bonaldo *et al.*, 1998). Thus, the *Col6a1* null mice is a good model to investigate the function of collagen VI *in vivo*.

Although *Col6a1*$^{-/-}$ mice undergo normal development, are fertile and do not display any obvious anatomical alteration, they are affected by an early onset myopathic disease with myofiber defects and muscle weakness (Bonaldo *et al.*, 1998; Irwin *et al.*, 2003). At the histological level, muscles of *Col6a1*$^{-/-}$ mice show an increased occurrence of centrally nucleated and degenerating myofibers, with variability in myofiber cross-sectional areas. Ultrastructural analysis revealed the occurrence of abnormal mitochondria and dilated sarcoplasmic reticulum cisternae in *Col6a1*$^{-/-}$muscles. Moreover, TUNEL analyses

revealed a markedly increased incidence of apoptosis in *Col6a1*$^{-/-}$ muscles. *Ex vivo* studies show the presence of a latent mitochondrial dysfunction that impinges on *Col6a1*$^{-/-}$ myofiber functionality (Irwin *et al.*, 2003). Mechanistic studies revealed an increased opening propensity of the permeability transition pore (PTP) of the inner mitochondrial membrane, thus leading to mitochondria depolarization and finally to apoptosis (Bernardi and Bonaldo, 2008). *In vivo* treatment with cyclosporin A, an inhibitor of the cyclophilin D that desensitizes PTP opening, was successful to rescue the apoptotic and mitochondrial defects and more importantly the myopathic phenotype of *Col6a1*$^{-/-}$ muscles. Independent studies in muscle biopsies and muscle cell cultures from BM and UCMD patients allowed to reveal the same pathomolecular defects in human collagen VI myopathies. As for *Col6a1*$^{-/-}$ mice, the latent mitochondrial dysfunction and spontaneous apoptosis of patients' muscle cultures were rescued by cyclosporin A treatment, as well as by adhesion onto native collagen VI as a substrate (Angelin *et al.*, 2007).

In 2010, further mechanistic studies allowed to demonstrate that lack of collagen VI leads to a failure of autophagy in skeletal myofibers (Grumati *et al.*, 2010). It was shown that *Col6a1*$^{-/-}$ muscles have a block of the autophagic flux, due to defective regulation of Beclin 1 and Bnip3, two key factors needed for activation of the autophagic process. Autophagosome formation is strongly reduced in muscles of *Col6a1*$^{-/-}$ mice , and they do not display activation of autophagy following 24-hour starvation, a well-known stimulus for induction of autophagy. As a consequence, *Col6a1*$^{-/-}$ muscles undergo a detrimental buildup of dysfunctional and damaged organelles. Interestingly, forced reactivation of autophagy in *Col6a1*$^{-/-}$ mice by genetic, pharmacological or nutritional means was successful in rescuing the myopathic phenotype and restoring muscle homeostasis and strength. The treatments to forcibly induce autophagy consisted of *i)* prolonged starvation (30-hour long) to study acute, short-term response; *ii)* feeding with a specifically designed chow with a lower protein content ("low-protein diet") for one month; *iii)* rapamycin administration for 15 days; and *iv) in vivo* transfection of tibialis anterior muscles with a Beclin 1 cDNA construct (Grumati *et al.*, 2010). Notably, these different approaches not only successfully reactivated autophagy in *Col6a1*$^{-/-}$ muscles, but also rescued the

apoptotic phenotype and ameliorated muscle histology and myofiber defects, leading also to recovery of functional properties with a significant increase of muscle strength in the low-protein diet approach.

Much interestingly, the same study also demonstrated that Beclin 1 and Bnip3 protein levels are reduced in muscle biopsies from BM and UCMD patients, thus revealing that defective regulation of autophagy is a shared feature of mice and men with collagen VI deficiency (Grumati *et al.*, 2010). Based on these findings, a pilot clinical trial with a nutritional approach and aimed at at restoring muscle autophagy was recently carried out in BM and UCMD patients (ClinicalTrials.gov Identifier NCT01438788; https://clinicaltrials.gov/ct2/show/NCT01438788). Towards this aim, seven patients affected by collagen VI deficiency underwent a voluntary 1 year-long low-protein diet with a normocaloric daily food intake (Merlini and Nishino, 2014). During the last part of my PhD I participated to this study, evaluating the autophagic response to this nutritional protocol by biochemical studies in protein extracts prepared from muscle biopsies of the different patients, obtained before and at the end of the 1-year trial. The results of this trail indicate a positive regulation of autophagy in muscles of enrolled patients, which is remarkably associated with a reduced progression of clinical symptoms and muscle pathology (Merlini *et al.*, manuscript in preparation).

Interestingly, a subsequent study, in which I was involved during my post-graduate research experience, was aimed at evaluating whether physical exercise may exert a beneficial effect in *Col6a1*$^{-/-}$ mice, with an obvious relevance for the treatment of human collagen VI-related myopathies. Physical training was not able to induce autophagy in *Col6a1*$^{-/-}$ muscles, but instead had detrimental effects leading to exacerbation of the muscle defects due to accumulation of damaged proteins and dysfunctional organelles (Grumati *et al.*, 2011). Of note, this work demonstrated for the first time that physical exercise is able to activate autophagy in skeletal muscles (Grumati *et al.*, 2011; Nair and Klionsky, 2011).

Although the phenotype of patients with collagen VI deficiencies and of *Col6a1*$^{-/-}$ mice clearly underline the critical role of this ECM component in skeletal muscles, as discussed

above collagen VI has a broad distribution in the body and likely exerts multiple functions in different tissues. Indeed, recent studies in *Col6a1*$^{-/-}$ mice also demonstrated a role for collagen VI in regulating *in vivo* Schwann cell differentiation, a function that is required for the proper maintenance of peripheral nerve myelination and function (Chen *et al.*, 2014a). In addition, further studies in *Col6a1*$^{-/-}$ mice revealed that collagen VI acts on macrophage recruitment and polarization, promoting nerve regeneration after injury (Chen *et al.*, 2014b).

Although all these studies point at collagen VI as a key ECM molecule exerting several important functions in different tissues, surprisingly very few literature works investigated the role of collagen VI in fibroblasts, i.e. the major cell type that primarily produces and secrete this ECM molecule in the different tissues including skeletal muscles (Hatamochi *et al.*, 1989; Braghetta *et al.*, 2008; Zou *et al.*, 2008). Given the peculiar pathway of intracellular assembly of this ECM molecule and the strict requirement of the synthesis and association of the three α1(VI), α2(VI) and 3(VI) chains in equimolar ratios for the proper assembly, secretion and ECM deposition of collagen VI, it can be assumed that mutation or ablation of a single chain, as it occurs in *Col6a1* null mice and in patients with dominant and recessive *COL6A1-A3* mutations, may have detrimental effects for fibroblasts. Initial studies in fibroblasts cultures derived from *Col6a1*$^{-/-}$ mice confirmed that lack of α1(VI) chain completely abolish the assembly and secretion of collagen VI by these cells. Interestingly, *Col6a2* and *Col6a3* genes are normally transcribed in *Col6a1*$^{-/-}$ mice, but in the absence of α1(VI) the other two chains cannot be assembled and are retained within fibroblasts (Bonaldo *et al.*, 1998). Studies in UCMD and BM patients confirmed that retention of collagen VI chains takes place in fibroblasts rather than myofibers or myoblasts, suggesting that fibroblasts themselves, responsible for the secretion of collagen VI, contribute significantly to the pathogenesis of UCMD and BM (Pan *et al.*, 2003; Zou *et al.*, 2008). It is therefore of great interest to elucidate how lack of collagen VI impacts on the homeostasis, survival and activity of fibroblasts. The major aim of my PhD project was to investigate whether collagen VI has an instructive role towards

fibroblast survival and autophagy and how lack of this ECM molecule affects fibroblast homeostasis.

1.3. Autophagy in mammalian cells

The autophagy-lysosome system is one of the major catabolic pathways of the cell. Based on their functions and mechanisms, different types of autophagy were described: microautophagy, chaperone-mediated autophagy and macroautophagy (Fig. 2). Microautophagy leads to the engulfment and degradation of small amounts of cytoplasm by the lysosomal membrane itself. Chaperone-mediated autophagy (CMA) targets unfolded soluble proteins for degradation, through direct translocation across the lysosome membrane by the chaperone hsc70 and the lysosomal receptor LAMP-2A (lysosome-associated membrane protein type 2A). Macroautophagy involves the formation of unique double-membrane vesicles (called autophagosomes) that engulf long-lived proteins, damaged organelles and pathogens, dispatching them to lysosomes for degradation and recycling, also in a selective manner (Mizushima *et al.*, 2008; Boya *et al.*, 2013). Macroautophagy (hereafter referred to as autophagy) will be of main interest for this discussion.

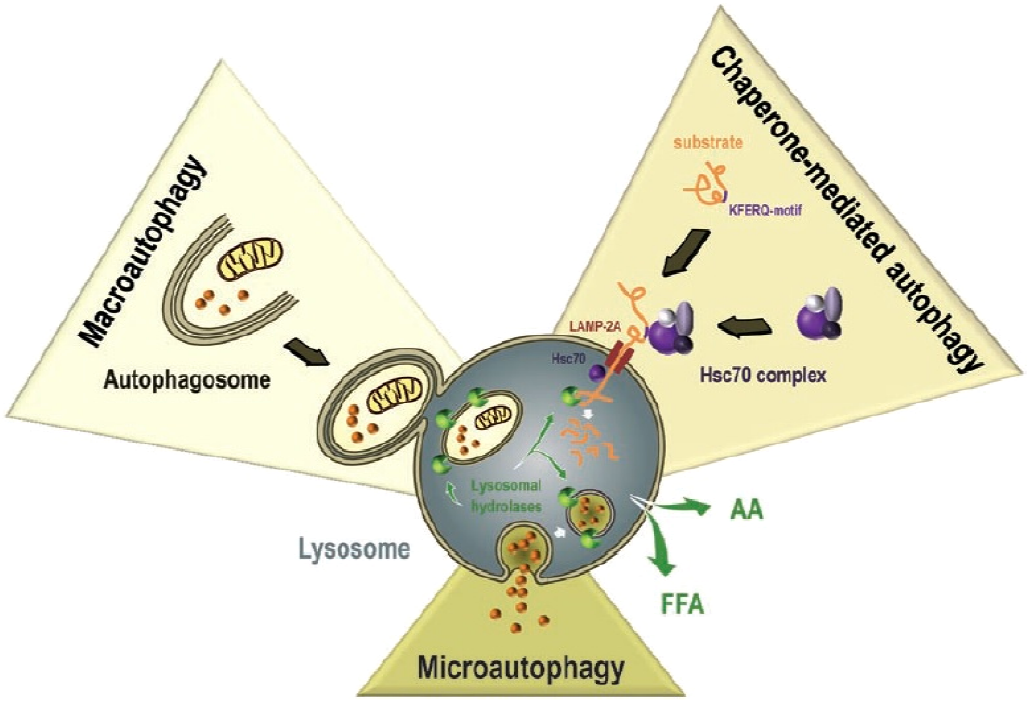

Figure 2. Schematic representation of the different types of autophagy (Wirawan et al., 2012).

Autophagy is finely regulated by extracellular and intracellular nutrient and growth factor sensing via a complex pool of receptors and interactors (Feng *et al.*, 2014; Stolz *et al.*, 2014), which are strictly required for the adaptive response of the cell and for global tissue homeostasis. Autophagy usually acts as a cytoprotective mechanism. However the precise regulation of autophagy is even more crucial, so that both excessive and defective activity of this process result in pathological outcomes (Mizushima *et al.*, 2008). Autophagic defects were shown to play a role in a broad number of human diseases, including neurodegenerative disorders, myopathies, heart and liver diseases, infections and immune diseases, and cancer (Levine and Kroemer, 2008; Mizushima and Komatsu, 2011; Schneider and Cuervo, 2014).

The key players in the autophagic process are a group of evolutionary conserved proteins, named autophagy-related (Atg) proteins. When autophagy is induced, Atg proteins assemble at specialized sites and initiate the formation of a double membrane structure called isolation membrane. This isolation membrane expands and recruits Atg proteins and membranes from Golgi, endoplasmic reticulum, endosome, mitochondria and/or plasma membrane compartments, to become a phagophore (Boya, Reggiori, and Codogno, 2013). Atg9 shuttles between the isolation membrane and the different recruitment sites, directing membranes for autophagosome elongation (Feng *et al.*, 2014). In mammalian cells, activation of the Beclin 1/class III phosphatidylinositol 3-kinase complexes is necessary to initiate the nucleation step of the phagophore. Association of Beclin 1 (Becn1, homologue of yeast protein Atg6) with Vps34, Vps15 and Ambra1 to form a core complex, and then also with UVRAG, Atg15, Barkor or Rubicon in multiprotein complexes, is involved in different functions in membrane trafficking (He and Levine, 2010). Ulk1/Atg1 kinase, which forms a complex with Atg13 and Atg17, is also a key regulator in autophagy initiation step (Mizushima *et al.*, 2010; Kim *et al.*, 2011). As detailed below, Ulk1 can be differently regulated by several kinases to modulate cell autophagy.

Following the initiation step, elongation of the phagophore takes place, thus generating the characteristic double-layered membrane vesicles called autophagosomes.

Two different ubiquitin-like conjugation systems act synergistically to add the Atg12–Atg5–Atg16L complex and the microtubule-associated light chain protein 3 (MAPLC3/LC3/Atg8) to the nascent pre-autophagosomal membranes (Ohsumi, 2001; Mizushima *et al.*, 2003; Fujita *et al.*, 2008). Atg5 forms a covalent complex with Atg12, thanks to Atg7 (an ubiquitin-activating E1 enzyme) and Atg10 (an E2-like enzyme). When Atg7 and Atg10 are released, Atg16L can bind the newly formed Atg5-Atg12 complex and together they lead to elongation of the pre-autophagosome (Nemoto *et al.*, 2003; Ferraro and Cecconi, 2007). At the same time, the cytosolic form of LC3 (called LC3-I) is cleaved by Atg4, and its C-terminal residue is transferred to a phosphatidyl ethanolamine (PE) by Atg7 (E1-like) and Atg3 (E2-like) enzymatic activities. The conjugation of LC3 with PE results in a lipidated, non-soluble form of LC3 (called LC3-II) that is inserted in the pre-autophagosomal membranes (Ichimura *et al.*, 2000).

The unique features of the LC3 protein make it the only reliable marker to follow in a spatial and temporal manner the formation and the dynamic changes of the autophagosomes. Indeed, generation of LC3-II specifically correlates with its insertion in the autophagosome membranes, in which this protein remains inserted until fusion with lysosomes and degradation (Kabeya *et al.*, 2004; Mizushima and Kuma, 2008; Klionsky *et al.*, 2012-guidelines). GFP-LC3 reporter mice are in this context a valuable tool to monitor autophagic flux *in vivo* (Mizushima and Kuma, 2008; Mizushima *et al.*, 2004). LC3 interacts with a wide range of proteins containing a specific domain, called LC3-interacting region (LIR). Among these interacting factors, the sequestosome-1 protein (p62 or SQSTM1) mediates selective degradation of ubiquitinated protein aggregates (Bjørkøy *et al.*, 2006; Komatsu *et al.*, 2007; Stolz *et al.*, 2014). Indeed, p62 also contains an ubiquitin binding domain thus targeting poly-ubiquitinated proteins to autophagosomal degradation. Following fusion with lysosomes, the autophagic adaptor p62 is also degraded. Therefore, p62 accumulation is a useful marker for autophagy flux and cell clearance (Stolz *et al.*, 2014; Klionsky *et al.*, 2012-guidelines). However, the expression of p62 can change at the transcriptional level due to many stimuli and conditions, such as nutrient starvation, making its interpretation more complex (Jiang and Mizushima, 2014). Furthermore, the

assembly of aggregation-prone proteins into large aggregates may also work as nucleation sites for the phagophore, promoting their uptake into autophagosomes. The selective removal of these aggregates, through specific chaperones or adaptor proteins, is called aggrephagy (aggresome-autophagy). Thanks to cargo-specific receptors, autophagosomes can selectively sequester and degrade different cargoes, such as mitochondria, peroxisomes, endoplasmic reticulum, endosomes, cytoplasmic aggregates, ribosomes and pathogens (Stolz *et al.*, 2014; Boya, Reggiori, and Codogno, 2013). The final step of autophagosome biogenesis is the sealing of the double membrane phagophore. This maturation process is interconnected with the fusion of autophagosome with the lysosome, that finally generate the autophagolysosome (or autolysosome) whose content is degraded by lysosomal hydrolases and can be recycled by the cell. Lysosomes integrity is also fundamental to complete autophagy (Shen and Mizushima, 2014).

Autophagy is controlled by multiple signaling pathways, most of which converge on the mammalian target of rapamycin (mTOR), a master regulator of cell growth. In mammalian cells, mTOR complex 1 (mTORC1) is controlled by the nutrient status of the cell and by the availability of amino acids and growth factors (Russell *et al.*, 2014). In physiological condition, mTORC1 negatively regulates autophagy by binding and phosphorylation of the Ulk1 complex at Ser 757, the major mTORC1 phosphorylation site *in vivo*, thus disrupting its interaction with AMP-activated protein kinase (AMPK) (Kim *et al.*, 2011; Shang and Wang, 2011). Conversely, when nutrients are scarce and/or ATP concentration is decreased, mTORC1 is inhibited leading to autophagy re-activation. Energy consumption leads to AMPK auto-phosphorylation. Active AMPK can subsequently trigger autophagy both by inhibiting mTOR and activating Ulk1 through phosphorylation (Egan *et al.*, 2011; Boya, Reggiori, and Codogno, 2013). Moreover, mTORC1 regulates autophagy at the level of Atg gene transcription, acting on downstream translational regulators, such as the initiation factor 4E binding protein (4E-BP1) and the p70 S6 kinase ($p70^{S6K}$, that in turn phosphorylates the S6 ribosomal protein).

Autophagy can be modulated also by controlling lysosome biogenesis, through mTORC1 regulation of the transcription factor EB (TFEB). TFEB is a master gene regulator

of several lysosomal and autophagy-related genes (Settembre and Ballabio, 2011). It localizes to the lysosome membrane together with mTORC1, whose phosphorylation leads to TFEB cytoplasmic sequestration. When mTORC1 is inactive, the dephosphorylated TFEB can migrate to the nucleus where it exerts its pro-transcriptional activity (Settembre *et al.*, 2012; Martina *et al.*, 2012). TFEB controls lysosomal biogenesis by positively regulating genes belonging to the Coordinated Lysosomal Expression and Regulation (CLEAR) network, and controls autophagosome biogenesis by direct targeting the promoters of several Atg genes, such as *UVRAG*, *MAPLC3B*, *SQSTM1* and *ATG9B* (Sardiello *et al.*, 2009; Settembre *et al.*, 2011).

Thus, mTOR has a major role in adapting cell metabolism in response to nutrient sensing, interacting with main autophagy regulators and impinging both on autophagy initiation and maturation steps (Russell *et al.*, 2014). Furthermore, via the mTOR pathway, also lysosomes show a crucial role in modulating the TFEB response, and hence the cellular response to nutrient changes (Settembre *et al.*, 2011).

1.4. Extracellular matrix regulation of autophagy

In all tissues and specialized microenvironments, ECM-derived signals are crucial for cytoprotection and homeostasis, in some cases converging to the autophagic machinery (Neill *et al.*, 2014). The role of the ECM on the regulation of autophagy is still under dissection. However, increasing evidence was recently provided regarding the involvement of ECM proteins (Nguyen *et al.*, 2007; Grumati *et al.*, 2010; Castello-Cros *et al.*, 2011; Tuloup-Minguez *et al.*, 2011; Buraschi *et al.*, 2013) and of integrin receptors (Fung *et al.*, 2008; Tuloup-Minguez *et al.*, 2013) in autophagy signaling, thus opening the field for further studies.

Epithelial cell survival depends on integrin-mediated adhesion to ECM. Upon matrix detachment, cells undergo a form of cell death called anoikis. Integrin disengagement is also able to trigger autophagy, as a prosurvival mechanism to skip anoikis in a non-tumorigenic manner. The reduced growth factor sensing by membrane receptors results in autophagy induction, despite of addition of other nutrients (Fung *et al.*, 2008). In this

process, autophagy induction is also correlated with activation of the endoplasmic reticulum kinase (PERK). In detached cells, PERK can promote autophagy and a concomitant antioxidant response through activation of a pathway that involves the eukaryotic translation initiation factor 2α (eIF2α), ATF4 and CHOP. This pathway subsequently induces Beclin 1/Atg6 and LC3/Atg8 expression, promotes ATP production, and reduces reactive oxygen species levels to delay anoikis (Avivar-Valderas *et al.*, 2011). The balance between autophagy induction and anoikis completion determines if one cell finally leaves the ECM and dies or if it is able to re-adhere (Avivar-Valderas *et al.*, 2011; Lock and Debnath, 2008).

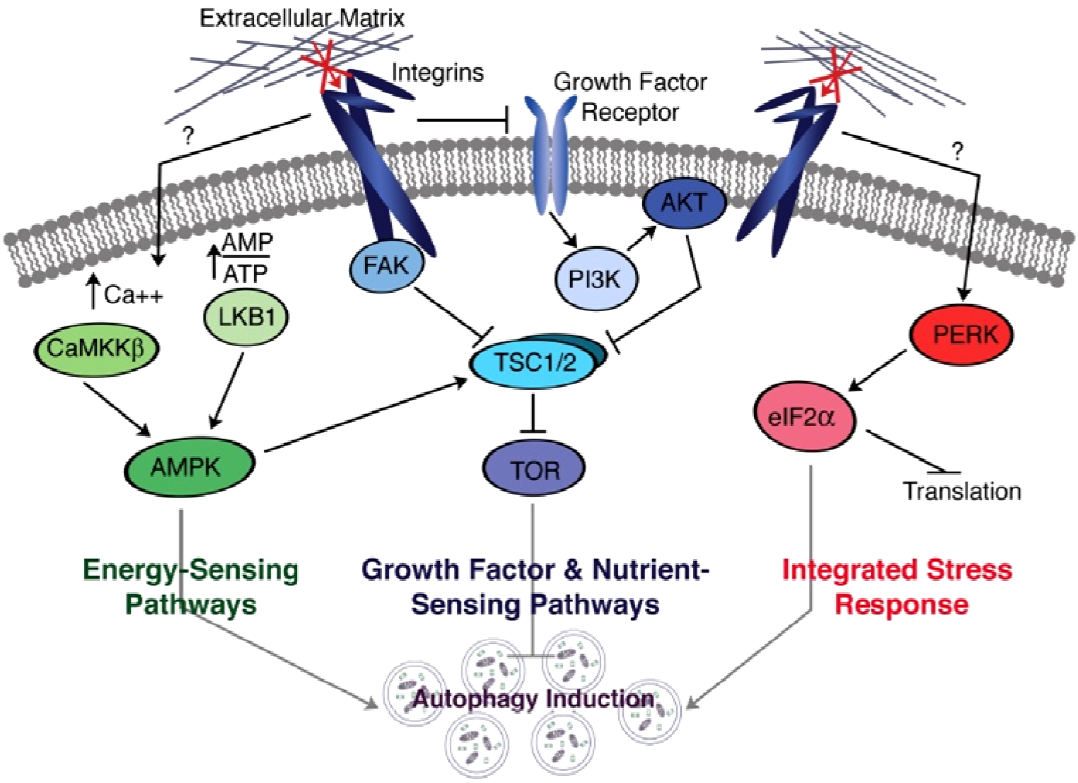

Figure 3. Candidate intracellular pathways linking the ECM to autophagy (Lock & Debnath, 2008).

ECM has also been proposed to modulate autophagy by other mechanisms, such as by activation of AMPK or FAK-dependent inhibition of mTOR, due to the disruption of cell-matrix contacts (Lock and Debnath, 2008) (Fig. 3). It is important to highlight that

autophagy modulation also occurs by extracellular soluble and non-soluble factors, usually thought to act at the level of cell adhesion and structure.

Several ECM proteins, including kringle V (Nguyen *et al.*, 2007), endostatin (Nguyen *et al.*, 2009), collagens (Grumati *et al.*, 2010; Tuloup-Minguez *et al.*, 2011), plasminogens (Castello-Cros *et al.*, 2011), laminin-2 (Carmignac *et al.*, 2011), decorin (Buraschi *et al.*, 2013; Goyal *et al.*, 2014), and endorepellin (Poluzzi *et al.*, 2014), are emerging as primary regulators of this process (Fig. 4).

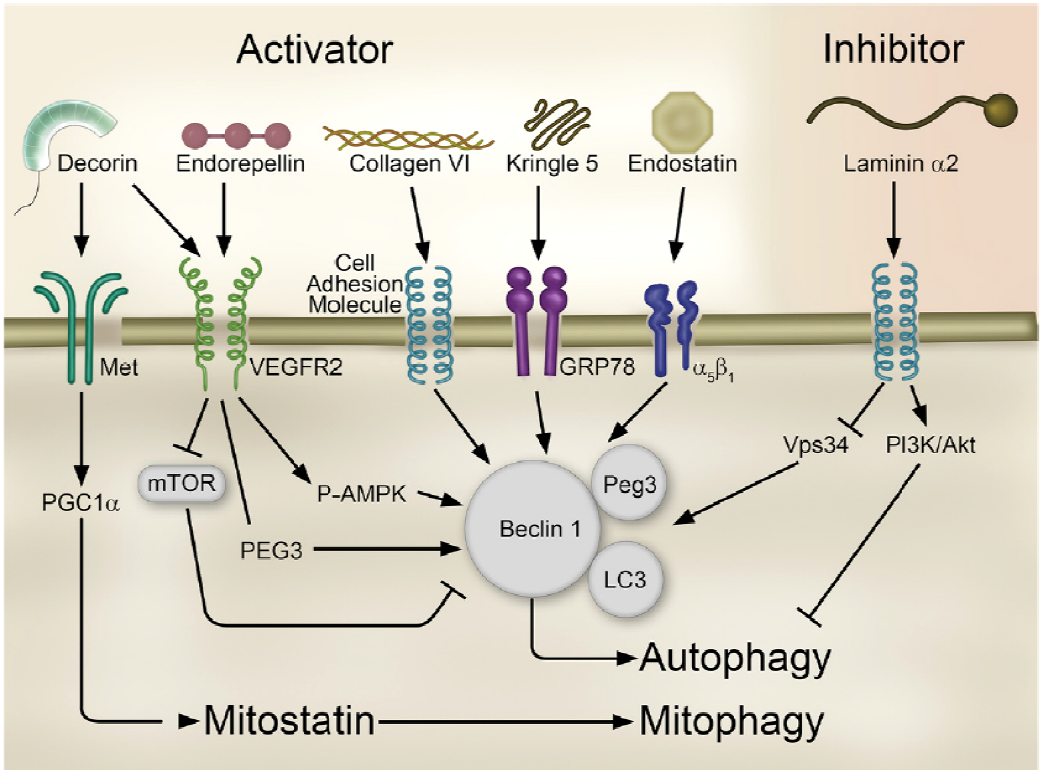

Figure 4. ECM proteins regulates autophagy (Neill et al., 2014).

It was recently demonstrated that decorin, a small leucine-rich proteoglycan, regulates a autophagosome formation via a novel Peg3-dependent process (Buraschi *et al.*, 2013). Peg3 (paternally expressed gene 3) is a tumor suppressor protein recently found to bind and promote Beclin 1 and LC3 expression upon decorin treatment on endothelial cells. Decorin interaction with VEGF receptor 2 (VEGFR2), and subsequent activation of AMPK, is required for the induction of Peg3-dependent transcriptional activity on autophagic genes. At the same time, soluble decorin is able to inhibit the

Akt/mTOR axis. Thus, decorin induces autophagy via a canonical Vps34/mTOR pathway by acting on a novel identified regulator of macroautophagy, Peg3 (Buraschi *et al.*, 2013; Goyal *et al.*, 2014).

Other ECM macromolecules, such as collagen types I and IV, display a role in autophagy modulation when present as adhesion substrates, but a mechanistic insight is still lacking (Tuloup-Minguez *et al.*, 2011).

In addition, ECM modulation of autophagy often takes place in a nutrient availability independent manner, suggesting an intrinsic ability to supervise and constrain extracellular factors that triggers this catabolic response, in order to harmonize cell responses (Neill *et al.*, 2014).

2. Methods

2.1. Cell culture and transfection.

Primary mouse embryonic fibroblasts (MEFs) were prepared by dissociation of 13.5 dpc mouse embryos from wild type (WT) C57BL/6 and *Col6a1*$^{-/-}$ pregnant female mice. MEFs at culture passage 2-4 were grown to 90% confluence in complete Dulbecco's modified Eagle's medium (DMEM) without antibiotics. Cells were harvested with 0.25% trypsin-EDTA (Life Technologies, Gibgo) and resuspended at a final density of 2.4 x 10^6 cells/ ml in buffer of the Microporation Solution Kit (MPK-10096, Digital Bio) together with 0.5 µg pMSE plasmid encoding for SV40 large T-antigen (SV40LT, kindly provided by Prof. M. Sandri, University of Padova). MEFs were then microporated with a 10 µl Gold Tip (Neon® Transfection System, MPT100, Life Technologies) at 1500 V for 20 millisec with the Microporator MP-100 Platform (Digital Bio), plated in 24-well plates prefilled with DMEM containing 10% fetal bovine serum (FBS, Life Technologies) without antibiotics and grown at 37° C in a humidified incubator with 5% CO_2. Cells were clonally diluted and passed for an additional 10 passes to ensure stable immortalization. We obtained at least three different WT and three different *Col6a1*$^{-/-}$ immortalized fibroblast lines. MEFs were cultured in DMEM supplemented with 10% FBS and maintained in a humidified incubator containing 5% CO_2 at 37° C. For collagen VI expression studies, cells were cultured three to seven days in DMEM containing 10% FBS supplemented with 0.25 mM ascorbic acid. GFP-LC3 stably expressing MEFs lines were generated from GFP-LC3 (kindly provided by Prof. N. Mizushima, University of Tokyo) and GFP-LC3;*Col6a1*$^{-/-}$ transgenic mice. When indicated, cells were plated on plastic coated with 5 µg/cm^2 purified murine native collagen VI (Irwin *et al.*, 2003) or collagen I (Sigma-Aldrich, C8919) and cultured for three days. 0.8 x 10^5 cells were plated on 12 mm glass coverslips, grown to 80% confluence and transfected with pMitoRed (kindly provided by Prof. L. Scorrano, University of Padova), mCherry-Parkin (Addgene plasmid 23956), YFP-Parkin (Addgene plasmid 23955, Narendra *et al.*, 2008) or GFP-TFEB (kindly provided by Prof. M. Sandri, University of Padova) using LipofectamineTM LTX (Life Technologies) in a 1:1 ratio, according to

manufacturer's guidelines. After 4 hr, transfected cells were washed in complete DMEM without antibiotics and cultured 18-20 hr before fixation. When indicated, the following additional treatments were used on 80% confluent cells: 3 hr or 6 hr serum starvation; 50 μM chloroquine (Sigma-Aldrich); 250-500 mM 3-methyladenine (3-MA, Sigma-Aldrich). Finally, cells were harvested and processed for FACS analysis or fixed for 10 min with ice-cold acetone/methanol (1:1) at -20° C. Carbonyl cyanide m-chlorophenylhydrazone (CCCP) was from Sigma.

2.2. Immunofluorescence on cells.

Fixed cells were washed three times in PBS, blocked with 10% goat serum (Sigma) for 30 min and incubated for 2 hr at room temperature or overnight at 4° C with the following primary antibodies: rabbit anti-collagen VI (AS72, kindly supplied by Prof. A. Colombatti, CRO Aviano), mouse anti-fibronectin (kindly supplied by Prof. A. Colombatti, CRO Aviano), rabbit anti-α1(VI) (Santa Cruz Biotechnology), guinea pig anti-α3(VI) (kindly supplied by Prof. R. Wagener, University of Cologne), rat anti-LAMP-2 (GL2A7, ab13524 Abcam), rabbit anti-LC3B (2775, Cell Signaling Technologies), rabbit anti-Tom20 (Santa Cruz Biotechnology). After three washing in PBS, slides were incubated for 1 hr with the following secondary antibodies: anti-mouse CY2, anti-rabbit CY2, anti-rabbit CY3, anti-rat CY3 (all Jackson Immunoresearch); IRIS anti-rabbit CY5.5 (Cyanine Technologies). Nuclei were stained with Hoechst 33258 (Sigma-Aldrich). Slides were mounted in 80% glycerol-PBS and analyzed with a Leica SP5 confocal microscope. Colocalization was quantified in merged images, after thresholding of individual frames, using the JACoP plugin of ImageJ (NIH). The percentage of cells with enlarged lysosomes was calculated by manual counting of the cells with at least two enlarged LAMP-2-positive lysosomes on total cell number per field, for thirty randomly chosen image fields. The percentage of cells with tubular or fragmented mitochondria was estimated by manual classification of mitochondrial morphology in at least thirty randomly chosen fields. Mean data are representative of at least five independent biological samples.

2.3. TUNEL assay.

Terminal deoxynucleotidyl transferase dUTP-mediated nick-end labeling (TUNEL) analysis was performed on acetone/methanol fixed MEFs using the Dead End Fluorometric In Situ Apoptosis Detection System (Promega). MEFs, grown on slides and fixed in acetone/methanol, were washed and incubated for 10 min with the equilibration buffer. Then the slides were incubated with a buffer containing fluorescent nucleotides, terminal deoxynucleotidyl transferase (TdT), and Hoechst 33258 (Sigma) for 1 hr at 37°C. The reaction was blocked with SSC solution (300 mM NaCl, 30 mM sodium citrate). After being washed three times in PBS, slides were mounted using 80% glycerol. Hoechst was used to counterstain all nuclei and TUNEL-positive nuclei were determined by counting randomly selected fields using a Zeiss Axioplan microscope.

2.4. Flow cytometry.

Wild type and *Col6a1*$^{-/-}$ MEFs were plated (200,000 cells/ well) in 12-well plates by adhesion on plastic, purified collagen VI or collagen I and cultured for a day. Cells were washed in PBS, and incubated for 3 hr or 6 hr in complete medium or in serum-free medium. When indicated, 1 μM staurosporine (STS) or 250-500 mM 3-methyladenine (3-MA, Sigma-Aldrich) were added to the serum-free medium. Apoptosis was determined using the Annexin V-FITC Apoptosis detection kit (eBioscience). Cells were harvested, washed with PBS and incubated in 195 μl of 1x binding buffer containing 5 μl annexin V-FITC for 15 min at room temperature in the dark according to the manufacturer's protocol. Cells were finally incubated with 1 μg/ μl propidium iodide (PI) and samples were immediately analyzed on a FACSCanto flow cytometer equipped with FACS Diva software (BD Biosciences), using the FL-1 and the FL-2 settings. Forward scatter and side scatter (morphology parameters) were performed to discriminate live cells (annexin V negative and PI negative), apoptotic cells (annexin V positive) and necrotic cells (annexin V negative and PI positive). For each sample 10,000 events were collected, for five independent biological replicates. Results were analyzed using Flowing Software v2.5.0 (Turku Centre for Biotechnology, University of Turku).

2.5. Quantitative RT-PCR (qRT-PCR).

500,000 MEFs of each genotype were plated in 6-well plates, in triplicate, and cultured for 2 days (autophagy studies) or 4 days (collagen VI expression). For the analysis of *Col6a1*, cells were cultured until post-confluence in DMEM containing 10% FBS, in the presence or absence of 0.25 mM ascorbic acid. For the analysis of autophagy genes, cells were washed in PBS, then media with or without FBS was replaced for 3 hr. RNA extraction was performed by adding 1 ml/well TRIzol Reagent (Life Technologies) directly on MEFs and following the manufacturer's protocol. RNA was quantified using a Nanodrop ND-1000 instrument (Nanodrop Technologies) and 1 µg total RNA was retrotranscribed using the SuperScript III First-Strand Synthesis System for RT-PCR (Life Technologies), following manufacturer's instructions. Resulting cDNAs were used to perform quantitative real time PCR using Rotor-Gene SYBR Green PCR Kit mastermix (Qiagen) with the RotorGeneQ instrument (Qiagen). Primer sequences are shown in Table 1.

2.6. Western blotting.

MEFs (0.5 x 10^6 cells/ ml) were cultured in 6-well plates for three days. When indicated, multiwell plates were coated with 5 µg/cm^2 collagen VI or collagen I as described above. Cells were washed once in PBS and harvested with a cell lifter in lysis buffer (100 µl 50 mM Tris-HCl, pH 7.5, 150 mM NaCl, 20 mM EDTA, 0.5% NP40) supplemented with phosphatase inhibitors (Cocktail II P5726, Sigma-Aldrich) and proteases inhibitors (Complete EDTA free, Roche). Cell lysates were then sonicated twice for 15 sec using a Bioruptor (Diagenode) and the cleared cell lysates were quantified with the BCA Protein Assay kit (Pierce). SDS-PAGE of protein lysates (20 or 30 µg) was performed using 3-8%, 4-12%, 10% or 12% polyacrylamide Novex NuPAGE Bis-Tris gels (Invitrogen) and electrotransferred onto PDVF membrane (Millipore). Membranes were blocked for 1 hr in 5% milk in TBST and incubated 1 hr at room temperature or overnight at +4° C with the following primary antibodies diluted 1:1000 in TBST, 5% BSA: anti-AMPK; anti-phospho-AMPK (Thr172), anti-Akt, anti-phospho-Akt (Ser473), anti-ERK1/2,

anti-Ulk1, anti -phospho-Ulk1 (Ser757 and Ser555), anti-4E-BP1, anti-phospho-4E-BP1, anti-S6, anti-phospho-S6, anti-Raptor, anti-phospho-Raptor (all Cell Signaling Technologies); guinea pig polyclonal anti-p62 (Progen); rabbit polyclonal anti-LC3B; rabbit polyclonal anti-Atg5 (Sigma-Aldrich); rat anti-LAMP-2 (Abcam); mouse monoclonal anti-β-actin (Chemicon International). Membranes were then washed three times and incubated for 1 hr at room temperature with HRP-conjugated secondary antibodies (Amersham Bioscience) diluted 1:1000 in TBST and 5% milk. Detection was performed by SuperSignal West Pico or Dura Chemiluminescent Substrate and CL-X Posure Film (Thermo Scientific), with β-actin as a loading control. When needed, membranes were stripped using a stripping buffer (25 mM glycine, 1% SDS, pH 2.0) and re-probed. Western blots were performed in at least three independent experiments. Densitometric measurements were obtained using ImageJ software (NIH), normalizing the signal of each band to the corresponding actin band or to the non-phosphorylated form of protein. We calculated the difference between the ratios of LC3 conversion (LC3-II/LC3-I) as an indicator of the rate of the autophagy flux: this difference was calculated as the ratio of LC3-II/LC3-I values obtained in basal condition, onto LC3-II/LC3-I values obtained after serum starvation:

$$\frac{\left(\frac{\text{LC3-II}}{\text{LC3-I}}\right)_{\text{serum-starved}}}{\left(\frac{\text{LC3-II}}{\text{LC3-I}}\right)_{\text{basal}}}$$

We defined this difference as serum-induced conversion rate of LC3.

2.7. Statistical analysis.

All results are expressed as means ± s.e.m. Statistical analysis of data was performed with Student's t test for unpaired data and a $P<0.05$ was considered statistically significant (*, $P<0.05$; **, $P<0.01$; ***, $P<0.001$).

3. Results

3.1. Immortalized MEFs produce collagen VI and organize an extracellular matrix

We first investigated the ability of immortalized MEFs to produce ECM proteins like collagen VI and fibronectin. Immunofluorescence using antibodies against whole collagen VI showed the deposition and the formation of organized filaments of collagen VI in the extracellular matrix of wild type MEFs, but not of *Col6a1*$^{-/-}$ MEFs (**Fig. 1A**). Fibronectin staining was detected in the extracellular matrix of both wild type and *Col6a1*$^{-/-}$ MEFs. As expected (Sabatelli *et al.*, 2001; Tillet *et al.*, 1994), collagen VI and fibronectin fibrils did not colocalize, but they were strictly interconnected in the extracellular matrix of wild type MEFs (**Fig. 1A**).

Culture media and cell extracts from wild type and *Col6a1*$^{-/-}$ MEFs that were grown from three to five days in 6-well plates, were separated by SDS-PAGE under reducing conditions and labeled with antibodies against either α1(VI) or α3(VI) collagen subunits (**Fig. 1B**). Cells were treated with ascorbic acid to promote collagen VI secretion in the extracellular environment. The α1(VI) chain was detected as a band at 140 kDa in culture media and cell extracts of wild type MEFs, but not of *Col6a1*$^{-/-}$ MEFs, in agreement with the complete null mutation of the corresponding *Col6a1* gene in homozygous knockout mice (**Fig. 1B**). In culture media and cell extracts of wild type MEFs, α3(VI) was detected as two major bands. The α3(VI) chain was abundantly present in wild type cell extracts and ascorbic acid treatment increased its secretion outside the cell. In culture media of *Col6a1*$^{-/-}$ MEFs, the α3(VI) chain was not detected except for a faint band below the 270 kDa marker. Cell extracts of *Col6a1*$^{-/-}$ MEFs displayed very low levels of α3(VI) (**Fig. 1B, C**). These data are in agreement with previous studies in *Col6a1*$^{-/-}$ mice, showing that in the absence of α1(VI) the other two chains are still expressed but cannot assemble nor lead to the secretion of functional collagen VI polypeptides.

To further investigate the expression of collagen VI in the immortalized MEFs, we performed qRT-PCR for the three collagen VI genes (**Fig. 1C**). Wild type MEFs expressed high levels of *Col6a1*, *Col6a2* and *Col6a3* transcripts. Treatment with ascorbic acid had no

significant effects on transcripts, except for α3(VI) mRNA that appeared increased. As expected, *Col6a1* mRNA in was almost undetectable in *Col6a1*$^{-/-}$ MEFs. Interestingly, *Col6a3* transcript levels were also decreased in *Col6a1*$^{-/-}$ MEFs, whereas *Col6a2* mRNA levels were similar in wild type and *Col6a1*$^{-/-}$ MEFs (**Fig. 1C**).

Given the presence of discrete amounts of intracellular α2(VI) and α3(VI) polypeptides in *Col6a1*$^{-/-}$ cells, we assessed whether the non-secreted single collagen VI chains are degraded through the autophagic pathway and are found into autophagosomes, which are accumulated in these cells as explained in detail below. However, we did not detect any co-localization of intracellular α3(VI) and autophagosome dots, suggesting that the unassembled collagen VI chains are eliminated by other mechanisms (**Suppl. Fig. S1**).

3.2. Autophagy is blocked at terminal stages in *Col6a1*$^{-/-}$ MEFs.

To examine whether autophagy was affected in *Col6a1*$^{-/-}$ MEFs, we studied autophagosome formation by evaluating LC3 conversion to its lipidated form and by monitoring protein degradation by consumption of p62, both in complete medium and after 3 hr serum withdrawal. Western blotting showed decreased LC3-I to LC3-II conversion (LC3-II/LC3-I ratio) in *Col6a1*$^{-/-}$ MEFs after serum withdrawal (**Fig. 2A**). However, total LC3-II protein content was not reduced *per se* when compared to the respective wild type condition. To investigate the autophagic flux we treated cells with chloroquine, an inhibitor of lysosome acidification. Interestingly, in wild type MEFs LC3-II/LC3-I ratio was increased both after starvation (two-fold increase) and in the presence of chloroquine, indicating an increase in autophagosome formation and autophagy induction (**Fig. 2B, C**). Differently, *Col6a1*$^{-/-}$ MEFs displayed only a small increase of the LC3-II/LC3-I ratio after serum starvation and no increase after chloroquine treatment (**Fig. 2B, C**). The results obtained by these experiments indicate that endogenous LC3 protein is accumulating in *Col6a1*$^{-/-}$ fibroblasts and that LC3-II conversion rate is decreased in *Col6a1*$^{-/-}$ cells when compared to wild type MEFs (**Fig. 2**).

To understand further the autophagic process in collagen VI deficient MEFs, we generated immortalized MEFs lines from GFP-LC3 and GFP-LC3;*Col6a1*$^{-/-}$ transgenic mice

and measured autophagosome formation by detection of GFP-positive puncta in cells maintained in complete medium or subjected to 3 hr serum withdrawal. In GFP-LC3 fibroblasts, few GFP-positive puncta formed in complete medium, while a six-fold increase of GFP-positive puncta was detected after serum withdrawal. In both conditions, 50 μM chloroquine treatment led to a marked accumulation of autophagosomes (**Fig. 2D, E**). In GFP-LC3;*Col6a1*$^{-/-}$ fibroblasts, we detected a massive formation of GFP-positive puncta already in complete medium conditions. In addition, no substantial variation in the number of fluorescent puncta was found in GFP-LC3;*Col6a1*$^{-/-}$ MEFs after serum starvation or following treatment with chloroquine. Moreover, GFP-positive autophagosomes were larger in collagen VI null fibroblasts when compared to wild type MEFs (**Fig. 2D**). These results suggest that the increased number and size of autophagosomes in *Col6a1*$^{-/-}$ fibroblasts may rely upon a slower "off rate" in the autophagic flux rather than an increase in autophagosome formation. Western blotting showed a decrease of p62 levels in *Col6a1*$^{-/-}$ MEFs , whereas total amounts of the Atg5-Atg12 conjugation complex increased in a similar manner in wild type and *Col6a1*$^{-/-}$ cells following serum starvation (**Fig. 2A**).

Gene expression analysis by qRT-PCR showed that p62 transcript levels were consistently down-regulated in *Col6a1*$^{-/-}$ MEFs, independently on serum starvation. Also the transcriptional activation of LC3 was defective in *Col6a1*$^{-/-}$ fibroblasts, as we did not detect any significant increase of LC3 mRNA levels after serum starvation, at difference from wild type MEFs (**Fig. 2F**). The mRNA levels of two other autophagic regulators, BNIP3 and Beclin 1, were not significantly affected by these experimental conditions or in the *Col6a1*$^{-/-}$ context (**Suppl. Fig. S3**).

3.3. AMPK is hyperactivated in *Col6a1*$^{-/-}$ MEFs, leading to a mild autophagy induction, but a residual activity of mTOR signaling is present.

Considering the latent mitochondrial dysfunction previously observed in *Col6a1*$^{-/-}$ myofibers (Irwin *et al.*, 2003; Grumati *et al.*, 2010), we investigated the activation state of AMP-activated protein kinase (AMPK), a sensor of energy status of the cell that becomes

active under metabolic stress (Russell *et al.*, 2014). AMPK phosphorylation was noticeably increased in *Col6a1*$^{-/-}$ MEFs, especially in basal conditions but also under serum starvation, indicating a general energy impairment (**Fig. 3A**). We analyzed the activation of extracellular signal-regulated kinases 1 and 2 (Erk1/2), two kinases acting on autophagy, and found that both Erk kinases were much less phosphorylated in *Col6a1*$^{-/-}$ MEFs compared to wild type MEFs both in basal conditions and after serum starvation (**Fig. 3B**).

Since the AMPK/Ulk1/mTORC1 signaling is essential for the autophagic response to nutrients (Russell *et al.*, 2014), we further analyzed AMPK-dependent Ulk1 activation, by investigating Ulk1 phosphorylation on Ser 555 (Egan *et al.*, 2011), and mTOR-dependent Ulk1 inactivation due to Ser 757 phosphorylation (Shang and Wang, 2011). Interestingly, we found that in both cases Ulk1 phosphorylation persisted after serum withdrawal in *Col6a1*$^{-/-}$ MEFs but not in wild type MEFs (**Fig. 3A, C**). Furthermore, the mTOR axis was persistently activated in *Col6a1*$^{-/-}$ MEFs after serum withdrawal, as demonstrated by phosphorylation of 4E-BP1 and of the S6 ribosomal protein, two major downstream targets of mTORC1 (**Fig. 3C**).

3.4. Adhesion onto collagen VI affects autophagy regulation in MEFs.

To evaluate whether addition of collagen VI was capable to impinge on the defective autophagy of *Col6a1*$^{-/-}$ MEFs, we cultured fibroblasts onto purified collagen VI provided as an adhesion substrate for three days, and then subjected cells to serum starvation. Growth of MEFs onto native collagen VI elicited an effect on LC3 lipidation and Ulk1 phosphorylation in both wild type and *Col6a1*$^{-/-}$ MEFs (**Fig. 4**). In particular, analyses of LC3-II/LC3-I ratios after western blotting showed that the serum-induced conversion rate of LC3 was increased in wild type MEFs, and a trend toward the increase was also found in *Col6a1*$^{-/-}$ MEFs (**Fig. 4A-C**). However, LC3 degradation in *Col6a1*$^{-/-}$ MEFs was enhanced in presence of collagen VI (**Fig. 4A**), leading to the rescue of LC3 accumulation in these cells (**Fig. 2B**). We also analyzed Ulk1 phosphorylation, in particular its mTOR-dependent inhibitory phosphorylation at Ser 757 that was found to be more phosphorylated in

Col6a1$^{-/-}$ MEFs (**Fig. 3C**), leading to Ulk1 inhibition in starving *Col6a1*$^{-/-}$ MEFs. Interestingly, after coating on collagen VI, Ulk1 phosphorylation in serum-starved condition was reduced also in *Col6a1*$^{-/-}$ MEFs (**Fig. 4A, D**). In wild type MEFs coated on collagen VI, Ulk1 phosphorylation was higher in basal conditions, and after serum depletion it decreased.

3.5. Lack of collagen VI affects lysosomes morphology and impairs autophagosome-lysosome fusion.

Based on the results discussed in § 3.2, which suggested an impairment of the "off rate" of the autophagic flux in *Col6a1*$^{-/-}$ MEFs, we analyzed lysosomes and their fusion with autophagosomes. Unexpectedly, immunostaining with the lysosomal marker LAMP-2 revealed a large amount of enlarged lysosomes in *Col6a1*$^{-/-}$ fibroblasts, whereas in wild type MEFs lysosomes appeared as smaller punctuate structures (**Fig. 5A, B**). Similarly enlarged lysosomes were detectable after serum depletion or following chloroquine treatment in wild type cells (**Fig. 5B, Suppl. Fig. S2**). Moreover, the increased number of enlarged lysosomes in *Col6a1*$^{-/-}$ MEFs appeared to be independent on autophagy induction by serum starvation (**Fig. 5B**). Wild type MEFs showed an increased number of enlarged lysosomes after serum depletion, that however was always of lesser extent when compared to *Col6a1*$^{-/-}$ cells (**Fig. 5B**). Interestingly, LAMP-2 protein levels were decreased in *Col6a1*$^{-/-}$ MEFs when compared to wild type MEFs, however LAMP-2 retained the capability to increase its levels in response to serum depletion (**Fig. 5C, D**). The decrease of LAMP-2 protein levels in *Col6a1*$^{-/-}$ MEFs was not paralleled by a reduction of LAMP-2 gene expression, which was also not influenced by serum depletion (**Fig. 5E**).

We further analyzed the final stages of fusion between autophagosomes and lysosome, by coimmunostaining for LC3 and LAMP-2. In wild type MEFs, colocalization of autophagosomes with lysosomes, indicating fusion events, was almost doubled upon serum depletion-induced autophagy (**Fig. 5F**). Notably, in *Col6a1*$^{-/-}$ MEFs colocalization of LAMP-2 and LC3 was not affected by serum depletion, indicating defective autophagosome-lysosome fusion (**Fig. 5F, G**). We also studied LAMP-2

immunolocalization on immortalized MEFs lines derived from GFP-LC3 transgenic mice, and obtained similar results for GFP-LC3;*Col6a1*$^{-/-}$ MEFs (data not shown).

It is well established that the transcription factor TFEB is a master regulator for lysosomal biogenesis, coordinating autophagy regulation to lysosomal biogenesis and function (Sardiello *et al.*, 2009; Settembre *et al.*, 2011) To evaluate whether TFEB contributed to the lysosomal defects found in *Col6a1*$^{-/-}$ MEFs, we investigated its cellular localization after transfection of a GFP-TFEB construct in MEFs. As expected (Settembre *et al.*, 2012), in wild type MEFs subjected to 3 hr serum depletion, the expressed GFP-TFEB transgene translocated from the cytosol to the nucleus (**Fig. 6A, B**), Differently, in *Col6a1*$^{-/-}$ MEFs the cellular localization of GFP-TFEB was markedly affected. In basal condition (complete medium), a sizeable fraction of GFP-TFEB was already seen in the nucleus in *Col6a1*$^{-/-}$ MEFs. Conversely, following serum depletion GFP-TFEB translocated to the nucleus only in a small fraction of *Col6a1*$^{-/-}$ MEFs (**Fig. 6A, B**).

3.6. Collagen VI ablation causes apoptotic cell death via caspase activation.

It is widely recognized that defects of autophagy impinge on cell survival and may lead to increased apoptosis and cell death. To evaluate the incidence of apoptosis in the immortalized wild type and *Col6a1*$^{-/-}$ MEFs, we first performed TUNEL assay. Apoptotic nuclei were markedly increased in collagen VI null fibroblasts (**Fig. 7A**). Notably, adhesion of cells onto purified collagen VI significantly rescued the apoptotic defects of *Col6a1*$^{-/-}$ MEFs, an effect which was not displayed by collagen type I, used as a control extracellular matrix substrate (**Fig. 7A**). The increased apoptosis incidence of *Col6a1*$^{-/-}$ MEFs was further confirmed by flow cytometry studies of annexin V and PI labeled cells (**Fig. 7B, C**). *Col6a1*$^{-/-}$ MEFs were less viable when compared to wild type MEFs, both under basal conditions and after 3 hr or 6 hr of serum depletion (**Fig. 7B** and data not shown). Furthermore, not only early apoptotic events, but also late apoptosis/ necrosis events (annexin V-FITC positive and PI positive cells) were increased in *Col6a1*$^{-/-}$ fibroblasts (**Fig. 7C**).

Interestingly, three days of culture onto native collagen VI significantly ameliorated the survival of *Col6a1*$^{-/-}$ MEFs both under basal conditions and after serum withdrawal. By contrast, when cultured onto a control coating made of collagen I, *Col6a1*$^{-/-}$ MEFs did not rescue cell viability after serum withdrawal (**Fig. 7B, C**). Adhesion onto collagen VI also elicited some beneficial effects on wild type cells, since apoptotic cells (annexin V positive) were significantly decreased when wild type MEFs were grown on collagen VI (**Fig. 7C**).

The above findings, together with the occurrence of a large number of aggregated autophagosomes in *Col6a1*$^{-/-}$ MEFs, suggest the possibility that an autophagic cell death may occur in this context. To test this hypothesis, we investigated autophagic cell death by treating cells with the autophagy inhibitor 3-MA in order to prevent the accumulation of autophagosomes and lysosomes. Notably, 3 hr treatment with 3-MA led to a dose-dependent increase of cell death both in wild type and in *Col6a1*$^{-/-}$ MEFs (**Suppl. Fig. S4**), thus excluding the possibility of an autophagic cell death. Next, we evaluated caspase activation by western blotting, and found that cleaved caspase 3 and 9 were present in *Col6a1*$^{-/-}$ MEFs (**Fig. 7D**). Moreover, the activated forms of both caspases were further increased by serum depletion in *Col6a1*$^{-/-}$ fibroblasts, similarly to the staurosporine-treated positive controls (**Fig. 7D**).

3.7. *Col6a1*$^{-/-}$ MEFs display fragmented mitochondria and mitophagy alterations.

As previously found in cell cultures derived from muscle biopsies of UCMD patients (Sabatelli *et al.*, 2012), *Col6a1*$^{-/-}$ MEFs displayed highly fragmented mitochondria with respect to wild type MEFs (**Fig. 8A**). We labeled mitochondria with different probes, using MitoTracker, pMitoRed and Mito-YFP plasmids, and consistently found that fragmented mitochondria were more than two-fold increased in *Col6a1*$^{-/-}$ MEFs when compared to the corresponding wild type MEFs (**Fig. 8A, B**).

We then analyzed the efficiency of mitochondria removal by selective autophagy, namely mitophagy, by performing coimmunolocalization studies of mitochondria and autophagosomes/autolysosomes after serum withdrawal. Towards this aim, we used GFP-

LC3 MEFs and stained mitochondria with Tom20 and lysosomes with LAMP-2. First of all, we confirmed a defect in mitochondria elongation and a decrease in autophagosome-lysosome fusion in *Col6a1*$^{-/-}$ MEFs (**Fig. 8C, D**). Then, interestingly, we noticed an increased rate of colocalization between mitochondria and autophagosomes/lysosomes in *Col6a1*$^{-/-}$ MEFs (**Fig. 8C, D**). To experimentally test if mitochondrial removal by autophagy was functional in *Col6a1*$^{-/-}$ MEFs, we transfected cells with a YFP-Parkin construct (Narendra *et al.*, 2008) and with pMitoRED plasmid (**Fig. 8E**). Interestingly, we found that YFP-Parkin was more frequently translocated to mitochondria in *Col6a1*$^{-/-}$ MEFs (more than ten-fold increase with respect to wild type MEFs) already in basal condition when complete medium was available (**Fig. 8F**). Mitochondria removal was estimated by monitoring Tom20 immunostaining after 24 hr of CCCP treatment (20 μM), used as mitochondrial uncoupler. We found that the mitochondrial pool was decreased in wild type MEFs after the CCCP-induced damage. Conversely, in *Col6a1*$^{-/-}$ MEFs the decrease of mitochondrial pool was lower (**Fig. 8G**).

4. Discussion

Collagen VI is an ECM protein forming a distinct microfibrillar network in most interstitial connective tissues including skin, cartilage, tendons, adipose tissue (Braghetta *et al.*, 1996; Kuo *et al.*, 1997; Keene *et al.*, 1988; Khan *et al.*, 2009). This ECM protein is concentrated near the basement membranes of several organs such as skeletal muscle, blood vessels and peripheral nerves (Kuo *et al.*, 1997). Notably, collagen VI is one of the major ECM component produced by human skin fibroblasts, together with collagen I and III (Olsen *et al.*, 1989).

A powerful tool to investigate the *in vivo* functions of collagen VI was provided by the generation of a knockout mouse model for collagen VI (*Col6a1*$^{-/-}$), through gene-targeted inactivation of *Col6a1* gene (Bonaldo *et al.*, 1998). *Col6a1*$^{-/-}$ mice display a distinctive phenotype with structural and functional defects of skeletal muscles and represent a valuable animal model of human collagen VI-related pathologies, including UCMD and BM (Bonaldo *et al.*, 1998; Irwin *et al.*, 2003; Grumati *et al.*, 2010). The first characterization of *Col6a1*$^{-/-}$ mice revealed a myopathic phenotype affecting primarily diaphragm and other skeletal muscles, with degeneration of myofibers and reduced strength (Bonaldo *et al.*, 1998). Electron microscopy analyses of *Col6a1*$^{-/-}$ muscles demonstrated ultrastructural alterations of sarcoplasmic reticulum and mitochondria, associated with a latent mitochondrial dysfunction and spontaneous apoptosis of myofibers (Irwin *et al.*, 2003). Further studies were carried out in muscle biopsies and primary muscle cell cultures derived from UCMD and BM patients, which demonstrated similar alterations to those found in *Col6a1*$^{-/-}$ mice (Angelin *et al.*, 2007). A highly influential study later demonstrated a failure of the autophagic process in collagen VI deficient muscles. Of note, this autophagic impairment plays a key pathogenic role in the onset of the myopathic phenotype. Indeed, failure to maintain a proper autophagic flux in *Col6a1*$^{-/-}$ myofibers causes retention of dysfunctional organelles and ultimately leads to myofiber apoptosis and degeneration (Grumati *et al.*, 2010). Furthermore, *in vivo* reactivation of a proper autophagic flux in *Col6a1*$^{-/-}$ muscles by different nutritional, pharmacological or genetic

approaches is highly beneficial and allows to rescue muscle structure and function (Grumati *et al.*, 2010). A more recent study, to which I collaborated before starting my PhD, showed that physical exercise promotes autophagy induction in skeletal muscle. Of note, physical training is unable to reactivate autophagic flux in *Col6a1*$^{-/-}$ muscles, leading instead to adverse effects and exacerbation of the muscle defects (Grumati *et al.*, 2011).

Various *in vitro* and *in vivo* studies in *Col6a1*$^{-/-}$ mice showed that lack of collagen VI has a strong impact on cell homeostasis and survival process, including apoptosis, cell differentiation, autophagy, stem cell niche and regeneration (Irwin *et al.*, 2003; Iyengar *et al.*, 2005; Grumati *et al.*, 2010; Urciuolo *et al.*, 2013). Collagen VI exerts a cytoprotective role in various cellular contexts and after different cell stresses, such as starvation, oxidative stress, Aβ peptide toxicity and injury (Irwin *et al.*, 2003; Grumati *et al.*, 2010; Menazza *et al.*, 2010; Cheng *et al.*, 2009; Cheng *et al.*, 2011). These findings highlight a key role of this ECM component in cell survival.

Generation of the *Col6a1*$^{-/-}$ mouse model was aimed at investigating the *in vivo* biological roles of collagen VI in the different tissues. During the past decade the main interest was focused on skeletal muscle given the relevant implications for human collagen VI-related myopathies. Although collagen VI clearly exerts a key role in muscle homeostasis, the protein is not synthesized by myofiber or by myoblasts. Previous work showed that expression of the *Col6a1* gene is finely regulated in a dynamic manner through a complex set of different transcription regulatory elements extending for about 10 kb upstream the *Col6a1* translated region (Braghetta *et al.*, 1996). Studies in transgenic mice expressing different *Col6a1* 5'-flanking regions fused to the *lacZ* reporter gene showed that expression of the *Col6a1* in skeletal muscle is conferred by an enhancer element located at about –5 kb from the *Col6a1* transcription start site (Braghetta *et al.*, 2008). Interestingly this enhancer has a strong activity in muscle fibroblasts, but not in myogenic cells, and activation of the –5kb *Col6a1* enhancer in interstitial fibroblasts of developing muscles requires the presence of the myogenic cells (Braghetta *et al.*, 2008). These findings point at a strict regulation of collagen VI expression and deposition in

muscles, where interstitial fibroblasts produce and secrete the protein in response to specific signals generated by the myogenic cells. This is also confirmed by studies with muscle-derived cultures containing both myoblasts and fibroblasts, showing that fibroblasts abundantly secrete collagen VI and organizes it into a microfibrillar network which takes contact with the surface of myogenic cells (Urciuolo *et al.*, 2013). *In vitro* studies showed that muscle primary cultures do not produce and secrete collagen VI into the ECM until muscle-derived fibroblasts are reintroduced in the culture (Zou *et al.*, 2008). Furthermore, studies in cell cultures from UCMD and BM patients showed that the mutated form of collagen VI is synthesized and retained by fibroblasts (Pan *et al.*, 2003; Zou *et al.*, 2008). Nevertheless, once secreted in the interstitial space, fibroblast-produced collagen VI tightly interacts with myofibers, thus explaining its biological functions deeply interconnected with muscle homeostasis (Zou *et al.*, 2008). Therefore, and at difference from other muscular dystrophies and inherited muscle disorders, collagen VI myopathies represent a unique type of non-cell-autonomous diseases of skeletal muscles, since the mutated protein downstream the primary genetic defect is not found or produced by the myofibers themselves, but by fibroblasts (Bönnemann, 2011). A major consequence of this is that restoration of collagen VI deposition by fibroblasts is expected to have a beneficial and strong impact, as demonstrated by a recent study from our laboratory showing that *in situ* grafting with wild type fibroblasts leads to proper deposition of collagen VI in the endomysial matrix of *Col6a1*$^{-/-}$ mice, with beneficial effects on muscle homeostasis (Urciuolo *et al.*, 2013)

Although the studies and findings discussed above unmistakably point at fibroblasts as the primary cell type producing collagen VI, no study until now has ever investigated the consequences caused by collagen VI deficiency in fibroblasts themselves. Besides the obvious significance for increasing our understanding on the roles exerted by collagen VI in different cells, such study would also have important implications for the diagnosis and therapy of human collagen VI-related diseases. Indeed, it is well know that fibroblasts and connective tissue actively cooperate with muscle and other tissues to maintain physiological properties and activities (Turrina *et al.*, 2013; Murphy *et al.*, 2011).

Therefore, during my PhD I performed several studies with fibroblasts derived from wild type and *Col6a1*$^{-/-}$ mice, aimed at throwing light on the intrinsic consequences on fibroblast survival and homeostasis elicited by collagen VI deficiency. My working hypothesis was that fibroblast damage due to collagen VI ablation may contribute and sustain the muscular defects that arise *in vivo*; and that collagen VI protein may exhibit distinctive autophagy instructive properties *per se* in fibroblasts. The study of fibroblasts *in vivo* is complicated, given the intricate interactions this cell type establishes in the different tissues. Therefore, I decided to set up an appropriate *in vitro* model for investigating various aspects of fibroblast biology in the presence or absence of collagen VI. First of all, I derived primary mouse embryonic fibroblast (MEF) cultures from wild type and *Col6a1*$^{-/-}$ mice, and immortalized them by transfection with a plasmid expressing the SV40 large T antigen. This allowed me to establish a stable *in vitro* fibroblast model to study collagen VI functions. Then, I demonstrated that these MEFs lines produced and secreted a proper ECM. Immunostaining and biochemical analyses showed that wild type MEFs secrete and deposit collagen VI. Moreover, collagen VI was tightly interconnected with fibronectin fibrils in the ECM and its secretion was increased by ascorbic acid treatment. As expected, *Col6a1*$^{-/-}$ MEFs were unable to assemble and secrete collagen VI but they were capable to produce fibronectin, collagen I and other ECM proteins, that also create a meshwork in the extracellular space. Once I established that this *in vitro* model is appropriate competent for ECM production, I investigated the cellular molecular and consequences caused by ablation of collagen VI in fibroblasts. In particular, I investigated whether lack of collagen VI has any impact on MEF survival processes, such as autophagy and apoptosis, as previously found in skeletal myofibers. Moreover, I performed studies aimed at dissecting the molecular pathway linked to *Col6a1*$^{-/-}$ defects in MEFs.

Considering the previous finding of autophagy deregulation in myofibers of *Col6a1*$^{-/-}$ mice (Grumati *et al.*, 2010), I investigated the involvement of collagen VI in the regulation of autophagy in MEFs. I first analyzed protein extracts from wild type and *Col6a1*$^{-/-}$ MEFs

to assess their ability to undergo autophagy in basal conditions and after serum deprivation. Under serum withdrawal, *Col6a1*$^{-/-}$ MEFs displayed less LC3 lipidation than the WT MEFs, as indicated by decreased LC3-II/LC3-I ratio. Based on this evidence, I investigated the autophagic flux by taking advance of chloroquine, an autophagy inhibitor drug that blocks autophagosome-lysosome fusion (Klionsky *et al.*, 2012). *Col6a1*$^{-/-}$ MEFs showed markedly increased accumulation of LC3 protein, both in the -I and -II forms, without any significant increase of the LC3-II/LC3-I ratio. In parallel, I monitored autophagosome formation using stable wild type and *Col6a1*$^{-/-}$ MEF lines expressing a GFP-LC3 reporter. Analysis of fluorescent puncta analyses revealed massive formation of LC3-positive autophagosomes in *Col6a1*$^{-/-}$ MEFs, without any significant increase following serum starvation stimuli, which was instead detectable in wild type MEFs. These findings revealed an accumulation of autophagosomes in *Col6a1*$^{-/-}$ fibroblasts, likely due to impaired autophagic flux rather than to increased autophagosome formation rate.

Analysis for p62, a selective autophagy substrate that also binds LC3 (Bjørkøy *et al.*, 2006), showed decreased p62 protein levels in *Col6a1*$^{-/-}$ MEFs, independently of serum starvation. Of note, p62 transcript levels were also decreased in *Col6a1*$^{-/-}$ MEFs both in basal condition and after serum starvation, thus explaining the decreased p62 protein levels in *Col6a1*$^{-/-}$ MEFs and preventing the monitoring of p62 as marker of protein consumption in these cells. In the experimental conditions applied here, analysis of p62 did not allow revealing any information about protein consumption due to the lack of p62 protein degradation after serum depletion in both wild type and *Col6a1*$^{-/-}$ MEFs. It was reported that p62 synthesis can change at the transcriptional level due to several factors, and p62 expression is upregulated during prolonged starvation (Mizushima and Yoshimori, 2007; Ichimura *et al.*, 2008; Jiang and Mizushima, 2014). Therefore, it will interesting to evaluate p62 turnover in wild type and *Col6a1*$^{-/-}$ MEFs after a shorter starvation time. Nonetheless, the present data suggest that p62 activity is altered in *Col6a1*$^{-/-}$ fibroblasts, due to the decreased expression at the translational level. Literature work indicate that a decline in p62 content and expression, which is related to a decrease of proteasome activity and of selective autophagic removal, may contribute to the

accumulation of insoluble polyubiquitinated protein aggregates and to the deregulation of the activity of the standard autophagic pathway as well as of other non-canonical pathways (Komatsu *et al.*, 2007; Wooten *et al.*, 2008; Kim *et al.*, 2014). Therefore, p62 deregulation in *Col6a1*$^{-/-}$ MEFs may contribute to a defective cellular state regarding autophagy. Moreover, decreased p62 mRNA translation may be linked to reduced phosphorylation of the extracellular signal-regulated kinases 1 and 2 (Erk1/2) (Kim *et al.*, 2014; Lee *et al.*, 2010), and/or to aberrant activation of TFEB translational program (Settembre *et al.*, 2011), as indeed displayed by *Col6a1*$^{-/-}$ MEFs.

To understand the signaling defects involved in the deregulated autophagy of *Col6a1*$^{-/-}$ MEFs, I analyzed the activation status of different protein kinases acting on autophagy. These studies allowed me to reveal that AMPK is hyperactivated in *Col6a1*$^{-/-}$ MEFs, and even more when cells are serum starved for 3 hr. As AMPK is a key metabolic energy sensor (Russell *et al.*, 2014), its markedly increased phosphorylation point at a strong energy impairment in *Col6a1*$^{-/-}$ MEFs, as we previously demonstrated in myofibers (Grumati *et al.*, 2010), which is worsened by autophagy induction stimuli. AMPK activation is also implicated in autophagy activation, via mTORC1 inhibition and Ulk1 phosphorylation at different serine residues (Egan *et al.*, 2010; Russell *et al.*, 2014). We therefore analyzed Ulk1 phosphorylation at Ser 555 and Ser 757, in order to assess its concurrent and opposite regulation by AMPK (acting positively) and mTORC1 (acting negatively) (Egan *et al.*, 2010; Kim *et al.*, 2011; Shang and Wang, 2011). Interestingly, and at difference from wild type MEFs, in *Col6a1*$^{-/-}$ MEFs we did not detected any decrease in Ulk1 phosphorylation at Ser 555 after serum starvation, which is fully consistent with the over-activation of AMPK. In *Col6a1*$^{-/-}$ MEFs, under serum starved conditions we also detected a slightly increased activity of Akt, a serine threonine kinase that plays central role in the regulation of a wide range of cell survival mechanisms. Increased Akt activation led us to speculate about a compensatory mechanism to assure cell survival of *Col6a1*$^{-/-}$ MEFs in the stressed condition (see also below discussion on apoptosis). Furthermore, Akt negatively regulates autophagy induction in mammalian cells, by acting on mTORC1

signaling (Manning and Cantley, 2007). In agreement with this, we found increased activation of mTORC1 in *Col6a1*$^{-/-}$ MEFs concurrently to autophagy induction stimuli, by means of enhanced phosphorylation of the downstream targets S6 and 4E-BP1. It is reasonable to speculate that mTORC1 is influenced by the abnormal Akt activation in *Col6a1*$^{-/-}$ MEFs. Indeed, mTORC1 activity further determined an increase in the inhibitory Ser 757 phosphorylation of Ulk1, which it is known to antagonize the interaction between Ulk1 and AMPK (Kim *et al.*, 2011; Shang and Wang, 2011). Although AMPK over-activation was expected to lead to premature autophagy induction in *Col6a1*$^{-/-}$ MEFs, both the initiation and maturation steps of autophagy were blocked by the concurrent activity of mTORC1, leading to autophagosome accumulation.

The inability to degrade autophagic vacuoles (a so called "off-rate" block) can be due to impaired capability for lysosomal degradation (Huynh *et al.*, 2007; Shen and Mizushima, 2014). Thus, I decided to investigate also the late stage of the autophagic process, evaluating lysosome contribution to the degradation of autophagosomes. Interestingly, *Col6a1*$^{-/-}$ MEFs exhibited enlarged lysosomes when compared to wild type MEFs. This condition is similar to the pattern displayed by wild type MEFs following treatment with the lysosome inhibitor chloroquine, a drug known to lead to lysosome dilation (Yoon *et al.*, 2010; Chen *et al.*, 2011). The massive presence of enlarged lysosomes in *Col6a1*$^{-/-}$ MEFs was independent from serum starvation, and furthermore correlated with impaired autolysosome formation and LAMP-2 protein depletion in basal condition. On the other side, LAMP-2 protein content was maintained after serum starvation, and LAMP-2 mRNA levels were unchanged in *Col6a1*$^{-/-}$ MEF. Thus, LAMP-2 was altered in *Col6a1*$^{-/-}$ MEFs only in basal condition, but this basal depletion was sufficient to block the proper fusion of autophagosomes with lysosomes, as confirmed by co-immunostaining for autophagosome and lysosome markers. Interestingly, literature studies showed that LAMP-2 depletion inhibits the autophagosome-lysosome fusion, thus causing a “traffic jam” that culminates in the accumulation of autophagosomes (Huynh *et al.*, 2007; Tanaka *et al.*, 2000). LAMP-1 and LAMP-2 are indeed required for proper autolysosome formation and hence for the removal of autophagosomes (González-Polo *et al.*, 2005; Huynh *et al.*,

2007; Fortunato *et al.*, 2009; Shen and Mizushima, 2014). As González-Polo and colleagues showed, LAMP-2 depletion in HeLa cells and MEFs correlates with starvation-induced cell death, with features of accumulation of autophagosomes and of apoptotic signaling activation (González-Polo *et al.*, 2005). On the other side, it is also known that during autophagy lysosomal function is regulated by the fusion of autophagosomes with lysosomes and relies upon mTORC1 suppression (Zhou *et al.*, 2013). Thus, the alteration of lysosome morphology and structure in *Col6a1*$^{-/-}$ MEFs is also linked with the sustained mTORC1 activity and the decreased autolysosome formation. Taken together, these results point at a failure to maintaining a proper off-rate of autophagy in *Col6a1*$^{-/-}$ MEFs, sustained both by lysosomal and mTORC1 contribution.

Given the striking lysosome defects in *Col6a1*$^{-/-}$ MEFs , I decided to examine the involvement of TFEB, a transcription factor that has been shown to have a master regulatory role in lysosome biogenesis and autophagy activity (Sardiello *et al.*, 2009; Settembre *et al.*, 2011). Towards this aim, I transfected wild type and *Col6a1*$^{-/-}$ MEFs with a GFP-TFEB expressing plasmid in order to analyze TFEB localization under basal conditions and after serum starvation. At difference from wild type MEFs, where GFP-TFEB relocalized from cytoplasm to nucleus after serum withdrawal as expected (Settembre *et al.*, 2012), *Col6a1*$^{-/-}$ MEFs exhibited a peculiar GFP-TFEB localization pattern in response to serum starvation. First of all, GFP-TFEB was largely localized in the nucleus already in basal conditions. Moreover, GFP-TFEB was not able to respond to starvation with the proper activation, and relocated to the cytoplasm when serum was depleted. Thus, we can argue that the translational program activated by TFEB was altered due to collagen VI ablation. Transcription of LC3 and p62 genes, two major targets of TFEB, was indeed abnormally regulated in *Col6a1*$^{-/-}$ MEFs after serum depletion, and LC3 in particular did not respond to serum withdrawal. We are currently investigating the transcriptional activity of other Atg genes known to be regulated by TFEB, as well as of endogenous TFEB. Interestingly, knockdown of Erk1/2 is known to induce nuclear translocation of TFEB to a similar extent as serum starvation (Settembre *et al.*, 2011). Erk

plays an important role in the maturation step of autophagy and in lysosome stabilization (Corcelle *et al.*, 2007; Duan *et al.*, 2014), and its inhibition can result in autophagic impairments, and eventually in cell death (Duan *et al.*, 2014). Of note, I found that Erk1/2 activation is compromised in *Col6a1*$^{-/-}$ fibroblasts. Thus it is reasonable to argue that Erk1/2 deregulation in *Col6a1*$^{-/-}$ fibroblasts may account for a premature nuclear translocation of the transcription factor TFEB and for lysosomal destabilization. The presence of a lysosomal stress in *Col6a1*$^{-/-}$ MEFs also contributes in this direction, despite the slight residual activity of mTOR should act in reverse towards TFEB translocation under serum starved conditions.

To further evaluate the role of collagen VI in autophagy regulation, I carried out biochemical analysis of LC3 lipidation in wild type and *Col6a1*$^{-/-}$ MEFs grown onto different ECM proteins, provided as adhesion substrates. In this context, my major aim was to evaluate the ability of collagen VI to regulate autophagy as adhesion substrate. Coating onto native collagen VI of wild type and *Col6a1*$^{-/-}$ MEFs showed a different pattern of LC3 lipidation: (*i*) in wild type MEFs, the LC3-II/LC3-I ratio was maintained, but LC3 was degraded to a bigger extent after serum depletion, suggesting an effect on autophagy induction; (*ii*) in *Col6a1*$^{-/-}$ MEFs, the LC3-II/LC3-I ratio was apparently unaffected, with only a small increase after serum depletion, but notably the total amount of LC3 protein was reduced. Thus, coating onto collagen VI reactivates LC3 degradation in *Col6a1*$^{-/-}$ MEFs. Adhesion onto collagen VI appeared to elicit also an effects on the autophagy initiation step, both in wild type and *Col6a1*$^{-/-}$ MEFs, showing a trend in restoring Ulk1 phosphorylation levels at the inhibitory site Ser 757. These findings highlight the ability of collagen VI to modulate autophagy, when in contact with fibrbolasts adhering on it. An increasing number of emerging *in vitro* studies demonstrate that ECM components are able to modulate autophagy in different manners (Tuloup-Minguez *et al.*, 2011; Neill *et al.*, 2014). Here, we show that collagen VI is an ECM protein exhibiting instructive properties towards autophagy regulation. We are currently investigating the role of collagen VI coating in the regulation of mTORC1 activity. In *Col6a1*$^{-/-}$ MEFs, in particular, I am evaluating whether collagen VI coating is able to rescue

mTOR residual inhibitory activity under autophagy induction. In addition, I am investigating whether collagen VI coating is capable to rescue the lysosomal defects of *Col6a1*$^{-/-}$ MEFs.

All the results concerning the autophagy deregulation displayed by *Col6a1*$^{-/-}$ MEFs converge to the concept of an altered basal condition due to the lack of extracellular collagen VI. Of note, the proper baseline regulation of autophagy is essential for cellular homeostasis, differentiation, development and survival (Mizushima and Komatsu, 2011). When nutrients or growth factors are scarce, collagen VI null fibroblasts, with altered basal rate of autophagy, are unable to readily respond to energy demands with the canonical catabolic and survival pathways. I speculate that in resting condition mTORC1 and TFEB deregulation affects lysosomal integrity and autophagy maturation steps (Shen and Mizushima, 2014). On the other side, it can be also inferred that AMPK over-activation, due to energy demand in *Col6a1*$^{-/-}$ MEFs, push the cell towards autophagy. Under stress conditions, indeed, the degradation of intracellular material through autophagy becomes an alternative source of energy (Kroemer *et al.*, 2010). Thus, *Col6a1*$^{-/-}$ fibroblasts try to ensure protein turnover and survival by generating a lot of autophagosomes that finally accumulate, exacerbating cell status. In parallel, *Col6a1*$^{-/-}$ MEFs exhibit reduced Erk1/2 activation, that relates with altered TFEB localization and activity (Settembre *et al.*, 2011). This leads to aberrant regulation of LC3 and p62 gene transcription during starvation, further impinging on cellular capacity for autophagy (Kim *et al.*, 2014; Settembre *et al.*, 2011).

Two other remarkable features I found affected in *Col6a1*$^{-/-}$ fibroblasts model are apoptosis and mitochondrial network. In past studies, we demonstrated that the presence of mitochondrial dysfunctions and spontaneous apoptosis in skeletal muscles of *Col6a1*$^{-/-}$ mice and UCMD/BM patients (Irwin *et al.*, 2003; Angelin *et al.*, 2007; Sabatelli *et al.*, 2012). I analyzed apoptosis in MEFs, using different experimental approaches as TUNEL and flow cytometric assays. I found that apoptosis occurrence was more than doubled in *Col6a1*$^{-/-}$ MEFs, with respect to wild type fibroblasts in the same culturing condition. In agreement

with the altered autophagic response to starvation, the rate of cell death in *Col6a1*$^{-/-}$ MEFs was further increased by serum depletion. In fact, a hallmark of cells defective for autophagy is an increased susceptibility to apoptotic stimuli, which normally would activate autophagy to promote cell survival (Levine and Kroemer, 2008; Fimia and Piacentini, 2010). Annexin V and propidium iodide stainings demonstrated that not only apoptosis is increased in *Col6a1*$^{-/-}$ MEFs, but that also final stages of late apoptosis and necrosis-like events are increased, indicating that collagen VI null fibroblasts are more sensitive to stress-induced cell death. Importantly, collagen VI was able to rescue the apoptotic phenotype and promote cell survival in *Col6a1*$^{-/-}$ MEFs, both basally and after serum starvation. On the contrary, coating with collagen I, used as a control, did not rescue apoptosis in *Col6a1*$^{-/-}$ MEFs, implying a specific effect elicited by collagen VI.

Considering the massive accumulation of autophagosomes in *Col6a1*$^{-/-}$ MEFs, the finding of a concomitant necrosis-like cell death prompted me to investigate whether some kind of autophagy-dependent cell death was occurring. In fact, it has beeen widely recognized that autophagic (or type II) cell death is associated with appearance of autophagosomes and membrane permeability to vital dyes (Wirawan *et al.*, 2012; Shen and Codogno, 2011; Yu *et al.*, 2004). If the altered autophagy regulation in *Col6a1*$^{-/-}$ MEFs contributed to cell death, one would expect that inhibition of autophagy leads to increased cell survival (Yu *et al.*, 2004). On the contrary, we found that only a minor fraction of necrosis-like cell death appeared to decrease in *Col6a1*$^{-/-}$ MEFs when autophagy was inhibited by chloroquine or 3-MA treatments, whereas the major percentage of fibroblasts were dying via apoptosis in a 3-MA dose-dependent manner. These results allow to argue that autophagic contribution to cell death in collagen VI null fibroblasts was irrelevant. Instead, the markedly increased incidence of apoptosis in *Col6a1*$^{-/-}$ MEFs was linked to increased activation of caspase 9 and caspase 3. Indeed, we found that these caspases were prematurely cleaved in *Col6a1*$^{-/-}$ MEFs in basal condition, and also to a major extent when serum was depleted. As expected, in wild type MEFs, caspase activation was only detected under apoptosis inducing stimuli, such as serum starvation or staurosporine treatment (González-Polo *et al.*, 2005; Zanotti *et al.*, 2011). Cleavage of caspase 9 implied

the activation of the intrinsic apoptotic pathway, linking the cell death found in *Col6a1*$^{-/-}$ MEFs to intracellular stress signals, such as mitochondrial damage (Shalini *et al.*, 2014). Up to date, we did not estimate the activation of the extrinsic pathway, by means of caspase 8 activation assays, but it will be interesting to understand whether both pathways contribute to the autophagic defects of *Col6a1*$^{-/-}$ MEFs. In any case, caspase activation further excludes the possible involvement of autophagic cell death in this context (Galluzzi *et al.*, 2015). Furthermore, adhesion onto collagen VI also exhibited a clear pro-survival effect in wild type fibroblasts. In fact, collagen VI coating ameliorated cell survival in wild type MEFs subjected to serum withdrawal, and this effect was not phenocopied by collagen I. This suggests a specific role of extracellular collagen VI on promoting cell survival and counteracting apopotosis. We postulate that native collagen VI exhibits distinct functions as cytoprotective factor for MEFs, in agreement with previously observations in avian corneal fibroblasts (Howell and Doane, 1998) and in fibroblasts protein extracts (Rühl *et al.*, 1999).

Mitochondria play an important role in cell homeostasis, given their key role in metabolism and adaptation to nutrient/growth factor stress (Scorrano, 2005; Liesa and Shirihai, 2013). Moreover, fusion and fission dynamics of mitochondrial network directly influence not only mitochondrial metabolism, but also cell death, autophagy, and a large number of signaling pathways (Kasahara and Scorrano, 2014). Thinking at mitochondrial dysfunction as a causative effect for apoptosis induction in *Col6a1*$^{-/-}$ MEFs, we analyzed mitochondrial network morphology, using different probes and markers. Interestingly, we found that *Col6a1*$^{-/-}$ MEFs displayed a fragmented mitochondrial network when compared to wild type cells, which exhibited tubular elongated mitochondria in the 70% of the cases. Defective mitochondrial elongation is often associated to mitochondrial dysfunctions, which dissipate cellular ATP and prime cell toward apoptosis (Scorrano, 2005; Gomes and Scorrano, 2011). Indeed, unbalanced rate of mitochondrial fusion and fission can have important effects on cell bioenergetics, because of the accumulation of irreversibly damaged mitochondria (Twig *et al.*, 2008; Liesa and Shirihai, 2013). These

dynamics, in concert with autophagy, are crucial for mitochondrial quality control mechanisms and cell survival (Liesa and Shirihai, 2013; Kasahara and Scorrano, 2014). Serum starvation induced a markedly increased rate of mitochondrial fragmentation in *Col6a1*$^{-/-}$ MEFs. In literature starvation is reported to cause elongation of mitochondria, by inhibiting Drp1 recruitment and mitochondria fission. Starvation-induced elongation is functional to prevent mitochondria removal by autophagy and to allow cell survival in starving cells (Gomes and Scorrano, 2011; Liesa and Shirihai, 2013). During starvation, mitochondria unable to elongate are latently dysfunctional and waste cellular ATP to sustain their membrane potential (Gomes and Scorrano, 2011). Therefore, sustained fission of mitochondria in *Col6a1*$^{-/-}$ MEFs was presumably linked to loss of mitochondria functionality and/or to aberrant mitochondria autophagic removal (mitophagy) during limited nutrient availability. Different signals are required to initiate the removal of damaged mitochondria. Loss of mitochondrial membrane potential and prior mitochondrial fragmentation represent major signals for mitophagy (Twig *et al.*, 2008; Gomes and Scorrano, 2008), as well as translocation of the PARK2-associated ubiquitin ligase, Parkin, from the cytosol to the mitochondrion (Narendra *et al.*, 2008; Youle and Narendra, 2011). To evaluated mitophagy involvement and functionality in *Col6a1*$^{-/-}$ MEFs, I studied Parkin translocation, by transfecting cells with YFP-Parkin (Narendra *et al.*, 2008). I found that in basal conditions YFP-Parkin was recruited more frequently to mitochondria in *Col6a1*$^{-/-}$ MEFs, suggesting a latent dysfunction of mitochondria, which activated massive Parkin recruitment and selective mitophagy. Mitochondrial removal, evaluated after both serum starvation and use of the mitochondrial uncoupler CCCP, is still under investigation. Up to date, the preliminary data obtained led us to speculate that, although Parkin recruitment should prime mitophagy in *Col6a1*$^{-/-}$ MEFs, the cell machinery was not able to activate a proper clearance of altered mitochondria, thus losing the capacity to restore mitochondria metabolism upon damage and to limit apoptosis activation. Further studies are required to strengthen this hypothesis. In addition, it will be important to determine mitochondria functionality in *Col6a1*$^{-/-}$ MEFs.

In conclusion, the data I collected in this PhD thesis work highlight a role for the ECM protein collagen VI as a factor able to modulate cell survival pathways in multiple ways. Indeed addition of collagen VI, used as a substrate for fibroblast adhesion, modulates autophagy and improves cell survival in serum withdrawal condition. Furthermore, genetic ablation of collagen VI in our fibroblast model impinges both on the initiation and the completion of the autophagy flux, leads to remodeling of mitochondrial shape, and causes apoptosis. Previous results I obtained in the first year of my PhD demonstrated that similar alterations in apoptosis and autophagy are present also in primary fibroblasts derived from diaphragms of *Col6a1*$^{-/-}$ mice (data not shown). The complex interplay between apoptosis and autophagy is critical to the overall fate of the cell (Mariño *et al.*, 2014; Booth *et al.*, 2014). Therefore, the remarkable alterations of both autophagy and apoptosis in *Col6a1*$^{-/-}$ fibroblasts indicate that this cell type likely plays a major role in the pathophysiological defects of collagen VI diseases and in the onset and progression of the muscle pathology of *Col6a1*$^{-/-}$ mice and of UCMD/BM patients, as previously postulated but never demonstrated (Zou *et al.*, 2008; Allamand *et al.*, 2011; Sabatelli *et al.*, 2012). Interstitial fibroblasts that are present in muscle tissue both during and after myogenesis not only play pivotal roles in muscle development but also protect myoblasts from apoptosis (Zhang *et al.*, 2010). Thus, a genetically inherited muscle defect, as in the case of collagen VI mutations, may lead to complex and additional pathological effects through the integration of fibroblast and myoblast related defects.

Although the involvement of collagen VI in apoptosis and autophagy is well documented, the molecular mechanisms involved in the intracellular transduction of the extracellular signals elicited by collagen VI are still unknown. In particular, it remains to be established whether and which transmembrane receptor is involved, or whether collagen VI mostly acts by regulating the biomechanical properties and fine-tuning the ECM three-dimensional organization. Recent independent work from our laboratory suggests that this ECM molecule has both biomechanical (stiffness) and biochemical (signaling) roles in the different tissues (Urciuolo *et al.*, 2013; Alexopoulos *et al.*, 2009).

Although future work is needed to understand in detail the intricate aspects of collagen VI biology and functions in skeletal muscles and in other tissues, the results of the present study provide further insight into the dynamic nature of the ECM and in particular of one of its major constituents. Collagen VI produced by fibroblasts in the muscle-associated connective tissues may serve as an ECM factor that allows for rapid reconstitution of skeletal muscle after different stress, and its deficiency is likely crucial for the appearance of the muscle pathology in mice and in patients.

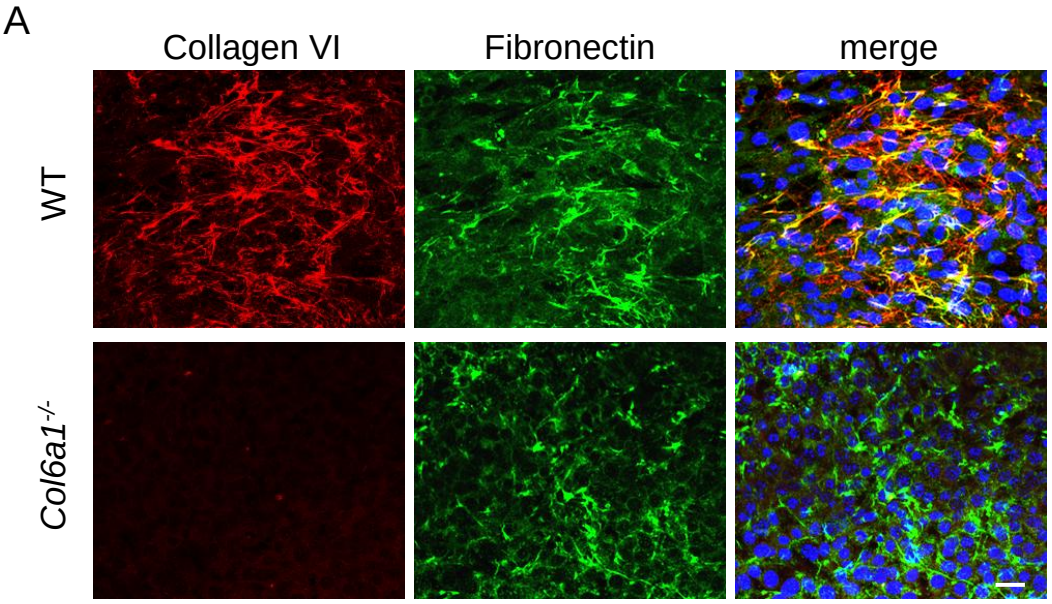
A
Collagen VI
Fibronectin
merge
WT
Col6a1-/-

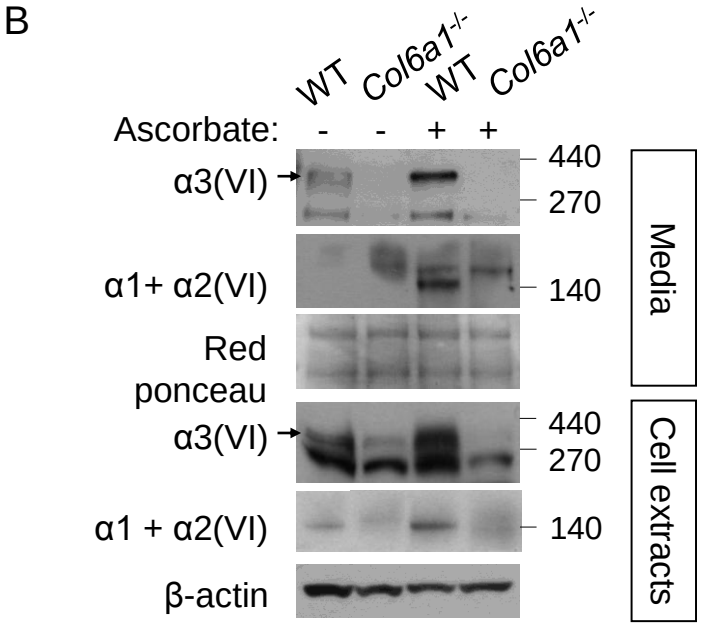
B
WT
Col6a1-/-
WT
Col6a1-/-
Ascorbate: - - + +
α3(VI)
440
270
α1+ α2(VI)
140
Media
Red ponceau
α3(VI)
440
270
α1 + α2(VI)
140
β-actin
Cell extracts

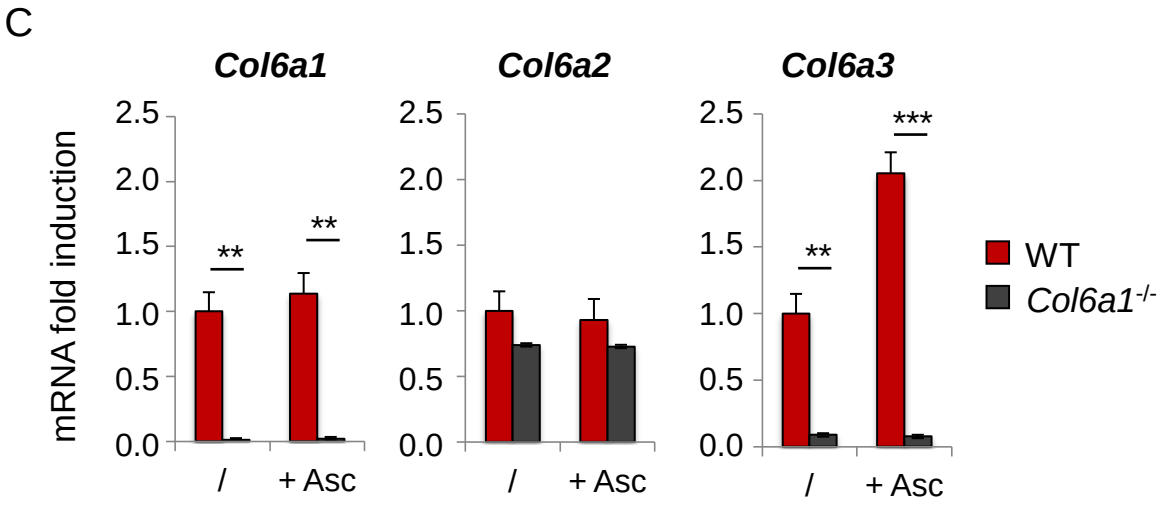
C
Col6a1
Col6a2
Col6a3
mRNA fold induction
2.5
2.0
1.5
1.0
0.5
0.0
**
**
**
***
/
+ Asc
WT
Col6a1-/-

Figure 1. Characterization of extracellular matrix (ECM) protein production by wild type and collagen VI null (*Col6a1*$^{-/-}$) MEF lines. (**A**) Immunofluorescence of collagen VI (red) and fibronectin (green) deposition in the ECM of WT and *Col6a1*$^{-/-}$ MEF lines. Nuclei were stained in blue with Hoechst 33258. Scale bar, 25 μm. (**B**) Western blot analysis of collagen VI α1 and α3 chain (α1(VI), α3(VI)) production in culture media and cell extracts from WT and *Col6a1*$^{-/-}$ MEFs. Where indicated 0.25 mM ascorbic acid was used to induce collagen secretion. (**C**) qRT-PCR analyses of *Col6a1*, *Col6a2* and *Col6a3* mRNA in WT and *Col6a1*$^{-/-}$ MEF lines. WT, wild type. **, $P < 0.01$; ***, $P < 0.001$.

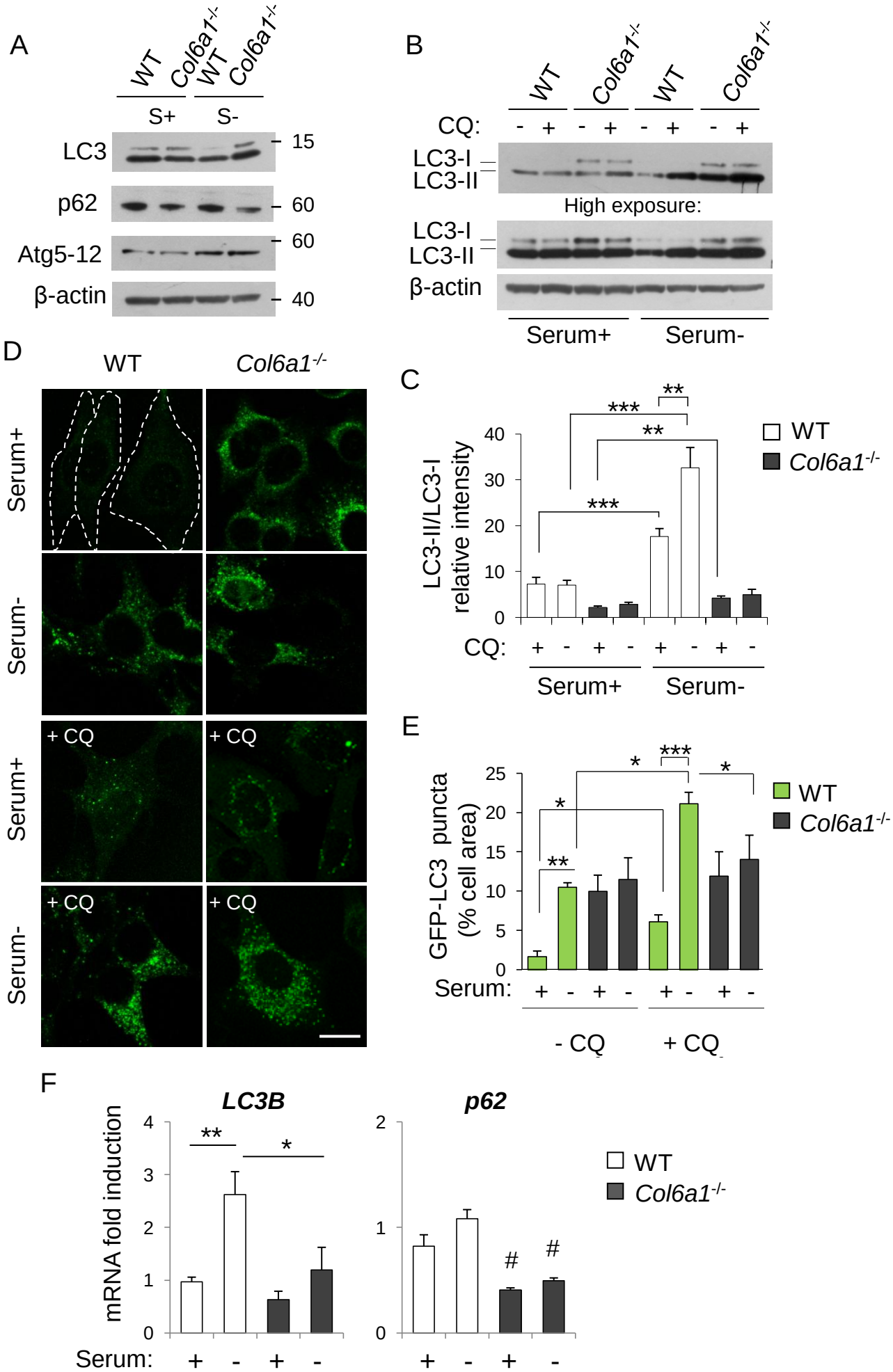
A
WT
Col6a1-/-
WT
Col6a1-/-
S+
S-
LC3
p62
Atg5-12
β-actin
15
60
60
40
B
WT
Col6a1-/-
WT
Col6a1-/-
CQ: - + - + - + - +
LC3-I
LC3-II
High exposure:
LC3-I
LC3-II
β-actin
Serum+
Serum-
C
LC3-II/LC3-I relative intensity
WT
Col6a1-/-
CQ: + - + - + - + -
Serum+
Serum-
D
WT
Col6a1-/-
Serum+
Serum-
+ CQ
E
GFP-LC3 puncta (% cell area)
WT
Col6a1-/-
Serum: + - + - + - + -
- CQ
+ CQ
F
LC3B
p62
mRNA fold induction
WT
Col6a1-/-
Serum: + - + - + - + -

Figure 2. Autophagy off-rate flux is blocked in *Col6a1*$^{-/-}$ MEFs. (**A, B**) Western blot analysis of total cell extracts from WT and *Col6a1*$^{-/-}$ MEFs in basal medium (Serum+, S+) and after serum withdrawal (Serum-, S-) for 3 hr. (**A**) LC3, p62 and Atg5-12 protein levels after serum starvation. (**B**) Monitoring of the autophagy flux through Western blot analysis of LC3 lipidation after 50 μM chloroquine (CQ) treatment. (**C**) Quantification of the relative intensity of LC3-II/LC3-I ratio showed in D (mean data of at least three independent biological samples). (**D, E**) Detection of LC3-II puncta in WT and *Col6a1*$^{-/-}$ MEFs from GFP-LC3 reporter mice. LC3 puncta (autophagosomes) accumulate in *Col6a1*$^{-/-}$ MEFs both in Serum+ and in Serum- condition. Scale bar, 25 μm. Corresponding quantification of GFP-LC3 puncta per cell area is shown in E. (**F**) qRT-PCR analysis of *LC3B* and *p62* mRNA expression. *, $P < 0.05$, **, $P < 0.01$, ***, $P < 0.001$; #, $P < 0.01$, *Col6a1*$^{-/-}$ versus WT MEFs . WT, wild type.

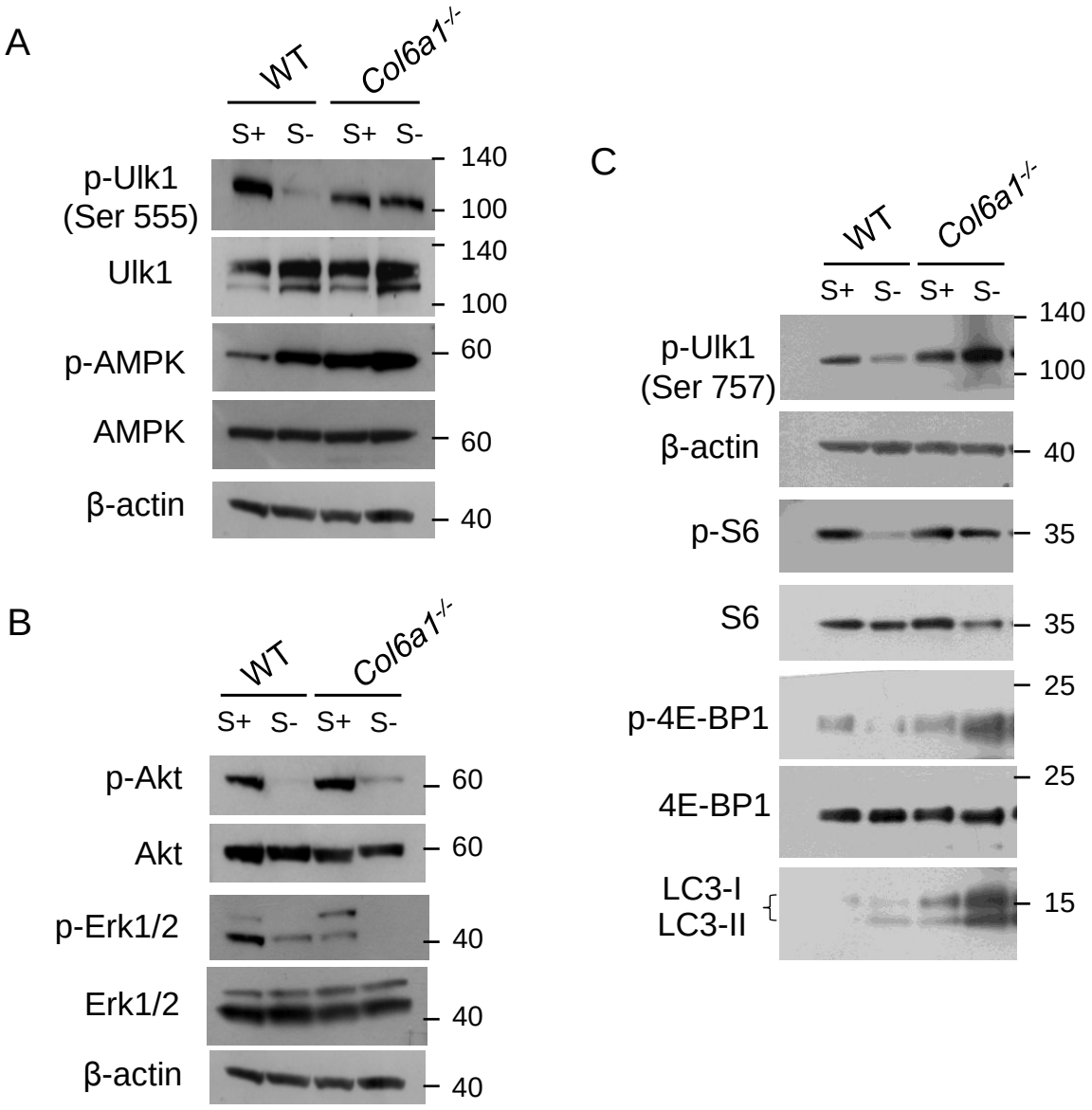

Figure 3. AMP-activated protein kinase (AMPK) is hyperactivated in *Col6a1*$^{-/-}$ MEFs, but persistent mTOR signaling is present. (**A-C**) Western blot analyses of total cell extracts from WT and *Col6a1*$^{-/-}$ MEFs in basal medium (S+) and after serum withdrawal (S-) for 3 hr. WT, wild type. (**A**) AMPK activation and its phosphorylation activity on Ulk1 at Ser 555. (**B**) Akt and Erk1/2 activation by phosphorylation. (**C**) mTOR downstream target analyses (4E-BP1 and S6) and its phosphorylation activity on Ulk1 at Ser 757. WT, wild type.

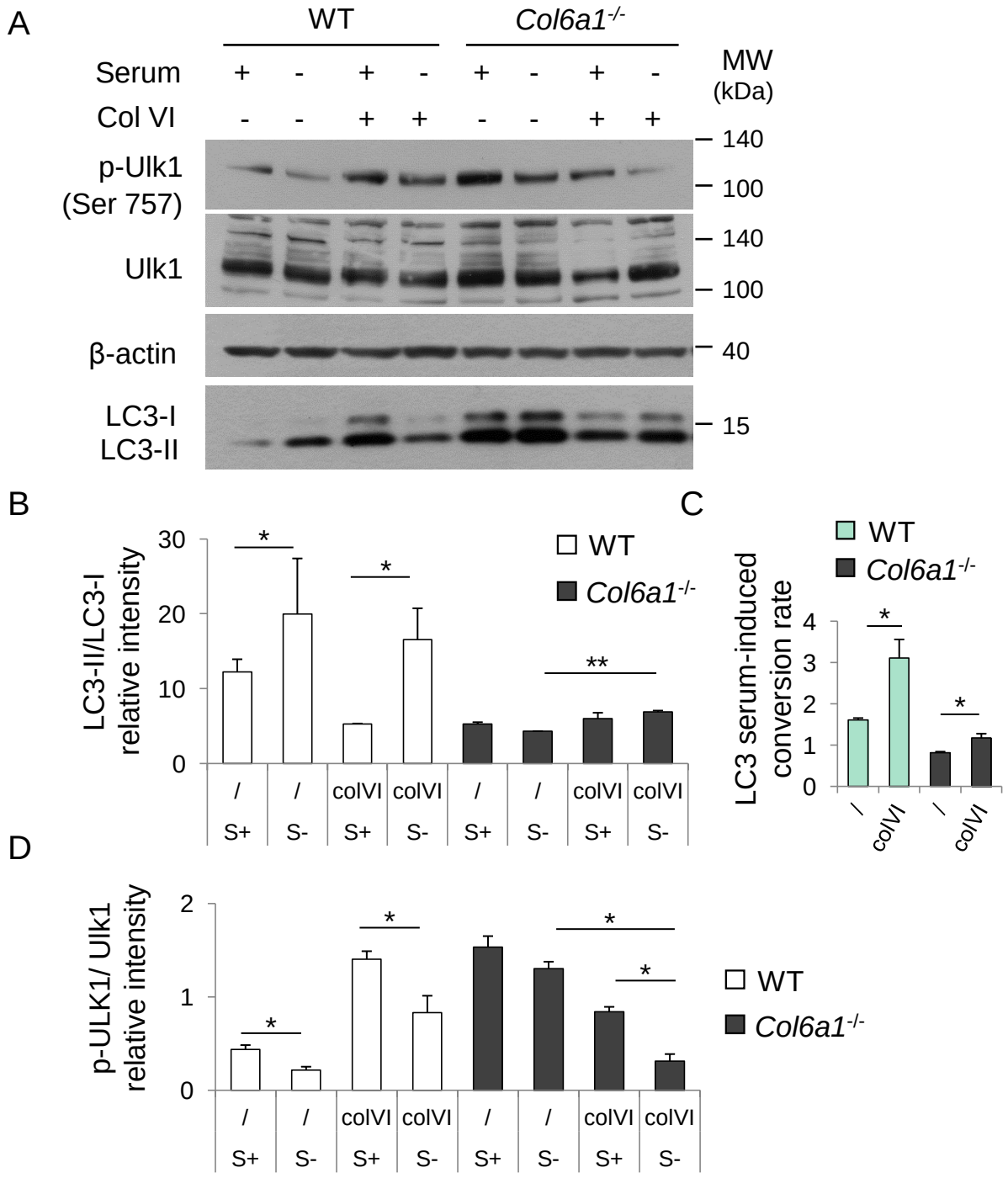

Figure 4. Autophagy modulation by collagen VI as adhesion substrate. (**A**) Western blot analyses of total cell extracts from WT and *Col6a1*$^{-/-}$ MEFs in basal medium (S+) and after serum withdrawal (S-) for 3 hr. When indicated, cells were grown onto collagen VI (Col VI) as adhesion substrate. (**B-D**) Densitometric quantifications of relative intensity of two independent blotting experiments as in A. Quantification of LC3-II/LC3-I ratio (**B**) and of p-Ulk1 (Ser 757) on Ulk1 total protein (**D**) are showed. (**C**) Serum-induced conversion rate of LC3. WT, wild type. *, $P < 0.05$, **, $P < 0.01$.

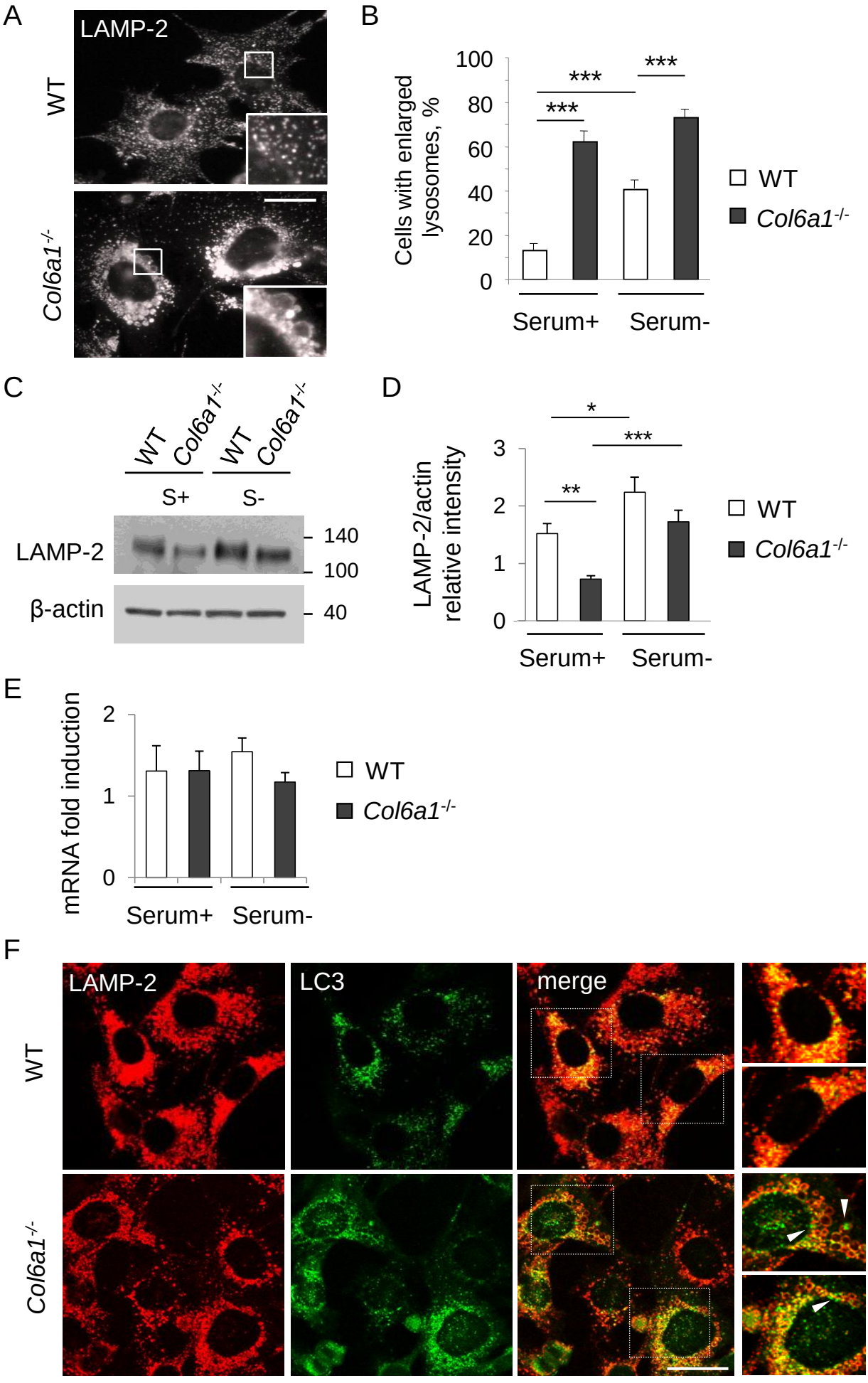
A
LAMP-2
WT
Col6a1-/-
B
Cells with enlarged lysosomes, %
100
80
60
40
20
0
***
***
***
Serum+
Serum-
WT
Col6a1-/-
C
WT
Col6a1-/-
WT
Col6a1-/-
S+
S-
LAMP-2
β-actin
140
100
40
D
LAMP-2/actin relative intensity
3
2
1
0
*
***
**
Serum+
Serum-
WT
Col6a1-/-
E
mRNA fold induction
2
1
0
Serum+
Serum-
WT
Col6a1-/-
F
LAMP-2
LC3
merge
WT
Col6a1-/-

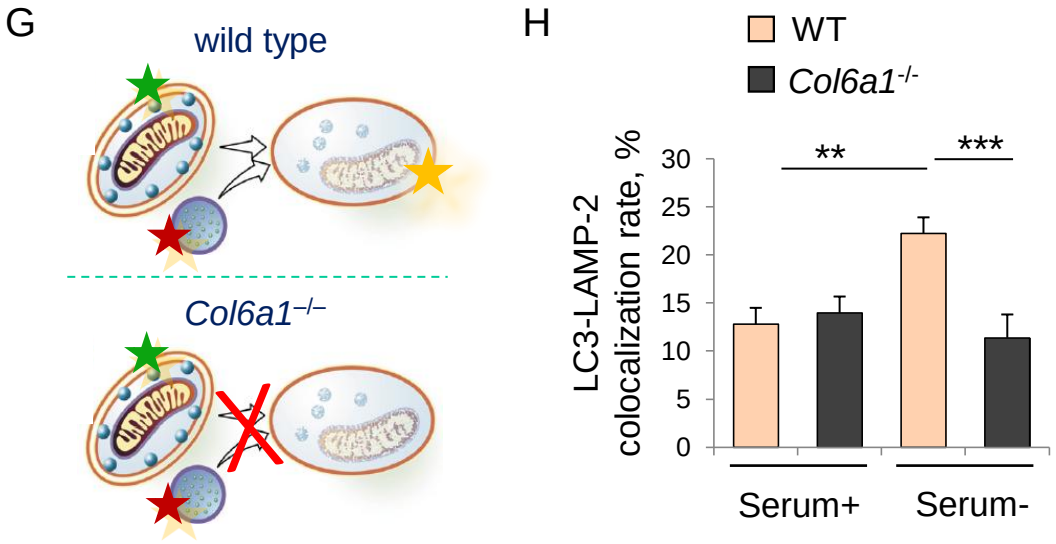

Figure 5. ***Col6a1*$^{-/-}$ MEFs showed enlarged lysosomes and decreased autolysosome formation.** (**A**) Immunofluorescence of LAMP-2 lysosome marker showing normal lysosomes in WT cells and enlarged lysosomes in *Col6a1*$^{-/-}$ MEFs. The inserts show a magnification of boxed area. (**B**) Quantification of cells containing at least two enlarged lysosomes. Data represent mean percentages ± s.e.m. of cells with enlarged lysosomes of thirty images per condition. (**C**) Western blot analysis of LAMP-2 in WT and *Col6a1*$^{-/-}$ MEFs, in basal medium (S+) and after serum withdrawal (S-) for 3 hr. (**D**) Quantification of the relative intensity of LAMP-2/actin of three independent immunoblottings, as in C. (**E**) qRT-PCR analysis of *LAMP-2* mRNA expression. (**F**) Coimmunostaining of LAMP-2 and LC3 on MEFs, after 3h of serum withdrawal. The right panels show the boxed areas of relative merged image. *Col6a1*$^{-/-}$ cells showed impaired autophagosome (green puncta) fusion to lysosomes (red) (arrowheads). Scale bars, 25 µm. (**G**) Schematic representation of the failure of autophagosome-lysosome fusion in *Col6a1*$^{-/-}$ MEFs (green star: autophagosome labeled by LC3; red star: lysosome labeled by LAMP2; orange star: autolysosome with merged LAMP2 and LC3 labeling). (**H**) Colocalization rate of LC3 and LAMP-2 staining. Mean percentages ± s.e.m. were calculated for at least fifteen images per condition. Serum+, basal medium; Serum-, 3 hr of serum withdrawal. Scale bar, 25 µm. WT, wild type. *, $P < 0.05$; **, $P < 0.01$, ***, $P < 0.001$.

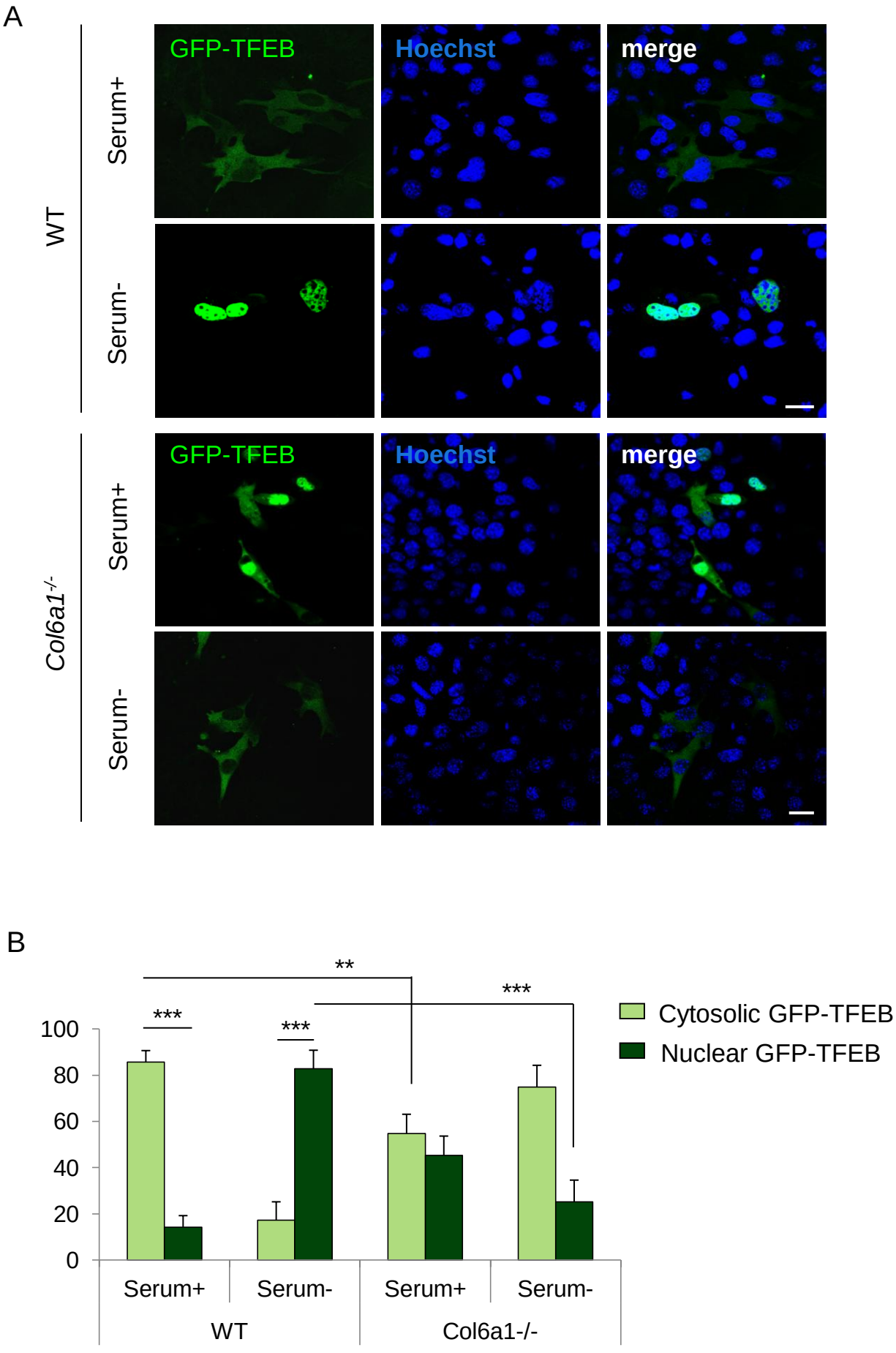
A
WT
Serum+
Serum-
GFP-TFEB
Hoechst
merge
Col6a1-/-
Serum+
Serum-
GFP-TFEB
Hoechst
merge
B
**
***
***
***
100
80
60
40
20
0
Cytosolic GFP-TFEB
Nuclear GFP-TFEB
Serum+
Serum-
Serum+
Serum-
WT
Col6a1-/-

Figure 6. GFP-TFEB nuclear translocation analysis in wild type and *Col6a1*$^{-/-}$ MEFs. (**A**) Representative micrographs of GFP-TFEB expressing MEFs in basal medium (Serum+) and after serum withdrawal (Serum-) for 3 hr, following plasmid transfection (GFP-TFEB). Nuclei were stained in blue with Hoechst. (**B**) Quantification of WT and *Col6a1*$^{-/-}$ cells showing cytosolic or nuclear-translocated GFP-TFEB, as showed in A. Mean data are representative of at least three independent biological samples. WT, wild type *, $P<0.05$; **, $P<0.001$; ***, $P<0.0001$.

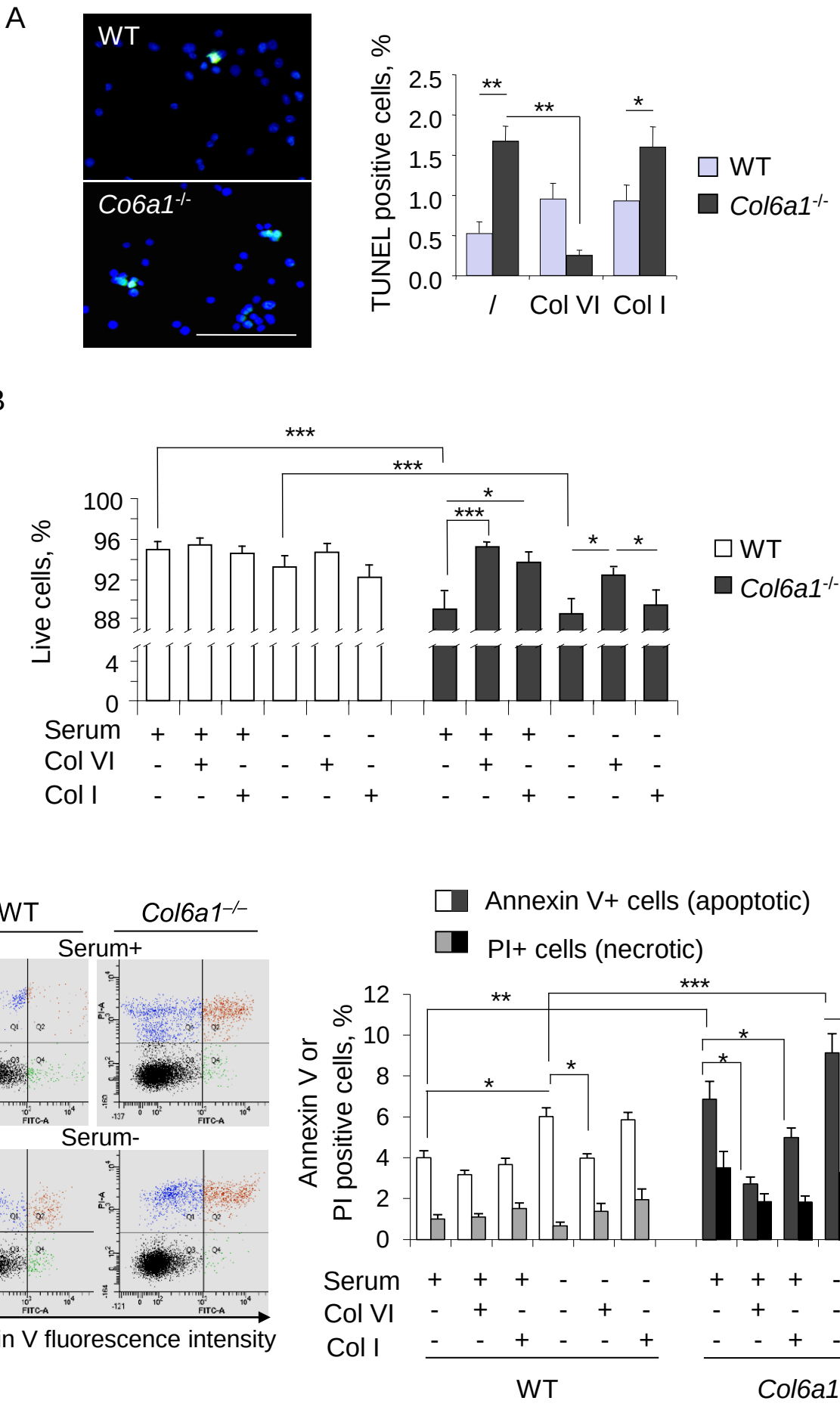
A
WT
Co6a1-/-
TUNEL positive cells, %
2.5
2.0
1.5
1.0
0.5
0.0
**
**
*
/
Col VI
Col I
WT
Col6a1-/-
B
***
***
*
***
*
*
Live cells, %
100
96
92
88
4
0
WT
Col6a1-/-
Serum + + + - - - + + + - - -
Col VI - + - - + - - + - - + -
Col I - - + - - + - - + - - +
C
WT
Col6a1−/−
Serum+
Serum-
PI fluorescence intensity
Annexin V fluorescence intensity
Annexin V+ cells (apoptotic)
PI+ cells (necrotic)
Annexin V or PI positive cells, %
12
10
8
6
4
2
0
**
***
*
*
*
*
*
Serum + + + - - - + + + - - -
Col VI - + - - + - - + - - + -
Col I - - + - - + - - + - - +
WT
Col6a1-/-

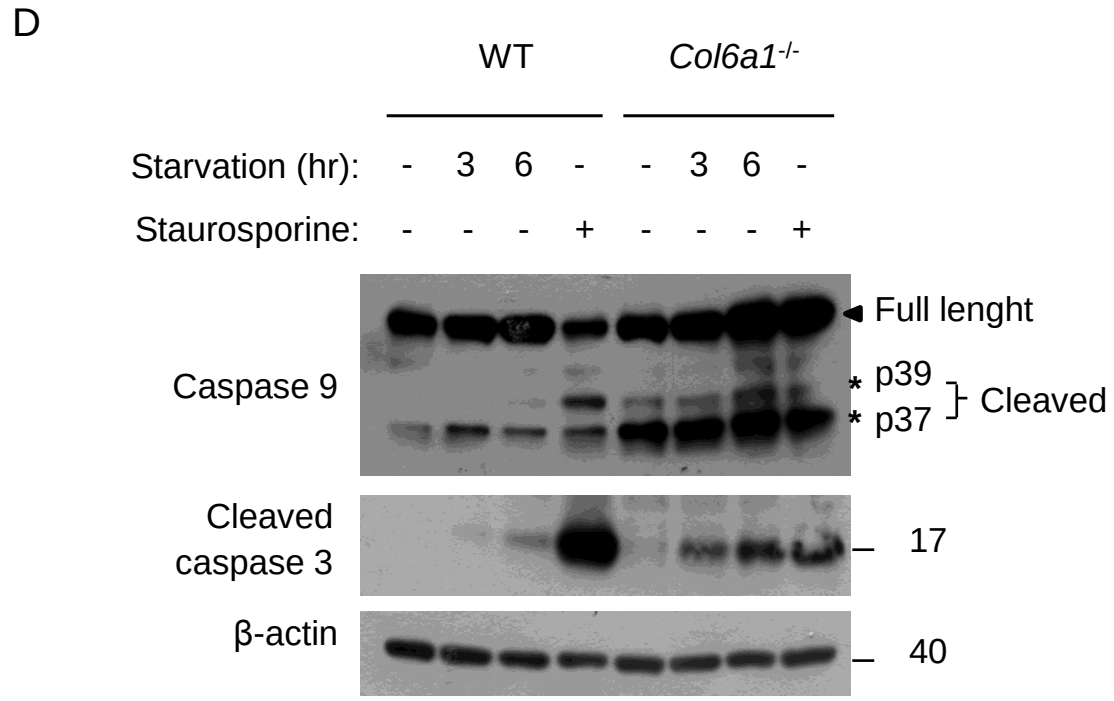

Figure 7. Apoptosis is increased in *Col6a1*$^{-/-}$ MEFs and collagen VI addition rescued the phenotype. (**A**) TUNEL assay. Left panel: representative micrographs; nuclei were stained in blue with Hoechst, TUNEL positive nuclei were in green. Right panel: quantification (n = 3) of TUNEL positive nuclei in WT and *Col6a1*$^{-/-}$ MEFs cultured on plastic wells (/), collagen VI (Col VI) or collagen I (Col I) proteins. (**B-D**) Annexin V/ PI (propidium iodide) flow cytometric analysis of WT and *Col6a1*$^{-/-}$ MEFs cultured for two days on plastic, collagen VI (Col VI) or collagen I (Col I) and serum depleted for the final 3 hr, where indicated. Data indicate the average for 10,000 cells collected in at least three independent biological samples. (**B**) Cell survival quantification. (**C**) Left panel: representative dot plots of flow cytometric analysis of annexin V/ PI for WT and *Col6a1*$^{-/-}$ MEFs. Right panel: quantification of annexin V (apoptotic) and PI positive (necrotic) cells. (**D**) Western blotting analysis of total cell extracts from WT and *Col6a1*$^{-/-}$ MEFs in complete DMEM with 10% serum, or without serum for the specified time (3 hr, 6 hr). Cells were treated with 1 μM staurosporine, where indicated. WT, wild type. *, $P < 0.05$, **, $P < 0.01$, ***, $P < 0.001$.

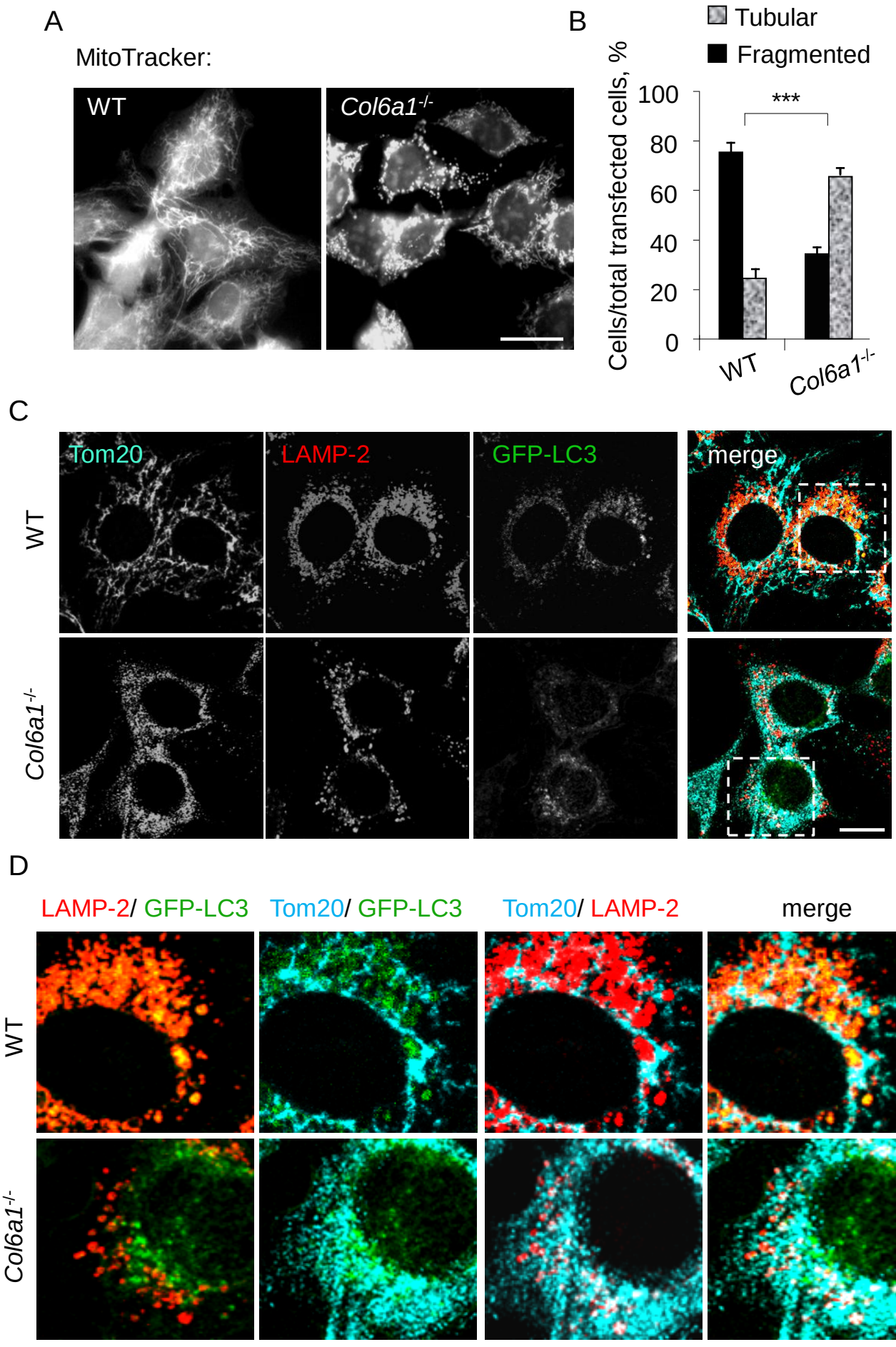
A
MitoTracker:
WT
Col6a1-/-
B
Tubular
Fragmented
Cells/total transfected cells, %
100
80
60
40
20
0
***
WT
Col6a1-/-
C
Tom20
LAMP-2
GFP-LC3
merge
WT
Col6a1-/-
D
LAMP-2/ GFP-LC3
Tom20/ GFP-LC3
Tom20/ LAMP-2
merge
WT
Col6a1-/-

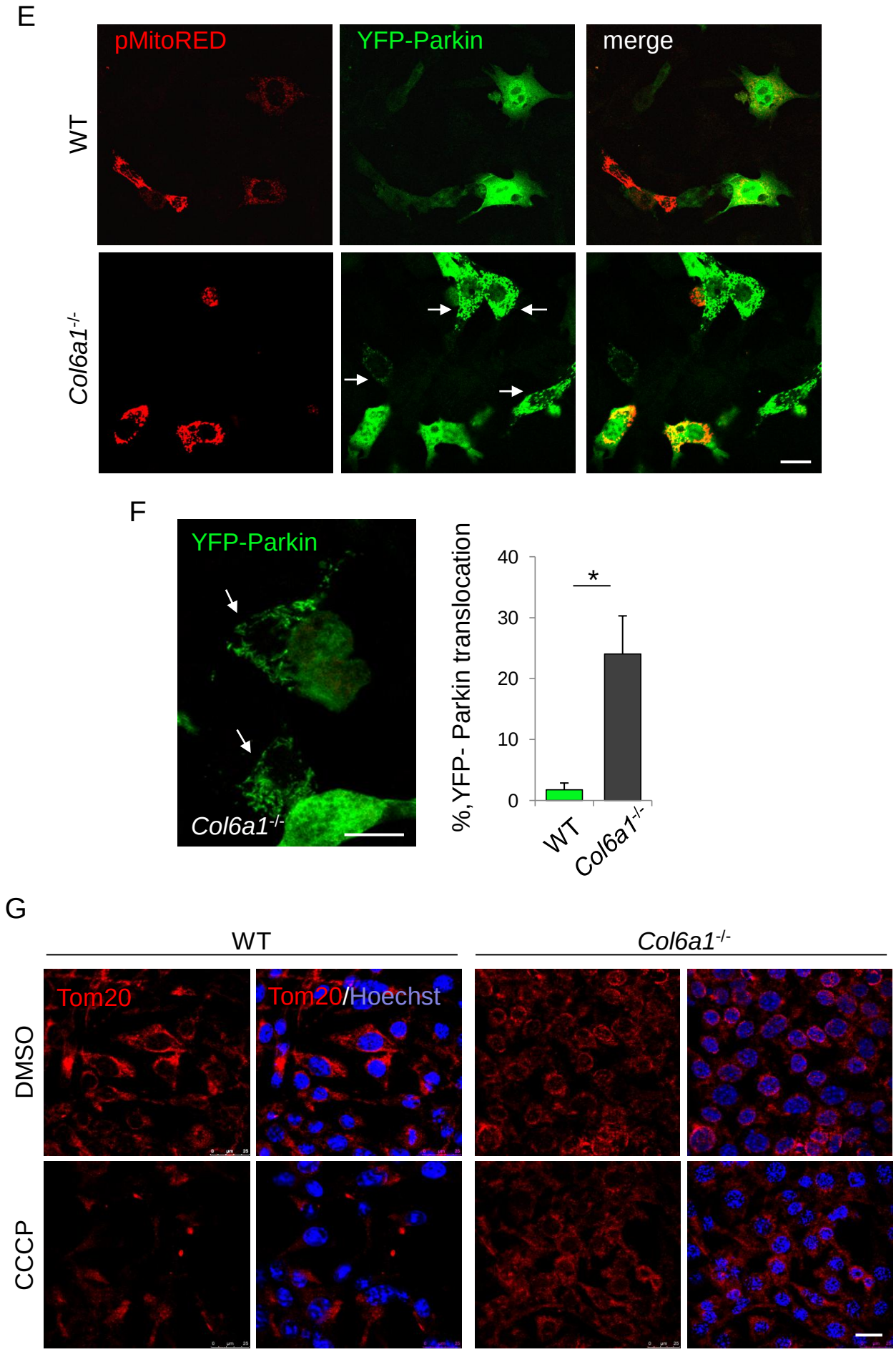
E
pMitoRED
YFP-Parkin
merge
WT
Col6a1-/-
F
YFP-Parkin
Col6a1-/-
%, YFP- Parkin translocation
40
30
20
10
0
*
WT
Col6a1-/-
G
WT
Col6a1-/-
Tom20
Tom20/Hoechst
DMSO
CCCP

Figure 8. Mitochondrial network is more fragmented and mitophagy is impaired in *Col6a1*$^{-/-}$ MEFs. (**A**) Representative micrograph of MitoTracker labeled mitochondria of WT and *Col6a1*$^{-/-}$ MEFs. (**B**) Quantification of cells showing tubular or fragmented mitochondria network in WT and *Col6a1*$^{-/-}$ MEFs, following transfection with mitochondrial fluorescent plasmids (pMitoRed or Mito-YFP). ***, $P<0.001$. Mean data are representative of at least five independent biological samples. (**C, D**) Coimmunostaining of LAMP-2 and Tom20 on GFP-LC3 MEFs, after 3 hr of serum withdrawal. (**D**) Image magnification of the boxed areas showed in C. Differential merged staining are showed. Scale bars, 25 μm. (**E**) Co-transfection of YFP-Parkin and pMitoRed plasmids in WT and *Col6a1*$^{-/-}$ MEFs. Arrows pointed to YFP-Parkin relocalized to mitochondria. (**F**) Left panel: representative micrograph of YFP-Parkin transfected *Col6a1*$^{-/-}$ MEFs. Arrows pointed to mitochondria-translocated YFP-Parkin. Right panel: quantification of cells showing YFP-Parkin translocation, as showed in the left panel, in WT and *Col6a1*$^{-/-}$ MEFs. (**G**) Immunostaining of Tom20 (showing mitochondria) in WT and *Col6a1*$^{-/-}$ MEFs, after 20 μM CCCP 24 hr treatment (or DMSO as a control). *, $P < 0.05$. WT, wild type.

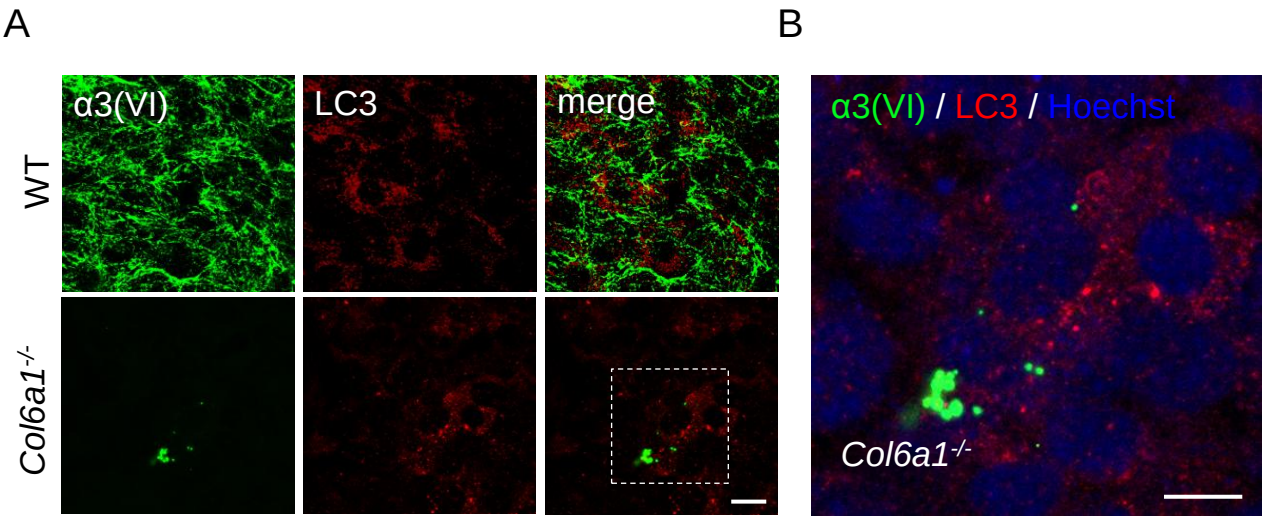

Figure S1. Coimmunostaining of LC3 and collagen VI α3 chain (α 3(VI)), in WT and *Col6a1*$^{-/-}$ confluent MEFs. (**A**) Scale bar, 20 µm. (**B**) Magnification of the boxed area in A. Intracellular dots of α3(VI) are detected in *Col6a1*$^{-/-}$ MEFs, without any colocalization with autophagosomes. Scale bar, 10 µm. WT, wild type.

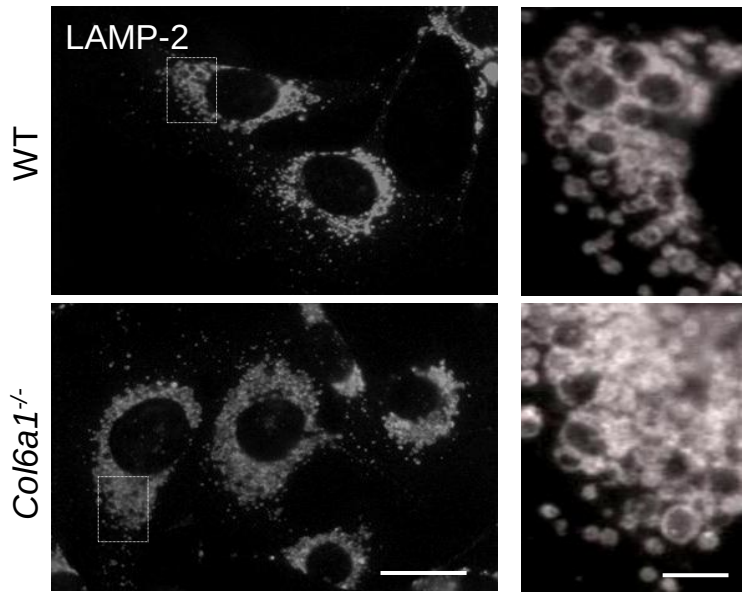

Figure S2. Chloroquine treatment induces lysosome enlargement in MEFs. WT and *Col6a1*$^{-/-}$ MEFs showing similar LAMP-2 immunostaining after 50 µM chloroquine treatment. Magnifications of the inserts show a detailed view of perinuclear swollen lysosomes. Scale bars, 25 and 5 µm. WT, wild type.

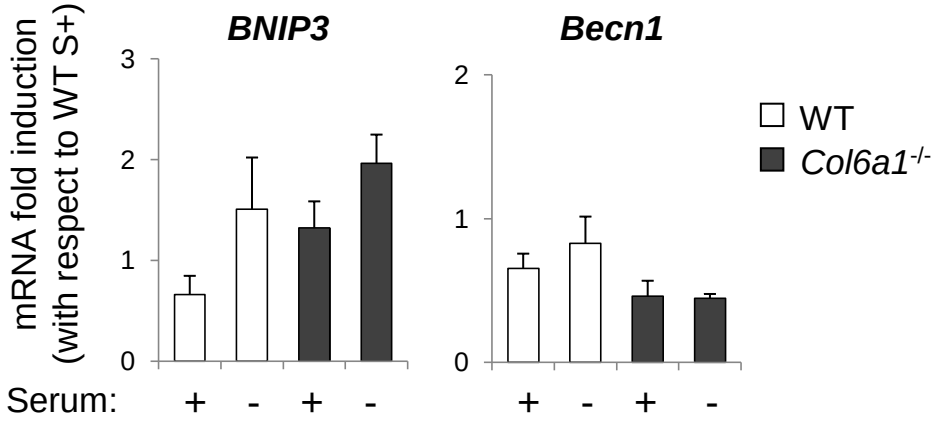

Figure S3. qRT-PCR analysis of *BNIP3* and *Becn1* mRNA expression in WT and *Col6a1*$^{-/-}$ MEFs in complete media or after 3 hr of serum withdrawal. WT, wild type.

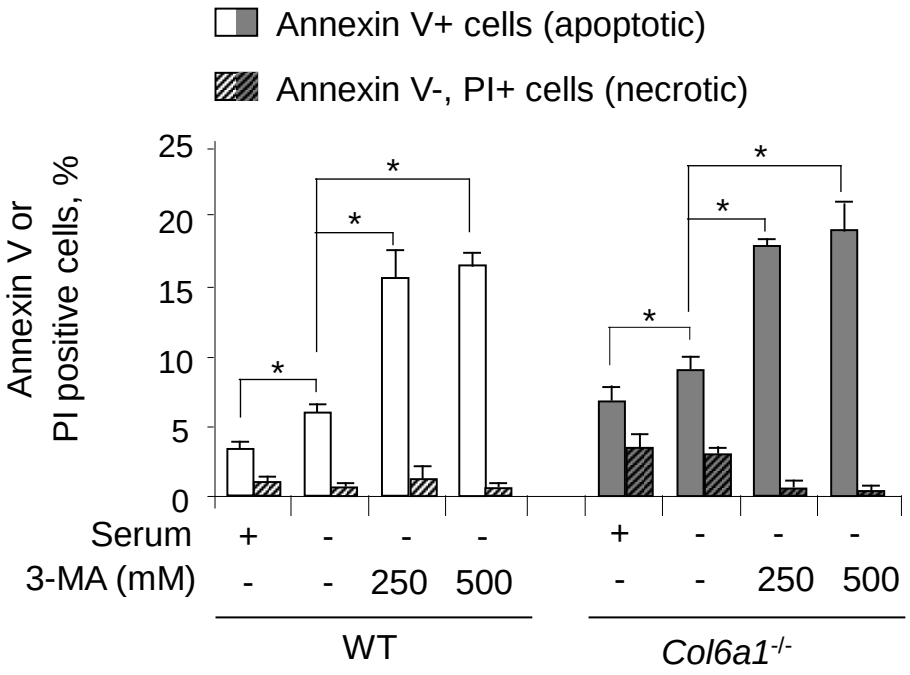

Figure S4. Quantification of annexin V/ PI (propidium iodide) flow cytometric analysis of WT and *Col6a1*$^{-/-}$ MEFs cultured for two days and treated with 3-MA in basal medium (Serum+) or without serum (Serum-). 3-MA increases apoptotis (annexin V+ cells) in a dose-dependent manner both in WT and *Col6a1*$^{-/-}$ MEFs. 3-MA autophagy inhibition is not sufficient to rescue cell death, indicating no contribution of autophagic cell death. WT, wild type.

Table 1. Sequence of the qRT-PCR primers used.

	Forward primer (5' > 3')	**Reverse primer (5' > 3')**
Col6a1	TGCCCTGTGGATCTATTCTTCG	CTGTCTCTCAGGTTGTCAATG
Col6a2	CAACCGCATCATCAAGGTCA	GGGTCTCCCTGTCGTCCTTT
Col6a3	AACCCTCCACATACTGCTAATTC	TCGTTGTCACTGGCTTCATT
LC3	CACTGCTCTGTCTTGTGTAGGTTG	TCGTTGTGCCTTTATTAGTGCATC
***p62* (*Sqstm1*)**	CCCAGTGTCTTGGCATTCTT	AGGGAAAGCAGAGGAAGCTC
LAMP-2	CAAAAGGACAGTATTCTACAGCTCA	CCACCGCTATGGGCACAA
GAPDH	CACCATCTTCCAGGAGCGAG	CCTTCTCCATGGTGGTGAAGAC

Part II: side projects

1. Autophagy regulation in skeletal muscles

Skeletal muscle is a tissue with a high intrinsic plasticity, able to readily respond to various stress conditions as contraction, physical exercise, nutritional changes, and aging. In order to display this plasticity and to maintain and preserve its high protein content, skeletal muscle needs a finely regulated catabolic system. Together with the ubiquitin-proteasome system, autophagy is crucial to assure proper protein and organelle turnover and assure muscle homeostasis (Bonaldo and Sandri, 2013; Vainshtein *et al.*, 2014).

Autophagy is constitutively active in skeletal muscle, and failure to maintain a proper autophagic flux can lead to muscle pathology. For example, different atrophic conditions as well as laminin α2 deficiency are associated with excessive autophagy (Carmignac *et al.*, 2011; Mammucari *et al.*, 2007; Masiero *et al.*, 2009). Conversely, inefficient autophagy allows the accumulation of unfolded proteins, macromolecular aggregates and dysfunctional organelles, as demonstrated in mouse modes for several inherited muscle diseases, such as collagen VI-related myopathies and Duchenne muscular dystrophy (Grumati *et al.*, 2010; De Palma *et al.*, 2012; Spitali *et al.*, 2013).

Forkhead box class O family member proteins (FoxOs) are highly conserved transcription factors exerting a key role in muscle energy homeostasis (Schiaffino *et al.*, 2013). In nutrient-rich conditions, Akt pathway inactivates FoxO factors by phosphorylation. When energy is required, autophagy initiation requires both the suppression of protein synthesis via inactivation of Akt/mTOR axis and the concurrent activation of FoxO3. Active FoxO3 translocates to the nucleus and induces the transcription of several autophagic genes, such as LC3, Bnip3, Vps34 and Beclin 1 (Mammuccari *et al.*, 2007). Atg5 and Atg7 are also necessary to sustain skeletal muscle autophagy flux and maintain myofiber integrity (Raben *et al.*, 2008; Masiero *et al.*, 2009).

Skeletal muscle is able to modulate its autophagic response in different physiological or stress conditions, such as contraction, fasting, mass wasting and metabolic

requirements, according to amino acids availability and energy consumption. This regulation occurs mainly through Akt/mTOR and AMPK axes, with different downstream cascades and pathway connections (Masiero *et al.*, 2009; Vainshtein *et al.*, 2014).

Several human myopathies display defects of the autophagy-lysosome system, indicating the critical role of this catabolic pathway for muscle homeostasis (Sandri *et al.*, 2013). Autophagic vacuolar myopathies (AVM), such as Danon and Pompe disease, are caused by mutation in non-Atg genes linked to lysosome or autophagolysosome functions. In these AVM diseases, autophagosomes accumulate inside myofibers due to their defective degradation, leading to myofiber degeneration and muscle weakness (Malicdan and Nishino, 2012). Recently, Vici syndrome, a multisystemic disorder also affecting skeletal muscles, was demonstrated to be caused by mutation of an autophagic gene called EPG5. Patients affected by Vici syndrome display lysosome-like vacuoles and p62 accumulation in muscles, associated with a block of the autophagosome-lysosome fusion process (Cullup *et al.*, 2013).

A detailed molecular understanding of the autophagy processes in skeletal muscles is fundamental for elucidating its role under physiological and pathological conditions and for uncovering new targets for therapy. The development of treatments and drugs able to restore proper autophagy in pathological contexts will be of outstanding interest to design new therapeutic approaches for human diseases.

1.1. AMBRA1 regulation of skeletal muscle development

Ambra1 is a key autophagy regulator and Beclin 1 interactor, with crucial role for embryogenesis and neural development in mammals (Fimia *et al.*, 2007; Mizushima *et al.*, 2010). *Ambra1* inactivation in mice by gene trap mutagenesis led to embryonic lethality. The E10-E14.5 homozygous *Ambra1* gene trap (*Ambra1*$^{gt/gt}$) mutant mouse embryos displayed a defective neural tube development, showing exencephaly and/or spina bifida. These defects were associated with excessive apoptosis, hyperproliferation and accumulation of ubiquitinated proteins in the nervous system, and to autophagy impairment in the developing embryo (Fimia *et al.*, 2007).

In basal conditions, Ambra1 tethers the Beclin 1/Vps34 complex to the microtubules, by directly binding the dynein motor complex (Di Bartolomeo *et al.*, 2010). Upon autophagy induction Ulk1 phosphorylates and unlocks Ambra1 from the cytoskeleton, allowing Beclin 1/Vps34 complex to translocate at the ER and to initiate autophagosome formation (Di Bartolomeo *et al.*, 2010).

Moreover, Ambra1 has a role in determining Ulk1 stability and kinase activity (Nazio *et al.*, 2013). In particular, mTOR phosphorylation inhibits Ambra1 activity in resting conditions; when autophagy is induced, Ambra1 is dephosphorylated and can interact with the E3-ligase TRAF6, to add Lys 63-linked ubiquitin chains to Ulk1, thus promoting its stabilization, self-association and function (Nazio *et al.*, 2013). As described before, Ulk1 can in turn activate Ambra1 by phosphorylation, to sustain autophagy through a positive loop (Di Bartolomeo *et al.*, 2010).

Other results confirmed the involvement of Ambra1 in the embryonic and larval development of the zebrafish (*Danio rerio*) model (Benato *et al.*, 2013).

During the second year of my PhD, I participated to a large project aimed at elucidating the role of Ambra1 in skeletal muscle homeostasis and development. To investigate the role of Ambra1 in muscle development, this project first involved studies in zebrafish embryos via knockdown of Ambra1 paralogue genes as well as in *Ambra1*$^{gt/gt}$ mouse embryos. These studies allowed demonstrating that Ambra1 is required for the proper morphogenesis of skeletal muscle, and that its depletion cause striking structural

and functional alterations of muscles. My own contribution to the project consisted in the histological and light microscopy analysis of skeletal muscles of *Ambra1*$^{gt/gt}$ mouse embryos.

OPEN ACCESS Freely available online

PLOS ONE

Zebrafish *ambra1a* and *ambra1b* Knockdown Impairs Skeletal Muscle Development

Tatjana Skobo[1], Francesca Benato[1], Paolo Grumati[2], Giacomo Meneghetti[1], Valentina Cianfanelli[3], Silvia Castagnaro[2], Martina Chrisam[2], Sabrina Di Bartolomeo[3], Paolo Bonaldo[2], Francesco Cecconi[3,4,5]*, Luisa Dalla Valle[1]*

1 Department of Biology, University of Padova, Padova, Italy, **2** Department of Molecular Medicine, University of Padova, Padova, Italy, **3** Department of Biology, University of Tor Vergata, Rome, Italy, **4** Department of Neuroscience, Istituto di Ricovero e Cura a Carattere Scientifico "Santa Lucia Foundation", Rome, Italy, **5** Unit of Cell Stress and Survival, Danish Cancer Society Research Center, Copenhagen, Denmark

Abstract

The essential role of autophagy in muscle homeostasis has been clearly demonstrated by phenotype analysis of mice with muscle-specific inactivation of genes encoding autophagy-related proteins. Ambra1 is a key component of the Beclin 1 complex and, in zebrafish, it is encoded by two paralogous genes, *ambra1a* and *ambra1b*, both required for normal embryogenesis and larval development. In this study we focused on the function of Ambra1, a positive regulator of the autophagic process, during skeletal muscle development by means of morpholino (MO)-mediated knockdown and compared the phenotype of zebrafish Ambra1-depleted embryos with that of *Ambra1*$^{gt/gt}$ mouse embryos. Morphological analysis of zebrafish morphant embryos revealed that silencing of ambra1 impairs locomotor activity and muscle development, as well as *myoD1* expression. Skeletal muscles in ATG-morphant embryos displayed severe histopathological changes and contained only small areas of organized myofibrils that were widely dispersed throughout the cell. Double knockdown of *ambra1a* and *ambra1b* resulted in a more severe phenotype whereas defects were much less evident in splice-morphants. The morphants phenotypes were effectively rescued by co-injection with human *AMBRA1* mRNA. Together, these results indicate that *ambra1a* and *ambra1b* are required for the correct development and morphogenesis of skeletal muscle.

Citation: Skobo T, Benato F, Grumati P, Meneghetti G, Cianfanelli V, et al. (2014) Zebrafish *ambra1a* and *ambra1b* Knockdown Impairs Skeletal Muscle Development. PLoS ONE 9(6): e99210. doi:10.1371/journal.pone.0099210

Editor: Zhiyuan Gong, National University of Singapore, Singapore

Received January 9, 2014; **Accepted** May 12, 2014; **Published** June 12, 2014

Funding: This work was financially supported by Telethon-Italy (Grant GGP10225) and by University of Padova (RFO-ex 60%). FC is also supported by AIRC (IG2010), FISM (2009), the Italian Ministry of University and Research (PRIN 2009 and FIRB Accordi di Programma 2011), the Italian Ministry of Health (Ricerca Finalizzata and Ricerca Corrente). The funders had no role in study design, data collection and analysis, decision to publish, or preparation of the manuscript.

Competing Interests: The authors have declared that no competing interests exist.

* E-mail: luisa.dallavalle@unipd.it (LDV); francesco.cecconi@uniroma2.it (FC)

Introduction

Autophagy is an evolutionarily conserved catabolic process in which cells, through the lysosomal machinery, degrade and recycle long-lived proteins and dismantle organelles in order to maintain a homeostatic intracellular environment. This process is tightly regulated and plays several important roles in normal physiology, differentiation, embryo development, and cell survival during starvation [1]. Defects of this degradative system play a role in various diseases, such as neurodegenerative and lysosomal storage disorders and in oncogenesis and cancer progression [2]. However, little is known about autophagy in muscular pathology.

In skeletal muscle, the role of autophagy was initially demonstrated in *Atg5* and *Atg7* muscle-specific knockout mice [3,4]. In both models, the muscle showed abnormal mitochondria and disorganized sarcomeres, confirming a homeostatic role of autophagy in this tissue. A direct connection between autophagy deregulation and muscular dystrophy was initially found in collagen VI null mice, where accumulation of abnormal organelles and spontaneous apoptosis was shown to strictly depend on defective autophagy regulation [5]. In agreement with this, reactivation of autophagy restored myofiber survival and ameliorated the dystrophic phenotype of collagen VI null mice. More recently, deregulation of the autophagic process was also demonstrated in other dystrophic mouse models [6–9] as well as in the Vici syndrome, a human genetic disease caused by recessive mutations of the *EPG5* gene, which codes for a key autophagy regulator involved in the formation of autolysosomes [10].

Ambra1, originally identified in a gene trap screening in mice, is a positive regulator of the Beclin 1 dependent programme of autophagy [11]. Ambra1 is an intrinsically disordered protein, whose capability of binding a number of other regulatory partners involved in many cell processes highlights its crucial role as a "relay" molecule for autophagy [12]. In mammalian cells, Ambra1 is normally docked at a specific cytoskeletal site, corresponding to the dynein light chain, where it is unleashed upon autophagy induction to translocate at the autophagosome origin sites on the endoplasmic reticulum [13]. Ablation of Ambra1, as demonstrated by loss-of-function in mice, leads to embryonic lethality and causes neural defects, suggesting a role for autophagy in nervous system development [11]. Results obtained with the zebrafish model confirmed the involvement of this protein in embryonic development and demonstrated that the duplicated fish *ambra1* paralogous genes are required for normal embryogen-

esis and larval development. Indeed, MO-induced ablation of the corresponding proteins was found to be associated with several developmental abnormalities and decreased viability [14].

The rapid development and transparency of zebrafish embryos, together with the high fecundity and amenability to genetic manipulation of this vertebrate model, as well as with the feature that skeletal muscles represent a large portion of the body and are easily accessible for analysis, have made this organism attractive for investigating muscle development and fiber-type specification (reviewed by [15]) as well as myopathies and muscular dystrophies (reviewed by [16]). In this study, we investigated the role of Ambra1 in skeletal muscle development by means of knockdown of *ambra1* paralogous genes in zebrafish. Depletion of zebrafish Ambra1 proteins results in abnormal locomotor activity and a severe myopathy characterized by irregular myofiber orientation and highly disorganized sarcomeres, suggesting a role for Ambra1 in muscle development. In agreement with this, histological analysis of mouse *Ambra1* gene trap mutant (*Ambra1*$^{gt/gt}$) embryos showed a disorganized three-dimensional structure of developing muscles and an increased proliferation of muscle cells.

Materials and Methods

Animal maintenance and handling

Zebrafish (AB strain) were raised, staged and maintained according to standard protocols [17,18]. Embryos were obtained by natural spawning and cultured in zebrafish fish water solution (50x: 25 g Instant Ocean, 39.25 g $CaSO_4$, 5 g $NaHCO_3$ for 1 l) at 28.5°C with a photoperiod of 14 h light/10 h dark. For *in vivo* imaging, embryos were anesthetized with 0.04% tricaine [18]. The touch-evoked motor behaviour was stimulated by touching the embryo with a thin tip. *Ambra1*$^{gt/+}$ mice (CD1 strain) were bred in order to obtain *Ambra1*$^{gt/gt}$ embryos [11]. Data were obtained in E13.5 embryos by comparing *Ambra1*$^{gt/gt}$ and wild-type (WT) animals. Mice were housed in individual cages in an environmentally controlled room (23 °C, 12 h light/12 h dark cycle) and provided with food and water *ad libitum*. All animal procedures were approved by the Ethics Committee of the University of Padova and Tor Vergata, Rome.

MO microinjection

MO (Gene Tools) treatment was performed with MOs against the ATG translation initiation sites of either *ambra1a* or *ambra1b* transcripts (MO-*ambra1a*-ATG and MO-*ambra1b*-ATG) and with splice-blocking MOs designed at the exon 3-intron 3 junction sequence of both genes (MO-*ambra1a*-splice and MO-*ambra1b*-splice). The designed splice-blocking MOs cause the skipping of exon 3, thus altering the translation reading frame of exon 4 with introduction of a premature stop codon, and the resulting proteins lack all known binding domains (Fig. S1). As controls, we used five-nucleotide-mismatched control MOs (MO-*ambra1a*-5m and MO-*ambra1b*-5m). All MOs were previously described and validated [14], however lower MOs dosages were used in this work in order to reduce embryo mortality. Specifically, for each MO, 10.3 ng were injected in the yolk of 1-cell stage embryos, whereas the dosage was halved in the co-injection experiments. Injections were performed under a dissecting microscope using a microinjector attached to a micromanipulator (Leica Microsystems). MOs-injected embryos were then incubated in 1x fish water solution at 28.5 °C up to the desired stages of development.

RNA synthesis and injections

For the *ambra1*-MO rescue experiments, human *AMBRA1* cDNA was removed from pLPCX-AMBRA1 [11] and subcloned in the pCS2+ vector. Full-length RNA was transcribed using the T3 promoter and the mMessage Machine kit (Ambion) according to the manufacturer's instructions and after plasmid linearization with *Hind*III restriction enzyme. After preliminary experiments with different dosages from 40 to 10 ng/embryo, the 10 ng/embryo dosage was selected for the injection of human *AMBRA1* RNA in one-cell stage embryos for rescue experiments.

Birefringence assay

Muscle birefringence was analysed by placing anesthetized embryos on a glass polarizing filter and covering with a second polarizing filter on a Leica DMR microscope. Embryos were photographed with a Leica DC500 digital camera. The top filter was twisted until it was possible to see the light refracting through the striated muscle. Pixel intensity in the trunk region was measured with ImageJ software. Values were expressed as the percentage to WT pixel intensity ± SEM ($n = 20$).

Whole mount in situ hybridization (WMISH)

Zebrafish embryos were fixed overnight in 4% paraformaldehyde (PFA, Sigma) in phosphate-buffered saline (PBS) at the required stages of development. WMISH was performed as previously described [19]. DIG-labeled *myoD1* riboprobe was synthesized by *in vitro* transcription with T7 RNA polymerases (Roche), following the manufacturer's instructions and after plasmid linearization with *Bam*HI restriction enzyme.

Imaging

For confocal microscopy, fixed embryos were embedded in 0.8% low-melting agarose and placed on a depression slide, and a Nikon C2 confocal system was used to record images. WMISH-stained embryos were mounted in 87% glycerol in PBT (PBS plus 0.1% Tween 20) or cleared and mounted in 2:1 benzyl benzoate/benzyl alcohol, observed under a Leica DMR microscope, and photographed with a Leica DC500 digital camera.

Histology and immunofluorescence

Zebrafish embryos were fixed overnight in 4% paraformaldehyde in PBS at 4 °C. For histology, 5 µm thin paraffin sections were cut and stained with haematoxylin and eosin. Embryos were fixed for antibody staining with 4% PFA and whole-mount immunohistochemistry was performed according to Dolez et al. [20], using the following primary antibodies: rabbit polyclonal anti-PH3 (1:1000; Millipore); mouse monoclonal anti-Pax7 (1:20; Hybridoma Bank), mouse monoclonal anti-F59 (1:100; Hybridoma Bank); mouse monoclonal anti-F310 (1:100, Hybridoma Bank); rabbit polyclonal anti-Laminin (1:400; Sigma). The following secondary antibodies were used: Alexa Fluor 488 goat anti-mouse IgG1(γ1) (A-21121, Invitrogen); Alexa Fluor 594 goat anti-rabbit IgG (H+L) (A-11012, Invitrogen). E13.5 mouse embryos were fixed in 4% paraformaldehyde, de-hydrated and included in paraffin. Haematoxylin-eosin staining was performed following standard protocols. Images were detected using a Zeiss Axioplan microscope equipped with a Leica DC500 digital camera.

Phospho-H3 immunostaining was quantified by counting positive cells present in the same six somites of the trunk region in ten embryos of each category.

Transmission electron microscopy

Samples were fixed in 6% glutaraldehyde in 0.1 M cacodylate buffer (pH 6.9) overnight at 4°C. After washing in cacodylate buffer, the specimens were post-fixed in 1% OsO_4 in the same

buffer for 2 h and dehydrated in a graded ethanol series followed by propylene oxide. The specimens were embedded in EPON 812 resin. Thick sections (1 μm) were cut with an Ultracut S Reichert ultramicrotome, counterstained with toluidine blue and examined with a light microscope. Thin sections (100 nm) were stained with uranyl acetate and lead citrate. Micrographs were taken with a FEI Tecnai G12 electron microscope operating at 100 kV.

Microinjection of the hsp70l:Lc3-RFP plasmid into fertilized eggs

A total of 25 ng/μl of hsp70l:Lc3-RFP [21] plasmid was co-injected with each ambra1-MO into zebrafish embryos at one-cell stage. Microinjected embryos were raised to 3 dpf stage and heat shocked by replacing the embryo medium with fish water preheated at 41 °C and then incubated in an air incubator at 38 °C for 30 min to induce hsp70 expression. Lc3-RFP labeled puncta were analysed by confocal microscopy.

Statistical analysis

Statistical analysis was performed by one-way analysis of variance (ANOVA) followed by Bonferroni's multiple comparison test (GraphPad Prism Software).

Results

Knockdown of *ambra1a* and *ambra1b* interferes with embryo motility and muscle integrity

To investigate the effects of *ambra1a* and *ambra1b* ablation during muscle development, we injected validated antisense MOs [14] into the yolk mass of 1-cell embryos to suppress translation of both maternal and zygotic mRNA (ATG MOs) or to silence zygotic transcription of the two genes (splice-blocking MOs). In agreement with a previous work [14], ATG-morphant embryos displayed severe abnormalities in their overall appearance that mainly consisted in body growth delay, curved shape, hemorrhagic pericardial cavity, as well as neural tube defects. The percentages of normal, abnormal and dead embryos at 3 dpf are reported on Fig. S2. More than 70% of ATG-morphant and about 35% of splice-morphant embryos had to be manually dechorionated (Fig. S3). The delay in hatching could be due to an overall developmental delay [14], but also to a reduction of the muscle activity that contributes to the exit of the embryos from their protective outer chorion. Moreover, after hatching, both *ambra1a* and *ambra1b* ATG-morphants, as well as co-injected morphant embryos, showed impaired or totally absent locomotor activity and did not respond to touch with the escape response normally observed in control embryos injected with mismatch MOs (Fig. S4). Less severe aspects of the phenotypes included uncoordinated movements in response to tactile stimuli and often swimming in a circular fashion. In agreement with the impaired locomotor activity, ATG-morphants exhibited a marked and statistically significant reduction of birefringence of the skeletal musculature when compared with control embryos, indicating decreased striated muscle formation and/or loss of myofiber organization (Fig. 1). Reduction of birefringence was comparable between co-injected and *ambra1a* ATG-morphants, and less marked in *ambra1b* ATG-morphants. Birefringence was also slightly reduced in both *ambra1a* and *ambra1b* splice-morphants, whereas it was normal in 5m-control embryos (Fig. 1). Co-injection of ATG-MOs with human *AMBRA1* mRNA resulted in the rescue of the morphants phenotypes (Fig. 1). Moreover, analysis of rescued embryos showed a marked and statistically significant improvement of skeletal muscle birefringence when compared to ATG-morphants (Fig. 1) as well as percentage of hatched embryos at 3 dpf (Fig. S3).

ambra1 depletion interferes with *myoD1* expression during myogenesis

To assess the requirement for *ambra1a* and *ambra1b* during embryonic myogenesis, we performed WMISH analysis with the somite-specific marker *myoD1*. At the bud stage (10 hpf), expression of *myoD1* in the adaxial cells was reduced in ATG-morphants, while the width between them was increased, particularly at the posterior end (Fig. 2). This was more evident in *ambra1a* ATG-morphants and in co-injected morphants. Expression of *myoD1* appeared normal in splice-morphants for both genes as well as in 5m-control morphants. At 20 hpf, ambra1 ablation resulted in abnormally shaped and less distinct somites, suggesting impaired somite organization, together with shortened anterior/posterior axes and undulated notochord. All defects were more evident in *ambra1a* ATG-morphants and in co-injected embryos. Segmentation pattern appeared normal in splice-morphants and in 5m-control morphants (Fig. 2).

ambra1 deficiency leads to abnormal myogenesis

To fully appreciate at a microscopic level the phenotype of *ambra1* morphants, we performed a histological analysis of haematoxylin/eosin stained longitudinal sections of muscles from 3 dpf embryos. This showed well-organized myofibers with elongated nuclei in WT and 5m-control muscles. In ATG-morphants, myosepta were not clearly evident, particularly in *ambra1a* ATG-morphants and co-injected embryos, and myofibers appeared misaligned with markedly disorganized shape and orientation. Moreover, ATG-morphants displayed an apparently increased number of myonuclei (Fig. 3). Morphological changes were much less evident in splice-morphants, although the myosepta were thinner and myofibers appeared less organized with respect to controls.

The irregular arrangement of muscle fibers was confirmed by toluidine blue stained semithin longitudinal sections of muscle fibers running between the vertical myosepta (Fig. 4). In both *ambra1a* and *ambra1b* ATG-morphants, the myoseptum was difficult to distinguish and in some places it appeared interrupted. Multiple areas devoid of staining were present within myofibers of both ATG-morphants, and amorphous opaque material replaced lost myofibers. In *ambra1a* ATG-morphants and in co-injected morphants many fibers appeared detached. Skeletal muscles of splice-morphants displayed only minor modifications. Cross sections of the trunk region analysed by toluidine blue staining showed extensive disruption of myofiber structure and organization, with empty spaces and regions filled with amorphous opaque material. Several myonuclei appeared large, abnormally rounded, and centrally localized (Fig. 4).

Immunostaining of 3 dpf embryos for phospho-histone H3, a mitotic marker, showed a higher proliferation rate in ATG-morphant embryos (Fig. 5), while the spots of phospho-histone H3 positive nuclei in splice-morphants were only weakly increased compared to controls. The increase of mitotic cells in ATG-morphant embryos resulted statistically significant (Fig. S5).

To evaluate the effect of zebrafish *ambra1a* and *ambra1b* knockdown on the autophagic process, we analysed autophagy in muscle fibers where transient expression of the lysosomal *Lc3*-RFP reporter protein was obtained by microinjection of zebrafish embryos with hsp70l:Lc3-RFP reporter construct, in which the zebrafish *Lc3* gene is driven by the hsp70l promoter and thus induced by heat-shock treatment [21]. Analysis at 3 dpf showed that several Lc3-RFP puncta were present in myofibers from WT and 5 m-control embryos. In contrast, knockdown of either *ambra1a* or *ambra1b* led to an almost complete lack of Lc3-RFP puncta in muscle fibers (Fig. S6).

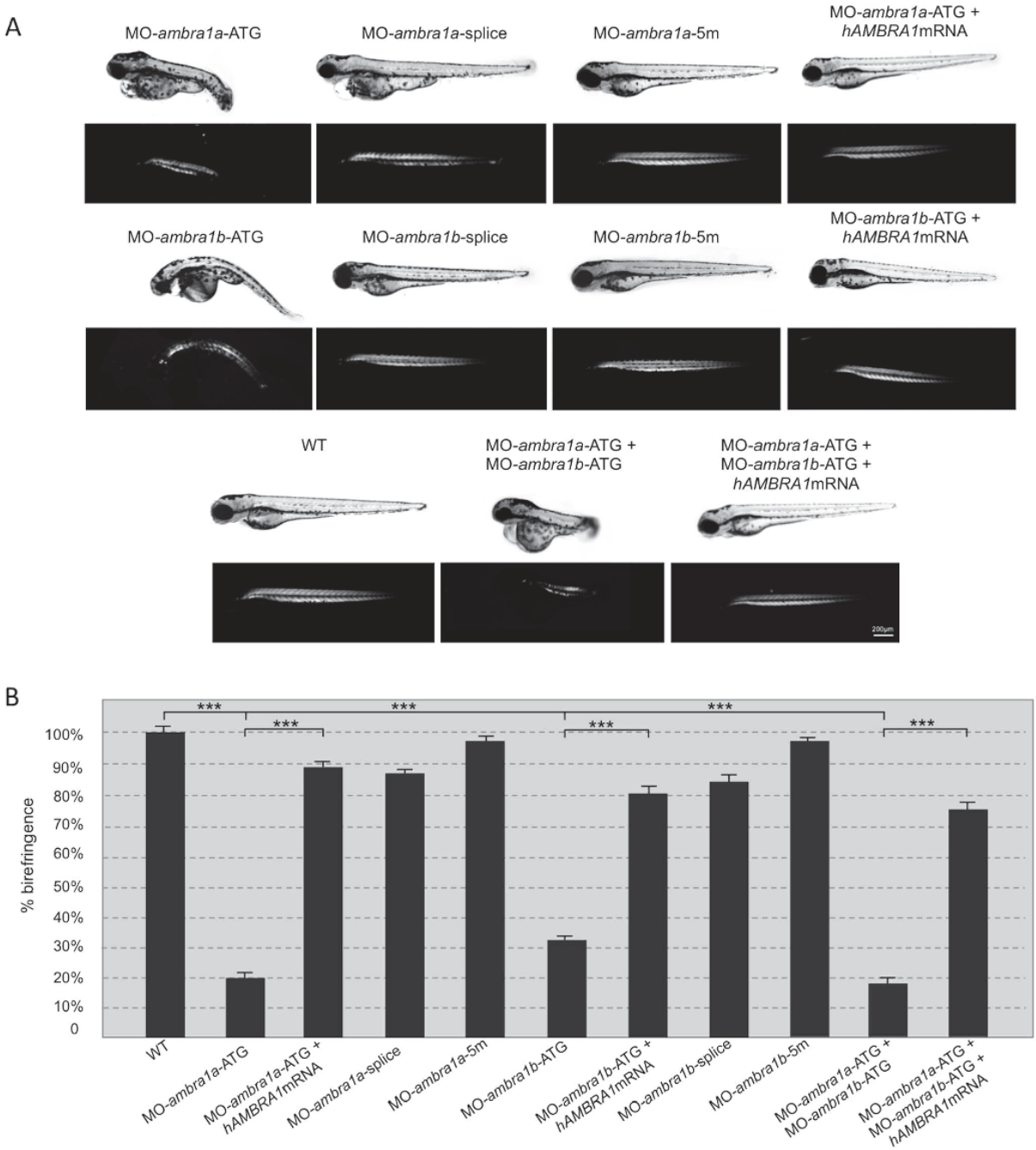

Figure 1. Ablation of *ambra1* results in reduced birefringence in zebrafish embryos. (**A**). Representative images under normal and polarized light of 3-dpf live embryos injected with the indicated MOs. ATG-morphant embryos show reduced size, curved shape, pericardial edema and reduced birefringence when compared to WT and 5 m-control embryos. No visible abnormalities are evident in splice-morphants. The phenotypic defects of ATG-morphant embryos, including birefringence, are rescued by co-injection with 10 ng/embryo of human *AMBRA1* mRNA. (**B**). Quantification of embryo trunk muscles birefringence shows a severe and statistically significant reduction in *ambra1* ATG- and in co-injected morphants. The birefringence is faintly reduced in *ambra1* splice-morphants, whereas WT and 5 m-control embryos display highly birefringent skeletal muscles. Muscle birefringence is statistically increased when ATG- and co-injected morphants are co-injected with human *AMBRA1* mRNA (***, $P<0.001$).

doi:10.1371/journal.pone.0099210.g001

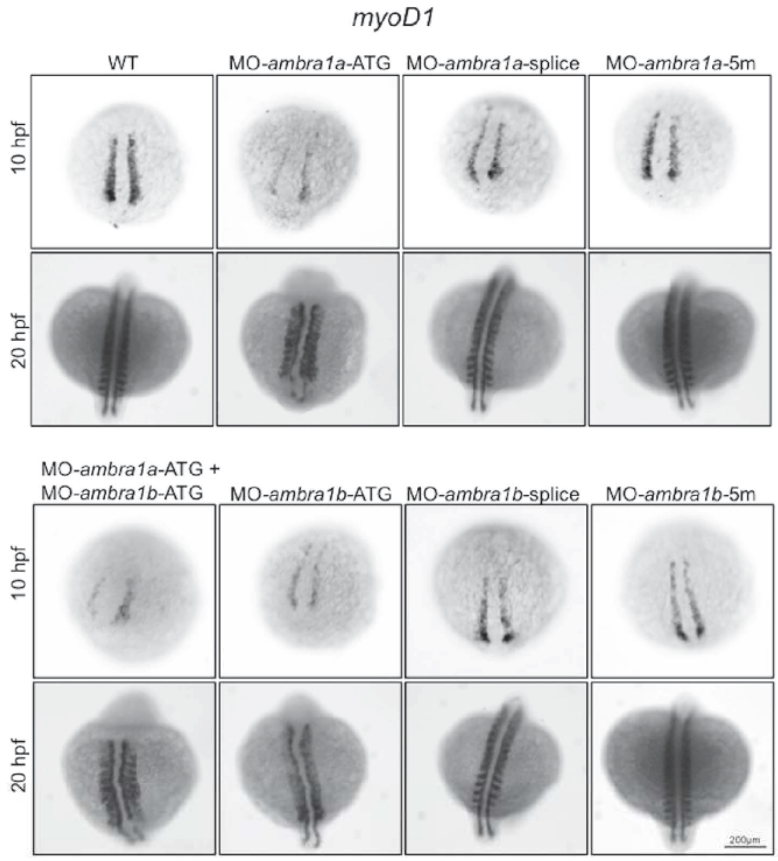

Figure 2. *In situ* hybridization analysis of *myoD1* expression in *ambra1* knockdown embryos. Expression of *myoD1*, analyzed in embryos injected with the indicated MOs at 10 and 20 hpf, is affected in *ambra1* ATG-morphants and in co-injected morphants. No differences are evident in *ambra1* splice-morphants when compared to WT and 5 m-control embryos. Embryos are shown by dorsal view, anterior side on the top.
doi:10.1371/journal.pone.0099210.g002

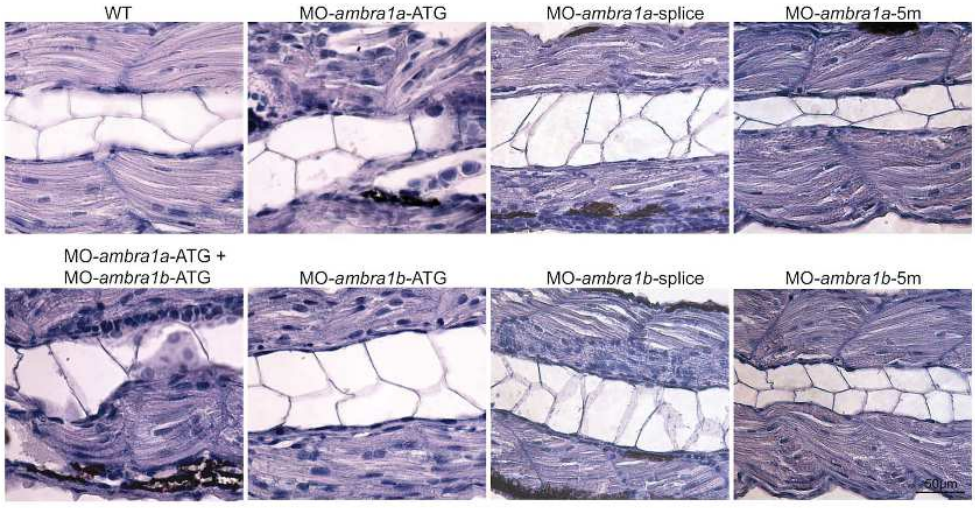

Figure 3. Abnormal morphology of *ambra1* knockdown embryos, as revealed by haematoxylin/eosin staining. Representative longitudinal sections of 3 dpf control and *ambra1* morphant embryos. Myofibers of ATG- and co-injected morphants muscles are highly disorganized and display irregular myosepta boundaries. The phenotype of splice-morphants is much less severe when compared to WT and 5 m-control embryos.
doi:10.1371/journal.pone.0099210.g003

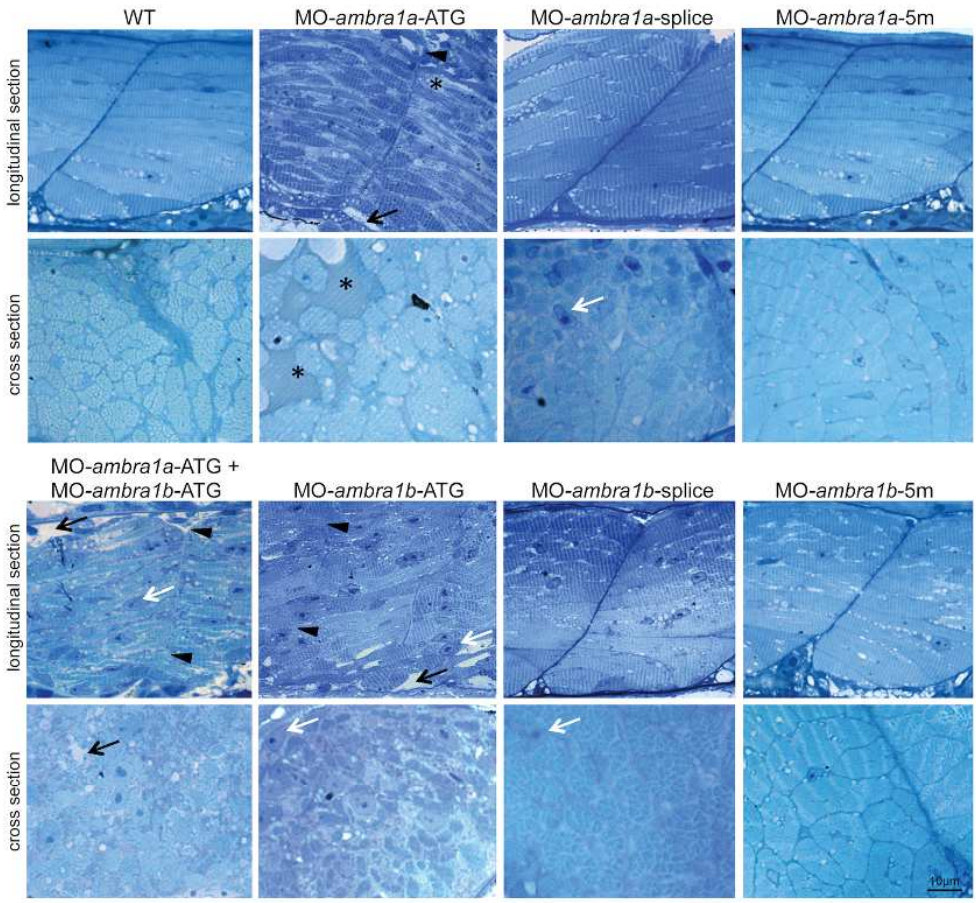

Figure 4. Abnormal morphology of *ambra1* knockdown embryos, as revealed by toluidine blue staining. Representative longitudinal and cross sections of 3 dpf control and *ambra1* morphant embryos. Muscles of *ambra1* ATG-morphants show a severe phenotype, with misaligned myofibers scattered in the somitic compartment. Black arrows, areas devoid of staining; white arrows, large myonuclei with condensed chromatin; black arrowheads, interruption of myoseptum; asterisks, opaque material replacing lost myofibers.
doi:10.1371/journal.pone.0099210.g004

Immunofluorescence at 2 dpf for Pax7, a key regulator of muscle progenitor cells [22], showed that both ATG- and splice-morphants had a higher incidence of Pax7-positive cells in the spaces between myosepta, instead of being regularly localized to the edges of the somites as in WT and 5 m-control embryos (Fig. 6).

Ablation of *ambra1* causes ultrastructural defects of myofibers

To better understand the subcellular alterations responsible for the observed fiber disturbances, we performed an electron microscopy analysis of longitudinal and cross-sections. Zebrafish embryos at 3 dpf showed that WT and 5 m-control embryos (not shown) had well-defined muscle fiber structure with normally developed sarcoplasmic reticulum encircling myofibrils and inter-myofibrillar mitochondria. In control embryos, sarcomeres were clearly visible and formed regular repeating units with alignment of well-defined Z-lines, mitochondria were aligned in rows and had tightly packed cristae, and myofibers were surrounded by very small areas of amorphous material (Fig. 7, panels A1–A4). In contrast, muscle fibers of ATG-morphants and of co-injected embryos contained only small areas of organized filaments, widely dispersed throughout the cells and surrounded by enlarged areas of disorganized cytoplasm devoid of normally appearing organelles. Remnants of degenerating myofibers were also seen in these regions (Fig. 7, panels B1–B4, D1–D4, F1–F4). Although ATG-morphants muscle fibers contained sarcomeres, they were substantially reduced in number, torn, not correctly aligned and dispersed within amorphous material. Areas with myofibrils showing orthogonal arrangement to each other were also visible (Fig. 7). The ultrastructural muscle defects were less severe in splice-morphants, where only small regions devoid of myofibrils were present together with a milder disorganization of sarcomeres (Fig. 7).

Patterning of internal membranes was also affected in ATG-morphants and in co-injected embryos, as the sarcoplasmic reticulum appeared dilated and often not closely associated with myofibrils (Fig. 8, row E). *ambra1* morphant embryos showed several ultrastructural abnormalities of T-tubules and sarcoplasmic reticulum, ranging from mild changes in splice-morphants to unrecognizable triad areas in co-injected morphants, whereas WT embryos and 5 m-control embryos displayed a normal pattern of T-tubules and sarcoplasmic reticulum resulting in regularly spaced triads (Fig. 8, row C). In *ambra1* morphant embryos, mitochondria

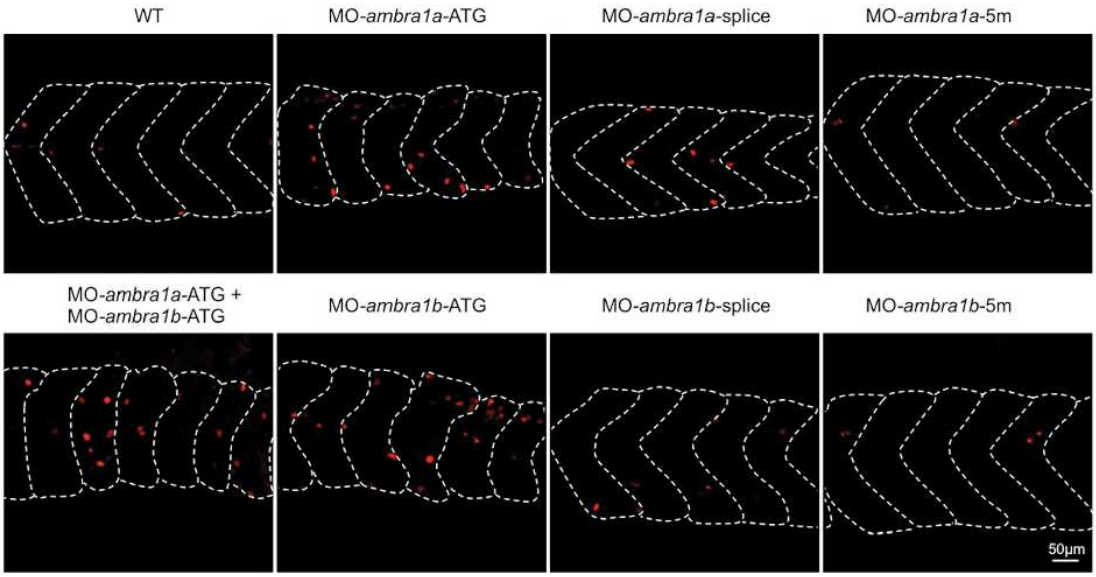

Figure 5. Cell proliferation in muscles of 3 dpf control and *ambra1* morphant embryos. Mitotic cells, detected by immunostaining for phospho-histone H3 in longitudinal sections, are more abundant in ATG-morphant embryos with respect to WT and 5 m-control embryos. Anterior is to the left and dorsal up.
doi:10.1371/journal.pone.0099210.g005

were scattered throughout the cytoplasm and their morphology was also markedly affected, as they were often swollen and devoid of cristae or, when present, these were disorganized or abnormal (Fig. 7, panel B2 and Fig. 8, row A). Ultrastructural analysis also confirmed that myonuclei were often larger in morphant embryos, with an irregular shape and more numerous when compared to control embryos (Fig. 8, row B). The abnormal myofiber ultrastructure of ambra1 depleted embryos was particularly evident in cross sections, where myofibers of control embryos showed a regular hexagonal arrays of thick and thin filaments while in *ambra1* morphants the hexagonal arrays were irregular, with areas in which thick filaments were not associated with thin filaments (Fig. 8, row D).

Taken together, these data highlight a severe disorganization of muscle tissue and cells upon ambra1 depletion. Also, alteration of mitochondria and ER structure seem to be causative of the phenotype.

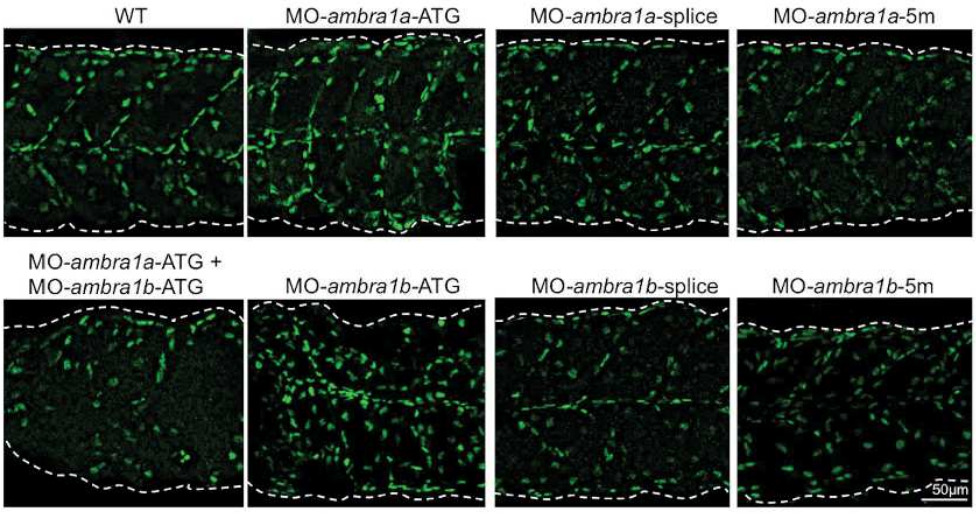

Figure 6. Pax7 expression in control and *ambra1* morphant embryos. Lateral views of 2 dpf muscles analyzed by immunofluorescence for Pax7. In WT and 5 m-control embryos, Pax7-positive cells are localized at the edge of somites, whereas in *ambra1* morphants many Pax7-positive cells are misplaced in the spaces between myosepta. Anterior is to the left and dorsal up.
doi:10.1371/journal.pone.0099210.g006

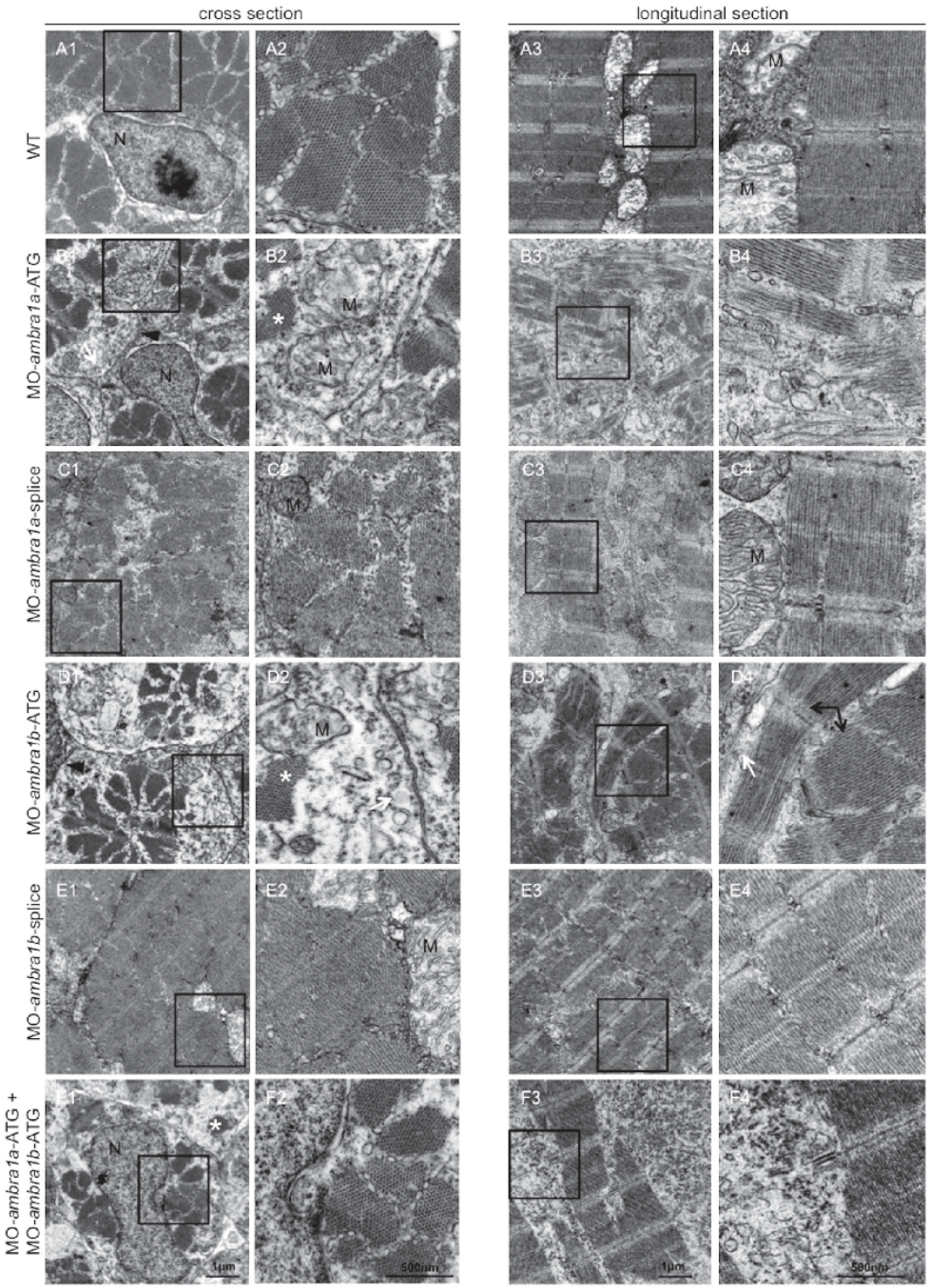

Figure 7. Ultrastructural analysis of *ambra1* morphants muscles reveals disorganized sarcomeres. Representative electron micrographs of cross and longitudinal sections of 3 dpf (WT, panels A1–A4), *ambra1a* ATG-morphant (panels B1-B4), *ambra1a* splice-morphant (panels C1–C4), *ambra1b* ATG-morphant (panels D1–D4), *ambra1b* splice-morphant (panels E1-E4), and co-injected morphant (panels F1–F4) zebrafish embryos. Columns 2 and 4 show higher magnification views of the boxed areas in column 1 and 3, respectively. Muscles of WT and 5 m-control (not shown) embryos display well-organized myofibers, showing densely packed sarcomeres with regular organization of thin and thick myofilaments. *ambra1* depleted muscles show a number of ultrastructural defects, with small patches of disorganized myofibers and mitochondria scattered throughout the cytoplasm. Black arrows, area with myofibrils having different orientations; white arrow, dilated sarcoplasmic reticulum not in contact with myofibrils; asterisks, fragments of torn myofibrils; M, mitochondria; N, nucleus.
doi:10.1371/journal.pone.0099210.g007

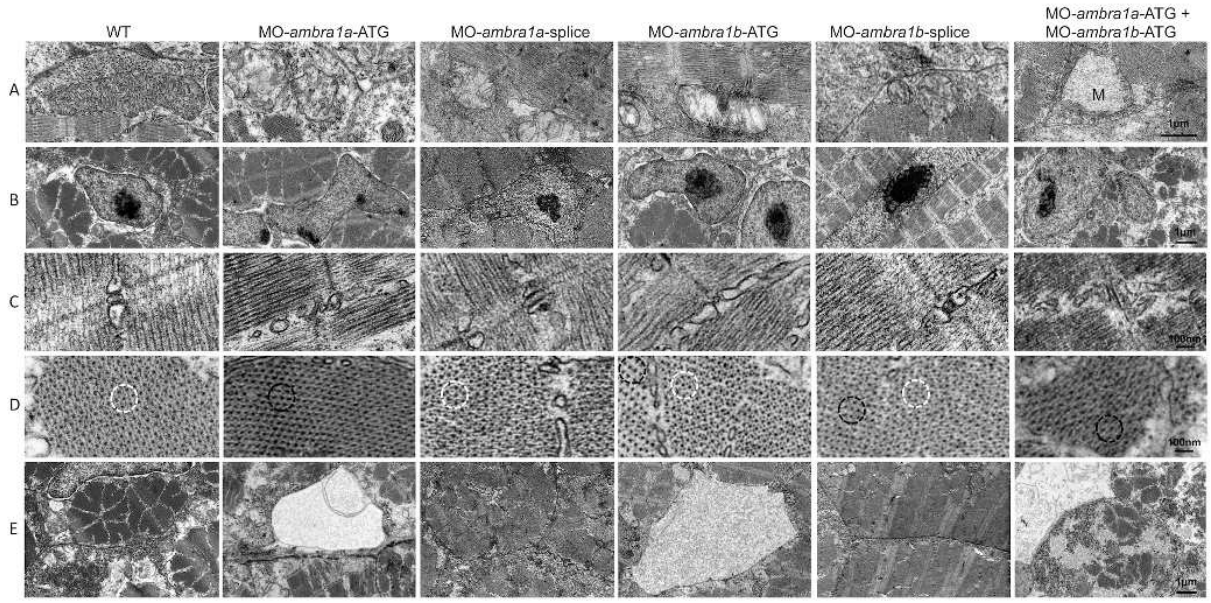

Figure 8. Ultrastructural analysis of *ambra1* morphants muscles reveals disorganized subcellular structures. When compared to WT and 5 m-control (not shown) embryos, *ambra1* morphant embryos display alterations of mitochondria (row A), nuclei (row B) and triads (row C), perturbation of the hexagonal arrangement of thick and thin filaments (row D), and dilations of the endoplasmic reticulum (row E). Muscles of morphant embryos show the presence of areas with reduced thin filaments (black circles in row D) adjacent to more normal-appearing hexagonal structures (white circles in row D). Co-injected double morphant embryos show exacerbated defects of these structures, whereas defects are barely evident in splice-morphants.
doi:10.1371/journal.pone.0099210.g008

Ablation of *ambra1* affects both myofibers and myosepta

Next, to assess whether knockdown of *ambra1a* and *ambra1b* expression results in defective specification and patterning of slow and/or fast muscle fibers, we examined myosin thick filaments in *ambra1* knockdown embryos by immunostaining with the F59 and F310 antibodies, which label slow and fast myosin isoforms, respectively. Slow muscle fibers were still present after *ambra1* knockdown, although myofiber density appeared lower in *ambra1a* ATG-morphants and in co-injected embryos (Fig. 9). However, whereas in control embryos the thick filaments were nicely organized and the myotomal segments were V-shaped and regularly spaced, thick filaments in slow muscles of ATG-morphant embryos appeared highly disorganized, with wavy and twisted myofibrils. Moreover, the characteristic V-shaped appearance of the vertical myoseptum was almost completely absent. Some muscle fibers were missing or detached from the myosepta, generating cell-free spaces in ATG-morphants. Combined injection of both ATG-MOs exacerbated the phenotype. The phenotype was almost normal in *ambra1* splice-morphants, where myofibrils presented only a slightly wavy morphology (Fig. 9). A similar disruption in myofiber organization was also evident in fast muscles. In WT and 5 m-control embryos, the fast muscle fibers appeared relatively uniform in size and were regularly arranged in parallel rows. Conversely, in ATG-morphants fast muscle fibers displayed variable shapes and were highly disorganized, showing a dystrophic appearance with detachment and retraction of myofibers from the vertical myosepta forming the somite boundaries and with irregular and wavy myofibers morphology (Fig. 9). Interestingly, splice-morphants displayed a more evident phenotype in fast muscle fibers than in slow muscle fibers. These data indicated that although slow and fast muscle fibers were still present and in the correct positions within the somites, myofiber organization was disrupted.

To further evaluate the myosepta defects suggested by the morphological analysis, we performed whole-mount immunofluorescence with an anti-Laminin antibody. Myotomes of ATG- and co-injected morphants embryos displayed an abnormal U-shape appearance, with myosepta presenting frequent interruptions of the structure, whereas myosepta appeared normal in control-MOs, as well as in splice-MOs injected embryos (Fig. 9).

Defects on both myofibers and myosepta morphology and organization were rescued by co-injection with human *AMBRA1* mRNA (Fig. 9).

Skeletal muscles in *Ambra1*$^{gt/gt}$ mouse embryos display morphological defects

To obtain further insight into the role of Ambra1 during muscle development, we investigated skeletal muscles from *Ambra1*$^{gt/gt}$ mutant mice, which bear a gene trap insertion in the *Ambra1* gene [11]. We first analyzed muscle morphology by haematoxylin-eosin staining in E13.5 mouse embryos, when differentiation of muscles is not yet complete and myogenic cells are undergoing fusion to form myofibers. In WT E13.5 mouse embryos, the structure of the developing muscles appeared normal, and myofibers were well organized and aligned to generate the ordered structure of the muscle, with many nuclei already localized at the periphery (Fig. 10A, upper panels). In *Ambra1*$^{gt/gt}$ E13.5 mouse embryos, skeletal muscles were formed but the three-dimensional tissue architecture was less organized (Fig. 10A, lower panels). The abnormal structure of developing muscles in *Ambra1*$^{gt/gt}$ embryos may be due to a failure in completing muscle development or to a delay in myofiber maturation. This was also supported by the presence of many immature myofibers displaying centrally located

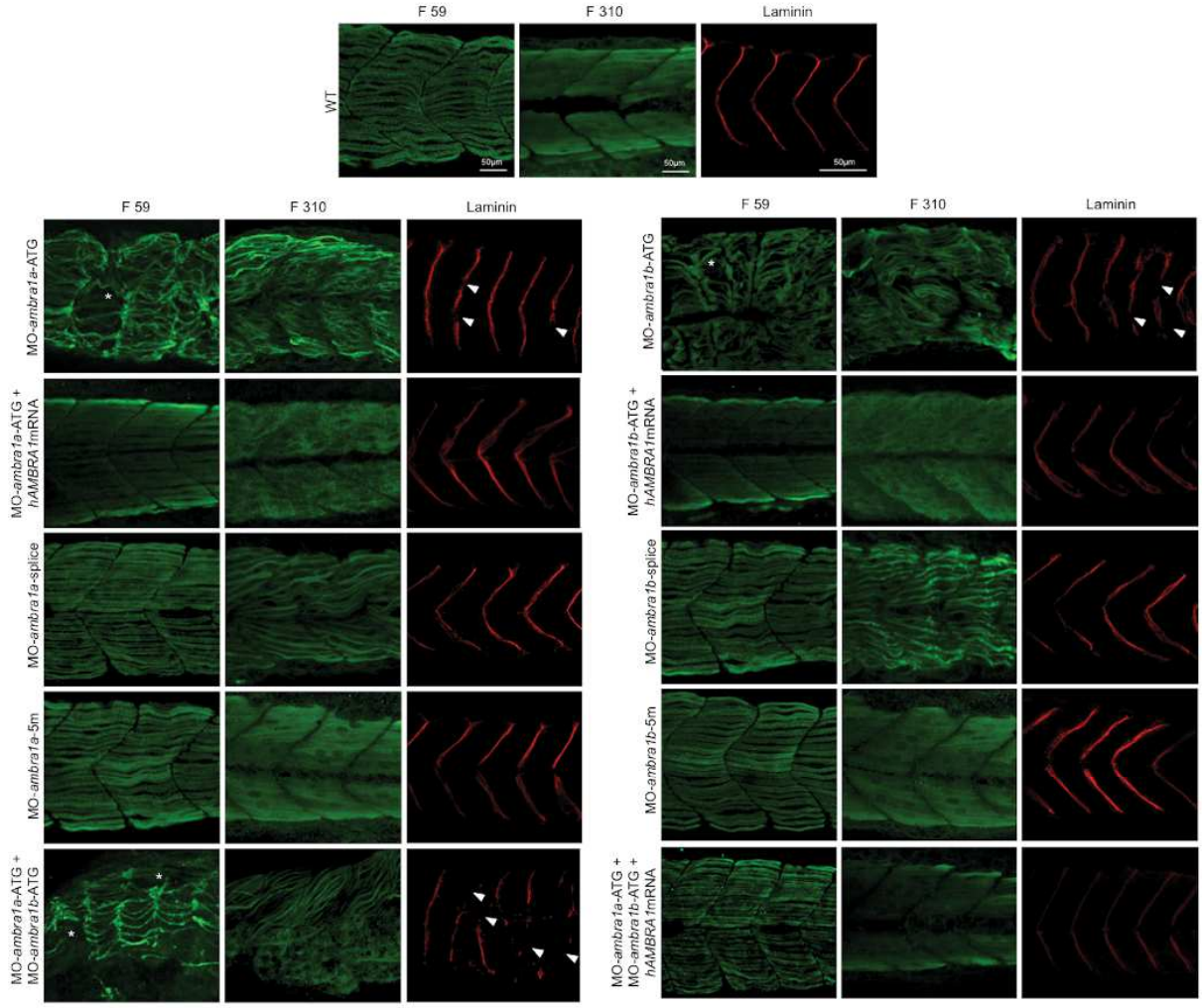

Figure 9. Knockdown of *ambra1* interferes with myosin organization in slow and fast muscles and with myosepta. Lateral views of 3 dpf embryos labeled with the F59 antibody (slow muscle fibers) and with the F310 antibody (fast muscle fibers), showing abnormally organized myofilaments in ATG-morphant embryos when compared to WT and 5 m-control embryos. Slow fibers are thinner in ATG-morphant embryos, whereas fast fibers of splice-morphant embryos display a wavy phenotype, visibly different from controls. The asterisks indicate broken or missing muscle fibers. Laminin labeling highlights the loss of the V-shape arrangement of somites and reveals interrupted myosepta (arrowheads) in ATG-morphant embryos. Defects in myosin organization and myosepta structure are rescued with the by co-injection with human *AMBRA1* mRNA. Anterior is to the left and dorsal up.
doi:10.1371/journal.pone.0099210.g009

nuclei in *Ambra1*$^{gt/gt}$ embryos (Fig. 10A, lower panels). These features, which were present in all muscles of *Ambra1*$^{gt/gt}$ embryos we analyzed, are clearly exemplified by the developing tongue. In WT E13.5 embryos, tongue showed a well-defined array of parallel myofibers distinctly organized in the three different planes of the developing intrinsic tongue muscles (Fig. 10B, upper panels). Conversely, in *Ambra1*$^{gt/gt}$ E13.5 embryos, the tongue displayed a general disorganization of the developing muscles and myofibers were less defined. In addition, there was a marked increase of cell density in the whole muscle tissue of *Ambra1*$^{gt/gt}$ embryos (Fig. 10B, lower panels). Similar morphological and cellular alterations were present in the developing dorsal and limb muscles of *Ambra1*$^{gt/gt}$ embryos, which also showed a noticeable increase of the interstitial connective tissue (Fig. 10C, D).

Discussion

In this work we used targeted protein depletion approaches to investigate the involvement of Ambra1 in muscle development. The severe phenotypes displayed by zebrafish *ambra1a/ambra1b* morphants and mouse *Ambra1*$^{gt/gt}$ embryos suggest a key role for Ambra1 in myogenesis. Our analysis on muscles of *ambra1a* and *ambra1b* zebrafish morphants was mainly focused on 3 dpf embryos, as at this stage muscles are fully developed. Our data indicate that ablation of Ambra1 leads to a severe myopathy with structural and functional defects of skeletal muscles, characterized by a marked reduction of myofiber density, abnormal orientation and decreased alignment of myofibers, disorganization of sarcomeres, alterations of the tubulo-reticular network and abnormal mitochondria morphology. The reduced locomotor activity of *ambra1a/ambra1b* zebrafish morphants, as well as the myofiber and

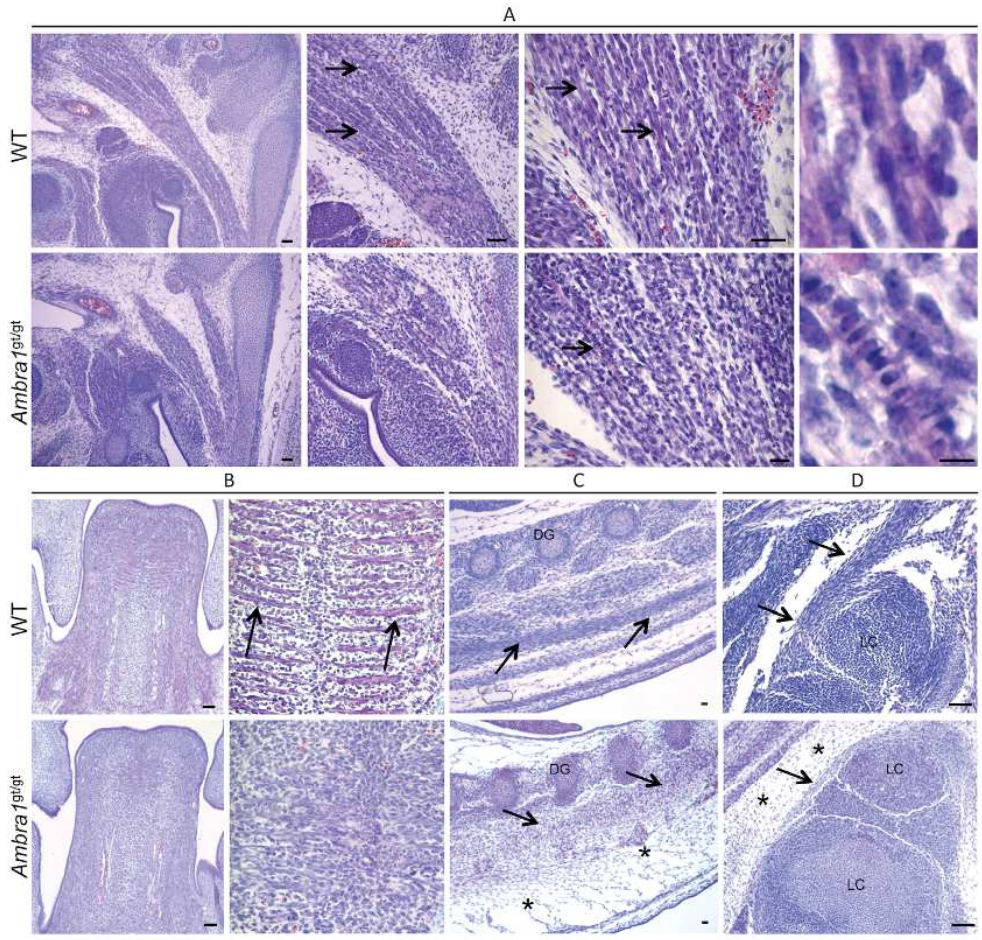

Figure 10. Morphological alteration of skeletal muscles in *Ambra*$^{gt/gt}$ mouse embryos. Representative pictures of skeletal muscles from WT and *Ambra1*$^{gt/gt}$ E13.5 mouse embryos, following haematoxylin-eosin staining. (**A**) Details of neck muscle. WT embryos display several well-organized and mature myofibers (black arrows), which have myonuclei already localized at the edge of the cell (right panel). In *Ambra1*$^{gt/gt}$ embryos, the muscle is much more immature, with poorly organized myofibers displaying centrally located nuclei (black arrows). (**B**) Details of the tongue. In WT embryos, myofiber are formed and well-organized (arrows), whereas in *Ambra1*$^{gt/gt}$ embryos there is a general disorganization of muscle architecture. (**C**, **D**) Representative pictures of dorsal (C) and limb (D) muscles (black arrows). *Ambra1*$^{gt/gt}$ embryos show abnormal muscle organization, together with a marked thickening of the connective tissue (black asterisks). All the analyzed muscles also display a noticeable increase of cell density in *Ambra1*$^{gt/gt}$ embryos. Scale bar, 50 μm.
doi:10.1371/journal.pone.0099210.g010

myosepta defects, were rescued by co-injection with human *AMBRA1* mRNA, thus confirming that these defects are caused by Ambra1 depletion and pointing at the conservation of Ambra1 functions during evolution. Although a role for Ambra1 in skeletal muscle was never proposed before now, our findings are in agreement with other recent studies indicating that autophagy plays a key role in skeletal muscles, as shown by the myopathic phenotype of *Atg5* and *Atg7* muscle-specific knockout mice [3,4] and by the connection between autophagy deregulation and muscular dystrophies [5–9].

In zebrafish, transcripts for both *ambra1* genes are present as maternal RNAs in the eggs and display a gradual decline until 8 hpf, being replaced by zygotic mRNAs from 12 hpf onwards [14]. To verify a possible role of these proteins in the early stages of skeletal muscle development, the commitment to the myogenic fate was analysed by WMISH for *myoD1*, whose expression normally begins in the adaxial cells prior to somite formation [23,24]. These cells, after migrating laterally through the somites, form the slow muscle cells [25], whereas those remaining near to the notochord form the muscle pioneer cells [26]. Later, *myoD1* expression takes place in the posterior half of each newly formed somite, giving rise to the fast muscle fibers [25]. Knockdown of zebrafish *ambra1* genes led to marked changes of *myoD1* expression, resulting in a reduced *myoD1* signal and a widening of the space between the bilateral adaxial cells of ATG-morphant embryos. At later stages, somites present a broad-shaped and non-homogeneous *myoD1* expression in ATG-morphant embryos. Interestingly, expression of *shh*, a gene coding for a secreted signalling protein implicated in the commitment of muscle precursors (reviewed in [15,26]), was also found to be abnormal in *Ambra1*$^{gt/gt}$ mouse embryos [11], as well as in zebrafish *ambra1* ATG-morphant embryos, resulting in notochord waving [14]. Depletion of Ambra1 proteins in zebrafish did not prevent the specification and differentiation of slow and fast muscle fibers, but clearly interfered with myofibrillogenesis leading to an anomalous pattern of both fiber types. As different levels, along with range and

timing, of Shh signalling specify different muscle subtypes [27,28], the displaced expression of this morphogen could explain the disorganization of the *ambra1*-morphant muscle fibers.

The changes in *myoD1* and *shh* expression, together with the reduced locomotor activity, observed in *ambra1* morphants occur at very early developmental stages, when embryonic cells are likely not yet competent for autophagy, e.g. the biological process in which Ambra1 has a well-established role. Actually, autophagy can be observed in zebrafish embryos starting from 32 hpf [29], and thus relatively late compared with the onset of the muscle developmental defects. Interestingly, *ambra1* depletion seems to interfere with the gene expression program responsible for correct muscle development, as suggested by the displaced expression of *shh* [14] and of *myoD1*, however it is still unclear whether these effects are related to Ambra1 pro-autophagic roles. On the other side, *ambra1* morphant embryos were also found to display reduced autophagy, as measured by immunoblot analysis for lipidated LC3 at 2 dpf [14]. A decreased activity of the autophagic process was also suggested by the lower incidence of puncta in muscle fibers isolated from zebrafish embryos expressing a hsp701:Lc3-RFP reporter plasmid.

Pax7 is a key regulator for myogenic progenitor cells in all vertebrates and Pax7-positive cells are already aligned along the vertical and horizontal myosepta at 2 dpf during zebrafish development [30]. In *ambra1* morphant embryos, the regular arrangement of Pax7-positive cells was disturbed and these also occurred in the spaces between myosepta, thus confirming the disorganization of somites. Although a significant increase of Pax7-positive cells was found in zebrafish with dystrophic phenotypes [30,31], our analysis did not reveal any obvious difference in the number of these cells between control and *ambra1* morphant embryos, This result seems to contrast with the apparently higher proliferation rate seen in *ambra1* morphants both by haematoxylin/eosin staining and by immunofluorescence for phosphorylated histone H3. However, this apparent discrepancy may be explained by a higher proliferation of fibroblasts, as also suggested by muscles of *Ambra1*$^{gt/gt}$ mouse embryos showing a conspicuous thickening of the interstitial connective tissue.

As for a number of other genes, the zebrafish ortholog of mammalian *Ambra1* gene is present as two duplicated paralogs coding for functional proteins. Although knockdown of one of these two paralogous genes is sufficient to alter muscle structure, the more severe phenotype of embryos deficient for both *ambra1* paralogs suggests that the two proteins not only work in similar biological process but also play distinct roles, thus justifying the retention of both genes as functional in the zebrafish genome after the fish-specific whole-genome duplication [32]. Notably, knockdown of only zygotic *ambra1a* and *ambra1b* transcripts by means of splice-MOs resulted in less severe muscle developmental defects, indicating the importance of maternally supplied *ambra1* transcripts and of the corresponding proteins in early embryonic development. Interestingly, and at difference from other parameters, splice-morphants showed a remarkably stronger phenotype than ATG-morphants with regard to fast fiber development, a finding that is in agreement with the different timing of slow and fast fiber differentiation [33]. Since fast fibers differentiate after slow fibers, the process in this case could be more affected by the silencing of zygotic transcripts because maternal transcript would be no longer available at that stage.

A number of recent studies indicated that autophagy plays important physiological and pathological roles in mature and fully developed skeletal muscles (reviewed in [34,35]). Our data, obtained from *ambra1a* and *ambra1b* zebrafish morphant embryos and from *Ambra1*$^{gt/gt}$ mouse embryos, indicate that this autophagy related-protein plays a critical and evolutionally conserved function during skeletal muscle development. In both animal models, ablation of Ambra1 leads to abnormal muscle morphogenesis. Ambra1 is critical not only for the correct architecture and maturation of myofibers, but it seems also implicated in cell proliferation control. Our data suggest a new function for Ambra1 during muscle biogenesis. While the presence of abnormal organelles is likely associated to the well-established role of Ambra1 in autophagy regulation, the altered morphology and the hypercellularity of the developing skeletal muscles may be due to a different function of Ambra1. Further studies will be needed to fully elucidate the functional roles of Ambra1 in the developing and postnatal skeletal muscles, in order to understand how this protein contributes to muscle homeostasis and identify possible human muscle pathologies linked to Ambra1 mutations.

Supporting Information

Figure S1 Schematic diagram showing the exon-intron structure of zebrafish *ambra1a* (A) and *ambra1b* (B) genes. The localization of known domains in the corresponding proteins is also indicated. The partial sequences of the abnormally spliced *ambra1a* and *ambra1b* transcripts, following targeting with the splice-MOs, highlights the loss of exon 3 (arrow) causing a codon frameshift and the introduction of a premature stop codon.
(TIF)

Figure S2 Percentage of dead, abnormal and normal 3 dpf embryos after injection with the different MOs.
(TIF)

Figure S3 Quantification of chorion hatching in 72 hpf embryos after injection with the different MOs.
(TIF)

Figure S4 Quantification of touch-evoked response and circular movement at 3 dpf. Embryos were quantified in three independent microinjections, and the number of embryos for each microinjection experiments was about 80.
(TIF)

Figure S5 Analysis of the number of mitotic cells present in the same six somites region of 10 embryos of each category. Data are presented as the mean ±SEM. ***, $P<0.001$.
(TIF)

Figure S6 Fluorescence detection in muscle fibers of control and *ambra1* morphant embryos following transfection with a Lc3-RFP reporter construct. Several fluorescent puncta have been detected in the transfected muscle fibers from WT and 5m-morphant embryos whereas only few puncta were visibile in ATG-morphant embryos.
(TIF)

Acknowledgments

The authors wish to acknowledge Dr. Michel Bagnat (Department of Cell Biology, Duke University Medical Center, Durham, NC) for providing hsp70l:Lc3-RFP plasmid, Dr. Gianfranco Bellipanni (Department of Biology, College of Science and Technology, Temple University, Philadelphia, PA) for providing *myoD1* plasmid and L. Pivotti and Dr. M. Milanetto for their valuable assistance in the fish facility.

Author Contributions

Conceived and designed the experiments: PB FC LDV TS PG. Performed the experiments: TS FB PG SC MC GM. Analyzed the data: TS PG VC SDB LDV. Wrote the paper: LDV PB FC TS.

References

1. Levine B, Kroemer G (2008) Autophagy in the pathogenesis of disease. Cell 132: 27–42.
2. Mizushima N, Komatsu M (2011) Autophagy: renovation of cells and tissues. Cell 147: 728–741.
3. Raben NV, Hill L, Shea S, Takikita R, Baum N, et al. (2008) Suppression of autophagy in skeletal muscle uncovers the accumulation of ubiquitinated proteins and their potential role in muscle damage in Pompe disease. Hum Mol Genet 17: 3897–3908.
4. Masiero E, Agatea L, Mammucari C, Blaauw B, Loro E, et al. (2009) Autophagy is required to maintain muscle mass. Cell Metab 10: 507–515.
5. Grumati P, Coletto L, Sabatelli P, Cescon M, Angelin A, et al. (2010) Autophagy is defective in collagen VI muscular dystrophies, and its reactivation rescues myofiber degeneration. Nat Med 16: 1313–1320.
6. Carmignac V, Svensson M, Körner Z, Elowsson L, Matsumura C, et al. (2011) Autophagy is increased in laminin α2 chain-deficient muscle and its inhibition improves muscle morphology in a mouse model of MDC1A. Hum Mol Genet 20: 4891–4902.
7. De Palma C, Morisi F, Cheli S, Pambianco S, Cappello V, et al. (2012) Autophagy as a new therapeutic target in Duchenne muscular dystrophy. Cell Death Dis 15: e418.
8. Choi JC, Muchir A, Wu W, Iwata S, Homma S, et al. (2012) Temsirolimus activates autophagy and ameliorates cardiomyopathy caused by lamin A/C gene mutation. Sci Transl Med 4: 144ra102.
9. Ramos FJ, Chen SC, Garelick MG, Dai DF, Liao CY, et al. (2012) Rapamycin reverses elevated mTORC1 signaling in lamin A/C-deficient mice, rescues cardiac and skeletal muscle function, and extends survival. Sci Transl Med 4: 144ra103.
10. Cullup T, Kho AL, Dionisi-Vici C, Brandmeier B, Smith F, et al. (2012) Recessive mutations in EPG5 cause Vici syndrome, a multisystem disorder with defective autophagy. Nat Genet 45: 83–87.
11. Fimia GM, Stoykova A, Romagnoli A, Giunta L, Di Bartolomeo S, et al. (2007) Ambra1 regulates autophagy and development of the nervous system. Nature 447: 1121–1125.
12. Fimia GM, Corazzari M, Antonioli M, Piacentini M (2013) Ambra1 at the crossroad between autophagy and cell death. Oncogene 32: 3311–3318.
13. Di Bartolomeo S, Corazzari M, Oliverio S, Nazio F, Lisi G, et al. (2010) The dynamic interaction of Ambra1 with the dynein motor complex regulates mammalian autophagy. J Cell Biol 191: 155–168.
14. Benato F, Skobo T, Gioacchini G, Moro I, Ciccosanti F, et al. (2013) Ambra1 knockdown in zebrafish leads to incomplete development due to severe defects in organogenesis. Autophagy 9: 476–495.
15. Jackson HE, Ingham PW (2013) Control of muscle fibre-type diversity during embryonic development: the zebrafish paradigm. Mech Dev 130: 447–457.
16. Gibbs EM, Horstick EJ, Dowling JJ (2013) Swimming into prominence: the zebrafish as a valuable tool for studying human myopathies and muscular dystrophies. FEBS J 280: 4187–4197.
17. Kimmel CB, Ballard WW, Kimmel SR, Ullmann B, Schilling TF (1995) Stages of embryonic development of the zebrafish. Dev Dyn 203: 253–310.
18. Westerfield M (1995) The Zebrafish Book. A Guide for the Laboratory Use of Zebrafish (Danio rerio), 3rd Edition. Eugene, OR, University of Oregon Press.
19. Thisse C, Thisse B (2008) High-resolution in situ hybridization to whole-mount zebrafish embryos. Nat Protoc 3: 59–69.
20. Dolez M, Nicolas JF, Hirsinger E (2011) Laminins, via heparan sulfate proteoglycans, participate in zebrafish myotome morphogenesis by modulating the pattern of Bmp responsiveness. Development 138: 97–106.
21. Ellis K, Bagwell J, Bagnat M (2013) Notochord vacuoles are lysosome-related organelles that function in axis and spine morphogenesis. J Cell Biol 200: 667–679.
22. Nord H, Nygård Skalman L, von Hofsten J (2013) Six1 regulates proliferation of Pax7-positive muscle progenitors in zebrafish. J Cell Sci 126: 1868–1880.
23. Coutelle O, Blagden CS, Hampson R, Halai C, Rigby PW, et al. (2001) Hedgehog signalling is required for maintenance of myf5 and myoD expression and timely terminal differentiation in zebrafish adaxial myogenesis. Dev Biol 236: 136–150.
24. Weinberg ES, Allende ML, Kelly CS, Abdelhamid A, Murakami T, et al. (1996) Developmental regulation of zebrafish MyoD in wild-type, no tail and spadetail embryos. Development 122: 271–280.
25. Devoto SH, Melançon E, Eisen JS, Westerfield M (1996) Identification of separate slow and fast muscle precursor cells in vivo, prior to somite formation. Development 122: 3371–3380.
26. Ochi H, Westerfield M (2007) Signaling networks that regulate muscle development: lessons from zebrafish. Dev Growth Differ 49: 1–11.
27. Du SJ, Devoto SH, Westerfield M, Moon RT (1997) Positive and negative regulation of muscle cell identity by members of the hedgehog and TGF-beta gene families. J Cell Biol 139: 145–156.
28. Wolff C, Roy S, Ingham PW (2003) Multiple muscle cell identities induced by distinct levels and timing of hedgehog activity in zebrafish embryos. Curr Biol 13: 1169–1181.
29. He C, Bartholomew CR, Zhou W, Klionsky DJ (2009) Assaying autophagic activity in transgenic GFP-Lc3 and GFP-Gabarap zebrafish embryos. Autophagy 5: 520–526.
30. Seger C, Hargrave M, Wang X, Chai RJ, Elworthy S, et al. (2011) Analysis of Pax7 expressing myogenic cells in zebrafish muscle development, injury, and models of disease. Dev Dyn 240: 2440–2451.
31. Berger J, Berger S, Hall TE, Lieschke GJ, Currie PD (2010) Dystrophin-deficient zebrafish feature aspects of the Duchenne muscular dystrophy pathology. Neuromuscul Disord 20: 826–832.
32. Postlethwait J, Amores A, Cresko W, Singer A, Yan YL (2004) Subfunction partitioning, the teleost radiation and the annotation of the human genome. Trends Genet 20: 481–490.
33. Blagden CS, Currie PD, Ingham PW, Hughes SM (1997) Notochord induction of zebrafish slow muscle mediated by Sonic hedgehog. Genes Dev 11: 2163–2175.
34. Sandri M, Coletto L, Grumati P, Bonaldo P (2013) Misregulation of autophagy and protein degradation systems in myopathies and muscular dystrophies. J Cell Sci 126: 5325–5333.
35. Vainshtein A, Grumati P, Sandri M, Bonaldo P (2014) Skeletal muscle, autophagy, and physical activity: the ménage a trois of metabolic regulation in health and disease. J Mol Med 92: 127–137.

1.2. Autophagic impairment in a sarcopenic patient with rigid spine syndrome and *FHL1* mutation

Four-and-half LIM domain 1 (FHL1) is a protein highly expressed in skeletal and cardiac muscle (Brown *et al.*, 1999; Morgan and Madgwick, 1999). FHL1 is shown to be involved in different regulatory pathways of the skeletal muscle, such as myogenesis and fiber size determination (Lee *et al.*, 2012; Cowling *et al.*, 2008). Mutations in the *FHL1* gene are associated with several muscle diseases, including X-linked myopathy with postural muscle atrophy (XMPMA), reducing body myophathy (RBM) and rigid spine syndrome (RSS) (MA) (Bertrand *et al.*, 2014).

In the last part of my PhD, I contributed to the characterization of the autophagic defects in a patient displaying sarcopenia and rigid spine syndrome and bearing a missense mutation in the *FHL1* gene (p.C150R). Muscle biopsies from this patient showed FHL1-positive aggregates inside myofibers and near the myonuclei. To better evaluate the impact of these aggregates in the onset of the myopathy, I participated to the evaluation of the aggregates composition and to the biochemical analysis of autophagy markers in patients' biopsies. This analysis revealed that ubiquitinated proteins and p62 were increased in patient muscles when compared to unaffected muscle controls. Beclin 1 and Bnip3 protein content was also increased, together with a slight induction in LC3 lipidation. Interestingly, the aggregates detected in patient muscles contained nuclear fragmented material and were positive for p62 and LC3 staining, suggesting the involvement of an aggrephagy-like process in this pathological context.

These results highlight the important contribution of a selective autophagy pathway in the pathogenesis of the myopathy linked to *FHL1* p.C150R mutation.

frontiers in
AGING NEUROSCIENCE

ORIGINAL RESEARCH ARTICLE
published: 19 August 2014
doi: 10.3389/fnagi.2014.00215

Aggresome–autophagy involvement in a sarcopenic patient with rigid spine syndrome and a p.C150R mutation in *FHL1* gene

Patrizia Sabatelli[1,2], Silvia Castagnaro[3], Francesca Tagliavini[1,2], Martina Chrisam[3], Francesca Sardone[1,2], Laurence Demay[4], Pascale Richard[5], Spartaco Santi[1,2], Nadir M. Maraldi[1], Luciano Merlini[2], Marco Sandri[6,7] and Paolo Bonaldo[3]*

[1] Institute of Molecular Genetics, CNR-National Research Council of Italy, Bologna, Italy
[2] SC Laboratory of Musculoskeletal Cell Biology, Rizzoli Orthopedic Institute, Bologna, Italy
[3] Department of Molecular Medicine, University of Padova, Padova, Italy
[4] UF Cardiogénétique et Myogénétique, Service de Biochimie Métabolique, Groupe Hospitalier Pitié-Salpêtrière, Paris, France
[5] UF Cardiogénétique et Myogénétique, Centre de Génétique, Hôpitaux Universitaires de la Pitié Salpêtrière, Paris, France
[6] Dulbecco Telethon Institute, Venetian Institute of Molecular Medicine, Padova, Italy
[7] Department of Biomedical Science, University of Padova, Padova, Italy

Edited by:
Emanuele Marzetti, Catholic University of the Sacred Heart, Italy

Reviewed by:
Heinz Jungbluth, King's College London, UK
Beril Talim, Hacettepe University, Turkey

***Correspondence:**
Paolo Bonaldo, Department of Molecular Medicine, University of Padova, Via U. Bassi 58/B, Padova I-35131, Italy
e-mail: bonaldo@bio.unipd.it

The four-and-half LIM domain protein 1 (FHL1) is highly expressed in skeletal and cardiac muscle. Mutations of the *FHL1* gene have been associated with diverse chronic myopathies including reducing body myopathy, rigid spine syndrome (RSS), and Emery–Dreifuss muscular dystrophy. We investigated a family with a mutation (p.C150R) in the second LIM domain of *FHL1*. In this family, a brother and a sister were affected by RSS, and their mother had mild lower limbs weakness. The 34-year-old female had an early and progressive rigidity of the cervical spine and severe respiratory insufficiency. Muscle mass evaluated by DXA was markedly reduced, while fat mass was increased to 40%. CT scan showed an almost complete substitution of muscle by fibro-adipose tissue. Muscle biopsy showed accumulation of FHL1 throughout the cytoplasm and around myonuclei into multiprotein aggregates with aggresome/autophagy features as indicated by ubiquitin, p62, and LC3 labeling. DNA deposits, not associated with nuclear lamina components and histones, were also detected in the aggregates, suggesting nuclear degradation. Ultrastructural analysis showed the presence of dysmorphic nuclei, accumulation of tubulofilamentous and granular material, and perinuclear accumulation of autophagic vacuoles. These data point to involvement of the aggresome–autophagy pathway in the pathophysiological mechanism underlying the muscle pathology of *FHL1* C150R mutation.

Keywords: myopathy, sarcopenia, FHL1, autophagy, protein aggregates

INTRODUCTION

Four-and-half LIM domain protein 1 (FHL1) is a cysteine-rich double zinc-finger protein encoded by the *FHL1* gene, localized on chromosome X (Dawid et al., 1995; Kadrmas and Beckerle, 2004). To date, three distinct FHL1 splicing isoforms have been identified (Brown et al., 1999; Morgan and Madgwick, 1999; Ng et al., 2001; Purcell et al., 2004; Johannessen et al., 2006; McGrath et al., 2006). FHL1A, also known as skeletal muscle LIM protein 1, is the full-length protein. FHL1B, or SLIMMER, is composed of the first three LIM domains and contains nuclear localization and export sequences and a RBP-J binding region. FHL1C, or KyoT2, is the shortest isoform, which contains only the first two LIM domains and a RBP-J binding region and interacts with PIAS1 (Taniguchi et al., 1998; Wang et al., 2007).

Four-and-half LIM domain protein 1 is highly expressed in skeletal and cardiac muscles (Lee et al., 1998; Brown et al., 1999; Greene et al., 1999; Morgan and Madgwick, 1999), where it localizes in the myofibrillar sarcomeres and in the sarcolemma (Bertrand et al., 2014). This protein has been demonstrated to be involved in several processes, including cellular architecture (McGrath et al., 2003, 2006), myoblast differentiation (Lee et al., 2012), mechanotransduction (Sheikh et al., 2008), and myofiber size (Cowling et al., 2008). FHL1 binds signaling and cytoskeletal proteins as well as transcription factors, acting as a transcriptional regulator of nuclear factor of activated T cells (NFATc1) to enhance the expression of genes that increase myofiber size (Cowling et al., 2008).

Mutations in the *FHL1* gene are responsible for a number of muscular disorders, which exhibit a broad spectrum of clinical features and disease severity ranging from severe childhood onset to milder adult-onset disorders. The diseases described so far include X-linked myopathy with postural muscle atrophy (XMPMA) (Windpassinger et al., 2008), reducing body myopathy (RBM) (Schessl et al., 2009; Shalaby et al., 2009; Selcen et al., 2011; Schreckenbach et al., 2013), X-linked dominant scapuloperoneal myopathy (Quinzii et al., 2008; Chen et al., 2010), rigid spine syndrome (RSS) (Shalaby et al., 2008), hypertrophic cardiomyopathy (Friedrich et al., 2012), and Emery–Dreifuss muscular dystrophy

(Gueneau et al., 2009; Knoblauch et al., 2010). RBM is characterized by the presence of intracellular protein aggregates called "reducing bodies (RBs)" mainly containing mutated FHL1 protein, cytoskeletal and intermediate filament proteins, and components of the unfolded protein response pathway (Liewluck et al., 2007). Although scapuloperoneal myopathy, XMPMA, RSS, hypertrophic cardiomyopathy, and Emery–Dreifuss muscular dystrophy share some overlapping clinical features and muscle pathology with RBM, the involvement of protein aggregation in these disorders remains unclear (Wilding et al., 2014).

Reducing bodies morphologically resemble aggresomes, structures proposed to facilitate the sequestration, and degradation of toxic misfolded proteins. Non-functional, damaged, and/or misfolded proteins are removed from the cell by the ubiquitin proteasome system. However, when the capacity of the proteasome is impaired or overwhelmed, polyubiquitinated misfolded proteins cannot be properly cleared and accumulate into the aggresome (Goldberg, 2003; Kawaguchi et al., 2003). Accumulating evidence suggests that aggresomes are substrates for autophagy. Autophagy is a degradation pathway that mediates bulk clearance of cytosolic proteins and organelles by the lysosome in a highly regulated process involving the coordinated actions of a large number of autophagy-related (Atg) genes. In response to particular stimuli, such as proteasomal dysfunction, an isolation membrane forms and expands to sequester portions of cytoplasm into double membrane structures called autophagosomes. The autophagosomes eventually fuse with lysosomes and their contents are degraded by lysosomal hydrolases. One hypothesis is that aggresomes may concentrate aggregated proteins for more efficient autophagic degradation (Bjorkoy et al., 2005, 2006; Iwata et al., 2005). Recent evidence indicates that aggresome formation is mediated by dynein/dynactin-mediated transport of misfolded proteins to the centrosome and involves several regulators, including the E3 ubiquitin-protein ligase parkin (Olzmann et al., 2008). Aggresome clearance is mediated by ubiquitin-binding proteins such as p62/SQSTM1 (Kirkin et al., 2009), an adaptor protein that decides the fate of protein degradation either through the ubiquitin proteasome system or the autophagy–lysosome pathway (Komatsu et al., 2007; Kirkin et al., 2009; Komatsu and Ichimura, 2010). Here, we report evidence of aggresome and autophagy involvement in the muscle of a sarcopenic patient with RSS and p.C150R mutation in the *FHL1* gene.

MATERIALS AND METHODS

GENOTYPING

The six coding exons and introns boundaries of FHL1 (NM_001159702) were screened for mutations by PCR on DNA from peripheral lymphocytes using primer pairs with a universal sequence (Table on demand). Exon 5 was sequenced with primers:

5PUF: 5′—ACCGTTAGTATGCGAGTTGGATTCAGGCAC TGGATCCTA — 3′

5PUR: 5′—TCGGATAGTCAGTCGTTTGCTGTCGTGAGG ATGGAATG — 3′.

Analysis of sequences was done with SeqScape software (Applied Biosystem).

MUSCLE BIOPSY

Peroneal muscle biopsy of the 34-year-old female was performed after written informed consent, and approval was obtained from the Ethics Committee of the Rizzoli Orthopedic Institute. The muscle sample was frozen in melting isopentane and stored in liquid nitrogen.

HISTOCHEMISTRY AND IMMUNOHISTOCHEMICAL ANALYSIS

Standard histochemical study was performed, and congophilic deposits were identified by Congo red staining (Bioptica) following the manufacturer's instructions. Cytochrome oxidase activity was assessed by conventional method. Acridine-orange staining was performed as previously reported (Darzynkiewicz, 1994). For double staining with menadione–nitro blue tetrazolium and anti-FHL1 antibodies, 10 μm-thick frozen sections were incubated with menadione-NBT solution in Gomori-Tris-HCl buffer at pH 7.4, without the addition of α-glycerophosphate substrate (Brooke and Neville, 1972), followed by incubation with anti-FHL1 antibody (Aviva System) and TRITC conjugated anti-rabbit secondary antibody (DAKO). Seven micrometer-thick non-fixed frozen sections were incubated with antibodies against laminin α2 chain, collagen VI, parkin (Millipore), desmin, developmental myosin heavy chain (d-MHC), fast myosin heavy chain, dystrophin (DYS1, DYS2, and DYS3 antibodies), emerin, lamin A/C (Novocastra), LC3 (Novus Biologicals), p62 (Progen Biotechnik), pericentrin, α-B-crystallin (Abcam), ubiquitin (Santa Cruz Biotechnologies), and histones (Chemicon), and revealed with FITC or TRITC conjugated anti-rabbit, anti-mouse, or anti-guinea pig secondary antibodies. Samples were stained with DAPI, mounted with anti-fading reagent (Molecular Probes), and observed with a Nikon epifluorescent/light microscope.

CONFOCAL IMAGING

The confocal imaging was performed with a A1-R confocal laser scanning microscope (Nikon), equipped with a Nikon 60×, 1.4 NA objective, and with a 488 and 561 nm laser lines to excite FITC (green) and TRITC (red) fluorescence signals. The 3D images were processed by stacking up 20–25 consecutive confocal images with surface shaded reconstruction. No deconvolution was applied to the images.

TRANSMISSION ELECTRON MICROSCOPY

Muscle biopsy was fixed with 2.5% glutaraldehyde in 0.1 M cacodylate buffer pH 7.4 for 3 h at 4°C, post-fixed with 1% osmium tetroxide in cacodylate buffer for 2 h, dehydrated in an ethanol series, infiltrated with propylene oxide and embedded in Epon 812 resin. Ultrathin sections were stained with uranyl acetate and lead citrate (Reynolds) and examined under a Philips EM400 operating at 100 kV.

WESTERN BLOTTING

Twenty micrometer-thick frozen sections were cut from the muscle biopsy of a healthy individual and of the proband patient. Sections were taken from two different portions of the patient muscle biopsy (referred as P_a and P_b). Muscle sections were lysed in 150 μl lysis buffer (50 mM Tris, pH 7.5, 150 mM NaCl, 10 mM $MgCl_2$, 1 mM EDTA, 10% glycerol, 0.5 mM DTT, 2%

sodium dodecyl sulfate, 1% Triton X-100) supplemented with phosphatase inhibitors (Sigma-Aldrich) and protease inhibitors (Roche), heated at 70°C for 10 min and centrifuged at 16,100 g for 10 min at 4°C. The protein content of each lysate was determined by the BCA Protein Assay kit (Pierce) and 30 μg of total proteins were separated by SDS-PAGE (Invitrogen) and immunoblotted as previously described (Chen et al., 2014). Membranes were probed with primary antibodies against FHL1 (ab23937 Abcam), LC3 (Thermo Scientific), p62 (Progen Biotechnik), ubiquitin (Cell Signaling Technologies), beclin 1 (Cell Signaling), BNIP3 (Sigma), vinculin (Sigma), or GAPDH (Millipore). Proteins were revealed with anti-rabbit, -mouse (Bethyl), -goat (Santa Cruz Biotechnologies), or -guinea pig (Sigma) HRP-conjugated secondary antibodies using the ECL reagent (Pierce-Thermo Scientific). Densitometric quantification of protein bands was performed by the ImageJ software (US National Institute of Health). Western blotting and quantifications are representative of at least three independent experiments.

RESULTS

The proband is a 34-year-old woman who noticed the inability to extend the right thumb at age 20. Soon after, she manifested neck weakness and limitation of flexion. Progression of weakness was rapid and she started to have difficulty in climbing stairs and getting up from the floor. At age 24, she started falling several times while walking. At age 26, the patient lost ambulation and was wheelchair bound. Examination at age 34 showed an atrophic phenotype with marked diffuse muscle wasting and weakness and prominent contractures. She had normal facial muscle strength, a minimal residual motor function in the elbow extensors and in the right biceps, but was profoundly weak in all the other muscles. She revealed marked contractures involving proximal and distal joints. The most striking contractures were in the neck muscles causing a fixed hyperextended neck that was also impossible to move in any direction. She showed a progressive decline in the respiratory function with a forced vital capacity 59% of predicted at age 25, 45% at age 27, and 13% at age 34. She refused to undergo mechanical ventilation. Cardiac investigation, including echocardiography and Holter, revealed no cardiac involvement. Muscle CT showed that all muscles were atrophic and substituted by fat and connective tissue, including the axial muscles, with a minimal sparing of the rectus femoris and vastus lateralis on the left, and of the peroneus on the right (**Figure 1A**). She was underweight (BMI = 17.1). However, according to her body composition, as revealed by DXA, she was sarcopenic/obese (appendicular lean body mass index of 3.27 kg/m^2 and total body fat of 44.4%) (Baumgartner et al., 2004). Her brother had a similar atrophic phenotype with marked rigidity of the spine and diffuse contractures but with more rapid progression, as he lost ambulation at age 18 and underwent tracheostomy at age 28. Their mother at age 58 had a mild lower limbs weakness and no contractures.

Sequencing of the *FHL1* gene in the index case identified a single missense mutation c.448T > C in exon 5 resulting in the replacement at codon 150 of a cysteine residue with an arginine residue (p.Cys150Arg). Nucleotide c.448 and residue p.150 of the *FHL1* gene are highly conserved among species and evolution, and all prediction softwares conclude for a pathogenic mutation. Analysis of the family showed that her brother and mother also have the same *FHL1* mutation.

Muscle biopsy showed fiber size variability, numerous internal nuclei, and increased endomysial and perimysial tissue. Several muscle fibers showed menadione-NBT positive aggregates, consistent with the presence of RBs (**Figure 1B**). RBs were devoid of oxidative enzyme activity and displayed an intense congophilia, indicative of the presence of amyloid deposits. Immunohistochemistry with FHL1 antibody revealed the presence of protein aggregates in about 20% of muscle fibers. Consistent with previous reports (Selcen et al., 2011; Feldkirchner et al., 2013; Bertrand et al., 2014), FHL1 deposits were detected throughout the cytoplasm and around myonuclei. Double staining with menadione-NBT revealed that FHL1 deposits strongly correlated with RBs, although with a more diffuse pattern. Desmin and α-B-crystallin (not shown) were strongly up-regulated in affected muscle fibers but they did not co-localize with FHL1 deposits (**Figure 1** and data not shown). Sarcolemmal components, such as dystrophin and laminin α2, were not detected in RBs; collagen VI was increased in the endomysium and perimysium, possibly as a consequence of active fibrosis (data not shown).

Reducing bodies displayed aggresome features as indicated by association with ubiquitin and with the luminal endoplasmic reticulum chaperone Grp78, in agreement with a previous work (Wilding et al., 2014). Consistent with aggresome formation, parkin, an E3 ubiquitin ligase involved in retrograde transport of misfolded proteins to centrosome (Garcia-Mata et al., 1999), and pericentrin, a marker of centrosome, were increased in affected myofibers (**Figure 2A**). Western blot analysis showed a patient-specific increase of ubiquitin (**Figure 2B**), confirming the massive presence of aberrant ubiquitinated proteins. Western blotting for FHL1 in the soluble fraction of patient muscle biopsy showed no significant change of FHL1 protein levels with respect to the control (**Figure 2C**).

Confocal imaging revealed a clear co-localization of FHL1 with p62 labeling (**Figure 2D**). FHL1/p62-positive aggregates also stained with DAPI, indicating the presence of nuclear material. Interestingly, DAPI-positive structures were not surrounded by nuclear lamina, as indicated by the absence of lamin A/C (**Figure 3A**) and emerin (not shown). In addition, DAPI-positive structures did not associate with histones (**Figure 3B**) and displayed an intense red fluorescence when stained with acridine orange (**Figure 3C**), a metachromatic dye that differentially stains double-stranded DNA and single-stranded DNA or RNA. Notably, DNase treatment strongly reduced the acridine-orange staining (**Figure 3D**). Altogether, these data suggest that FHL1/p62 aggregates also include single-stranded DNA, possibly due to nuclear degradation.

Recent studies have suggested that aggresomes are substrates for autophagy (Yao, 2010). LC3 immunolabeling on the patient muscle biopsy revealed the presence of autophagosomes in proximity of p62 aggregates (**Figure 4A**), suggesting the involvement of the autophagic pathway in aggresome clearance. Moreover, analysis of the protein levels of several autophagic markers showed a strong accumulation of p62, confirming the presence of an elevated number of aggresomes (**Figures 4B,C**). Notably, Beclin 1 and BNIP3, two well-known positive regulators of autophagy, were

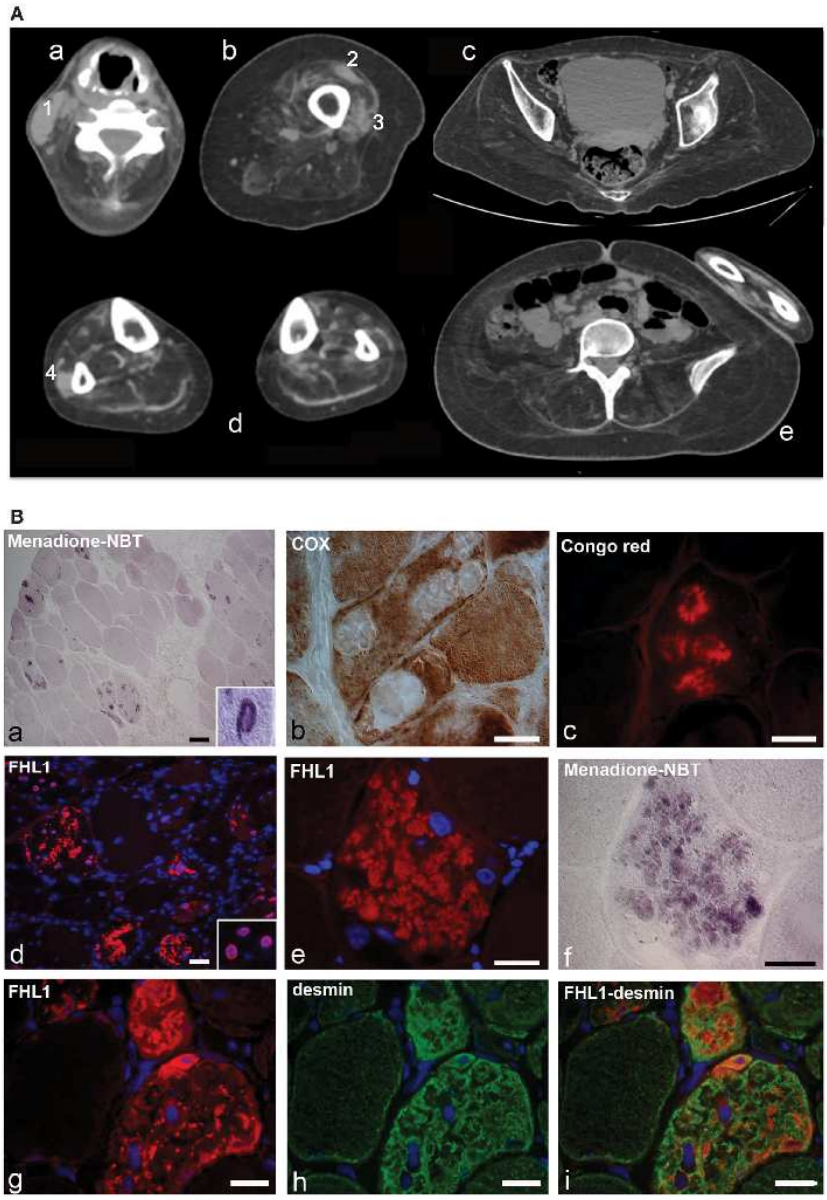

FIGURE 1 | (A) Patient with FHL1 mutation: index case. Muscle CT imaging of the neck (a), left thigh (b), pelvis (c), lower legs (d), and abdominal (e) muscles. In the neck, there is a relative preservation of the left sternocleidomastoideus (1) and almost complete involvement of all the other muscles (a). In the left thigh, only the rectus femoris (2) and vastus lateralis (3) are relatively spared (b). In the pelvis (c) and in the abdomen (e), there is a marked degeneration of all muscles. In the lower legs, only the peroneus (4) of the right leg is relatively spared (d). **(B)** Histochemistry and immunohistochemical analysis of patient muscle biopsy. Cross-sections show the presence of RBs in several muscle fibers, as revealed by menadione-NBT staining (a). Granular deposits are detectable at the nuclear rim of some myonuclei (a, inset). RBs appear devoid of oxidative activity (cytochrome oxidase, COX in b) and display affinity to Congo red staining (c). Immunofluorescence analysis of FHL1 shows protein accumulation throughout the cytoplasm of several muscle fibers (d) and around myonuclei (d, inset). FHL1 immunolabeling (e), followed by menadione-NBT staining (f), demonstrates that FHL1 accumulates in RBs (f). Double labeling for FHL1 and desmin (g–i) shows a marked increase of desmin in FHL1-accumulating myofibers. Scale bar, 20 μm.

strongly increased in the patient biopsy, indicating that autophagy induction is taking place, likely in response to the need of clearing the accumulating aggregates. This was further confirmed by the slight increase of LC3 lipidation observed in the patient biopsy (**Figures 4B,C**). All together, these data indicate that autophagy is strongly induced in the muscle biopsy from the patient.

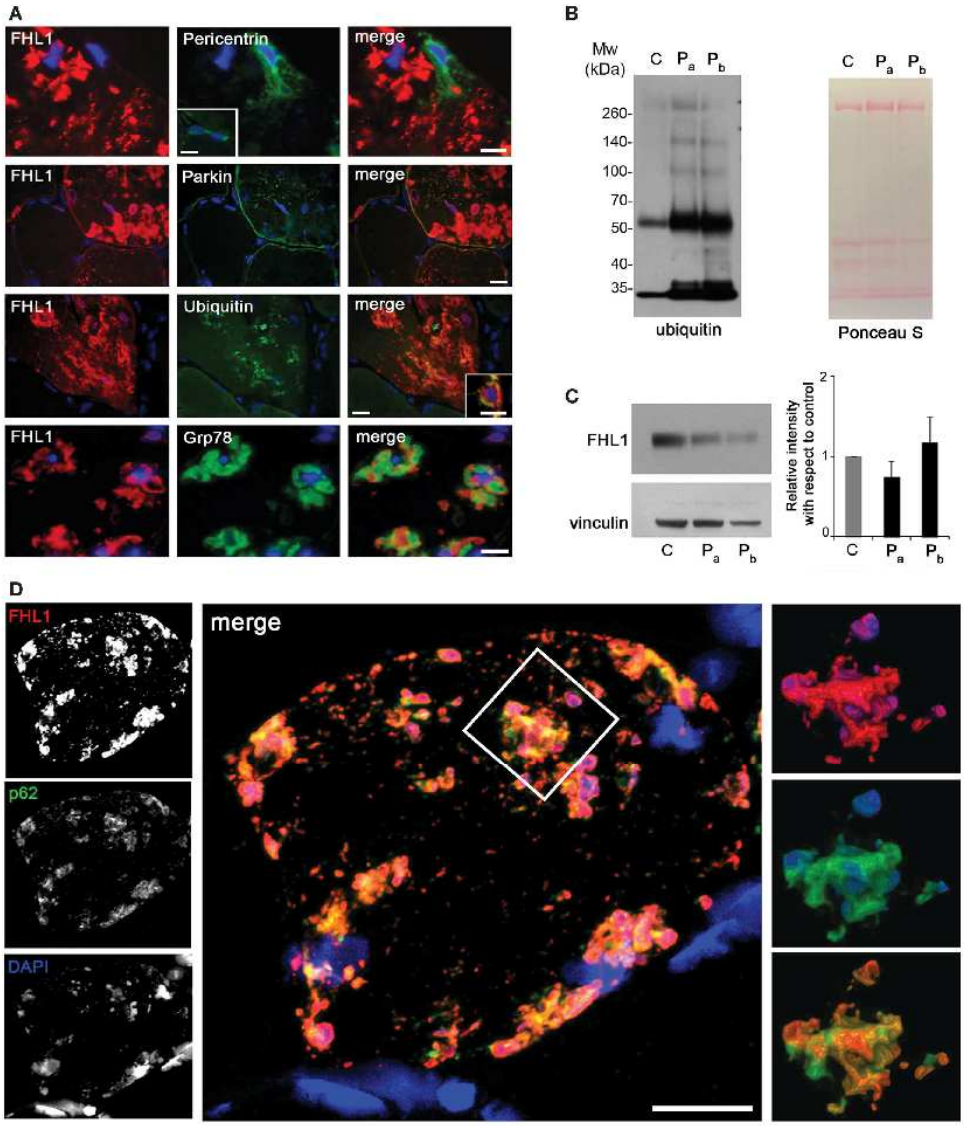

FIGURE 2 | (A) Double labeling of FHL1 with pericentrin, parkin, ubiquitin, and Grp78 in cross-sections of patient muscle biopsy. Scale bar, 20 μm. **(B)** Western blot analysis for ubiquitin in total protein extracts from muscle biopsies derived from a healthy donor **(C)** and from the patient (two different fragments of the index case biopsy, P_a and P_b). Increased reactivity for ubiquitin is clearly detectable in patient extracts. Ponceau S staining is shown as loading control. **(C)** Western blot analysis for FHL1 and vinculin in total protein extracts from muscle biopsies derived from a healthy donor **(C)** and from the index case (P_a and P_b). Quantification of the FHL1 protein level showing the relative western blot intensity with respect to control. Densitometric quantification was performed by three independent western blot experiments ($P > 0.05$, P_a and P_b vs C). **(D)** Confocal immunofluorescence imaging of the patient muscle biopsy labeled with FHL1 antibody (red), p62 antibody (green), and DAPI (blue). The maximum intensity projections of the single channels (white) are shown on the left, the merged image of confocal projections are shown in the middle, and the 3D surface shaded reconstruction of an enlargement of the area defined by the white box is shown on the right. Scale bar, 10 μm.

Ultrastructural analysis showed cytoplasmic bodies and tubulofilamentous material associated with nuclear alterations and autophagic vacuoles (**Figure 5**). Tubulofilamentous aggregates ranged from 14 to 1.2 nm. Dysmorphic nuclei showed condensed heterochromatin, ribonucleoprotein aggregates, enlarged nucleoli, and condensed granular material at the outer face of the nuclear cisterna. In addition, a reduced number of nuclear pores were also detected in nuclei with hypercondensed heterochromatin. Autophagic vacuoles, and in particular autophagolysosomes as indicated by the presence of a single membrane, were frequently

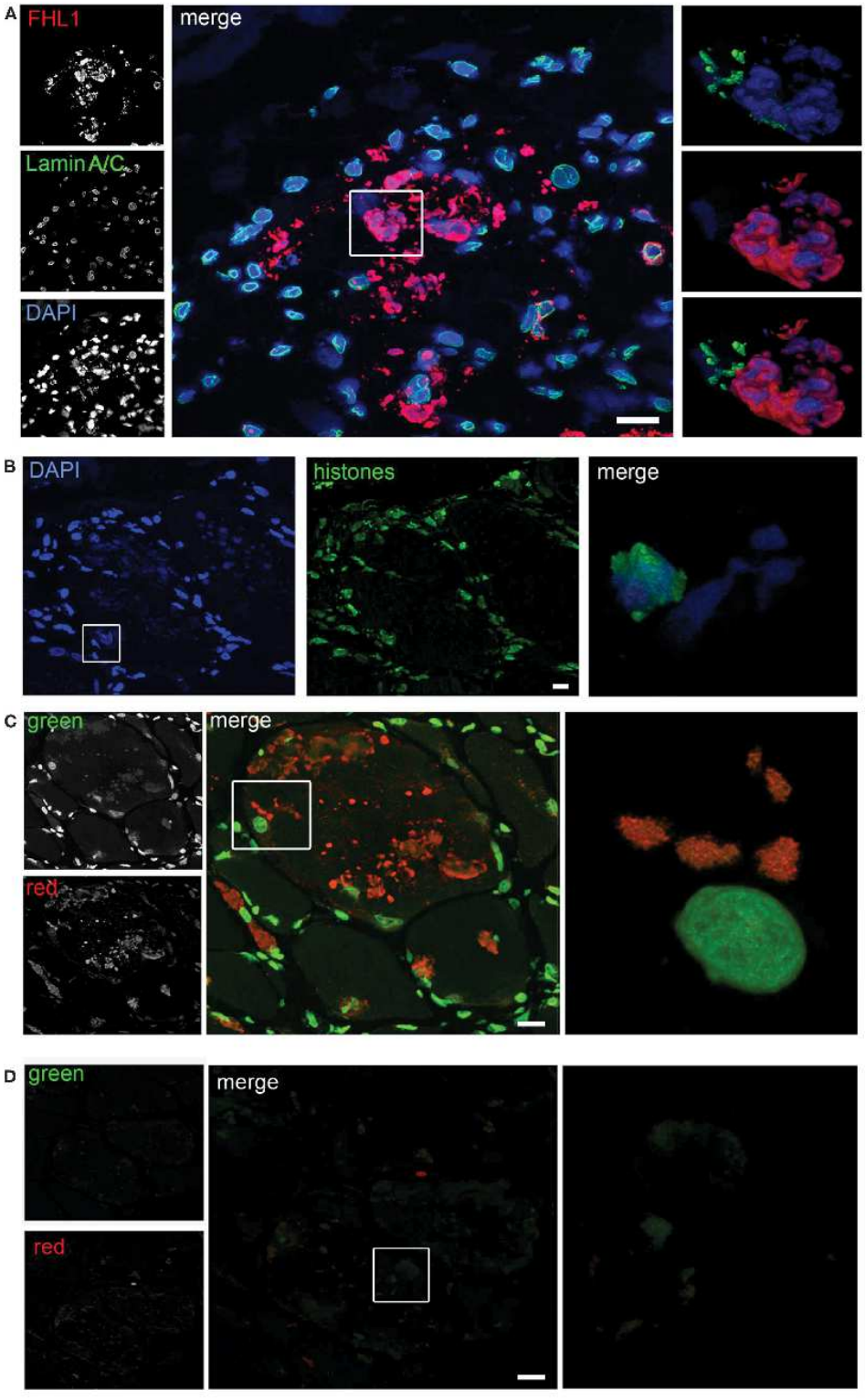

FIGURE 3 | Continued

FIGURE 3 | Continued
(A) Confocal immunofluorescence imaging of the patient muscle biopsy labeled with FHL1 antibody (red), lamin A/C antibody (green), and DAPI (blue). The maximum intensity projections of red and green channels (white) are shown on the left, the merged image of confocal projections are shown in the middle, and the 3D surface shaded reconstruction of an enlargement of the area defined by the white box is shown on the right. **(B)** Confocal immunofluorescence imaging of the patient muscle biopsy labeled with an anti-histones antibody (green) and DAPI (blue), together with 3D surface shaded reconstruction (merge). **(C)** Acridine-orange staining. The maximum intensity projections of the single channels (white) are shown on the left, the merged image of confocal projections are shown in the middle, and the 3D surface shaded reconstruction of an enlargement of the area defined by the white box is shown on the right. **(D)** Acridine-orange staining after DNase digestion on frozen sections of the patient's muscle biopsy showing that the treatment completely removed nuclear and RBs associated DNA. The maximum intensity projections of the red and green channels (white) are shown on the left, the merged image of confocal projections are shown in the middle, and the 3D surface shaded reconstruction of the area defined by box is shown on the right. Scale bar, 10 μm.

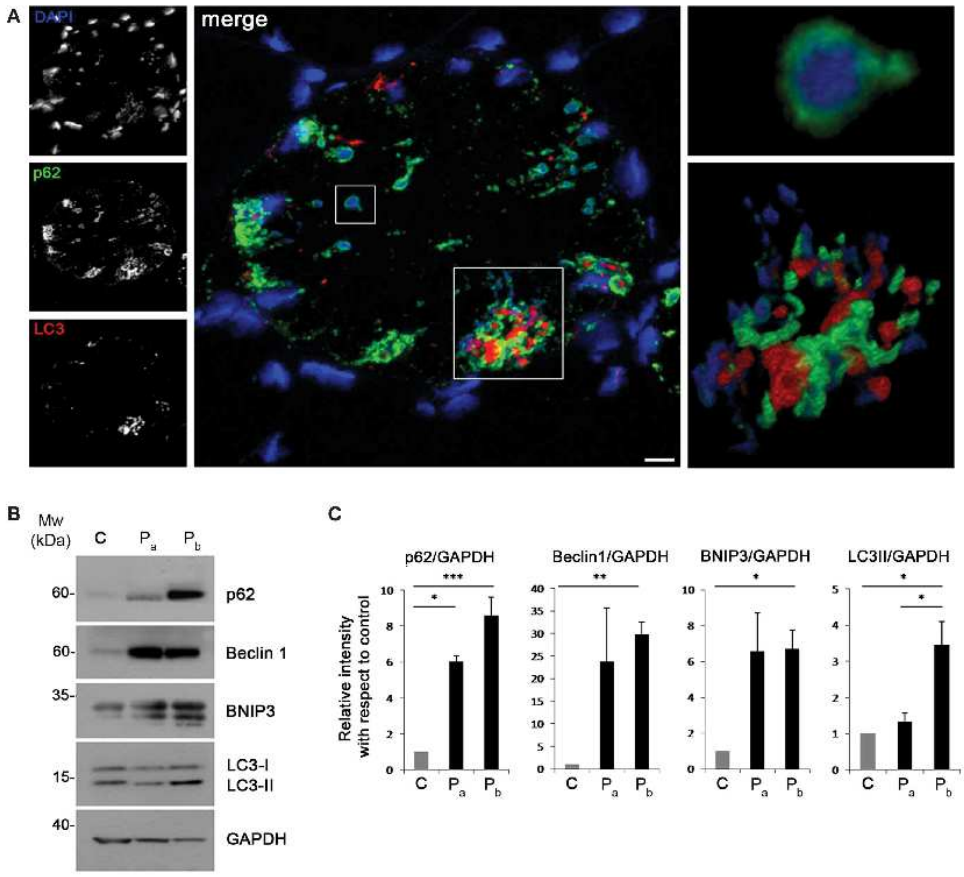

FIGURE 4 | (A) Confocal immunofluorescence imaging of the patient muscle biopsy labeled with LC3 antibody (red), p62 antibody (green), and DAPI (blue). The maximum intensity projections of the single channels (white) are shown on the left, the merged image of confocal projections are shown in the middle, and the 3D surface shaded reconstruction of an enlargement of the areas defined by the white boxes are shown on the right. Scale bar, 10 μm. **(B)** Western blot analysis for the autophagic markers LC3, Beclin 1, BNIP3, and p62 in muscle biopsies derived from a healthy donor **(C)** and from the index case (P_a and P_b). GAPDH was used as a loading control. **(C)** Quantification of the protein levels showing the relative western blot intensity with respect to control. Densitometric quantification was performed by three independent western blot experiments (***$P < 0.001$; **$P < 0.01$; *$P < 0.05$).

found in proximity of altered nuclei. Other inclusions consisted of myelinic bodies and aggregates of sarcoplasmic reticulum.

DISCUSSION

In this work, we provided data showing that aggresome and autophagy are involved in the pathophysiological defects underlying the muscle pathology of a sarcopenic patient with RSS and carrying a *FHL1* p.C150R mutation.

In our family, the female index case and her brother had a typical RSS (Moghadaszadeh et al., 2001). The p.C150R mutation has already been reported in patients with RSS (Schessl et al., 2010; Selcen et al., 2011). Interestingly, another female patient

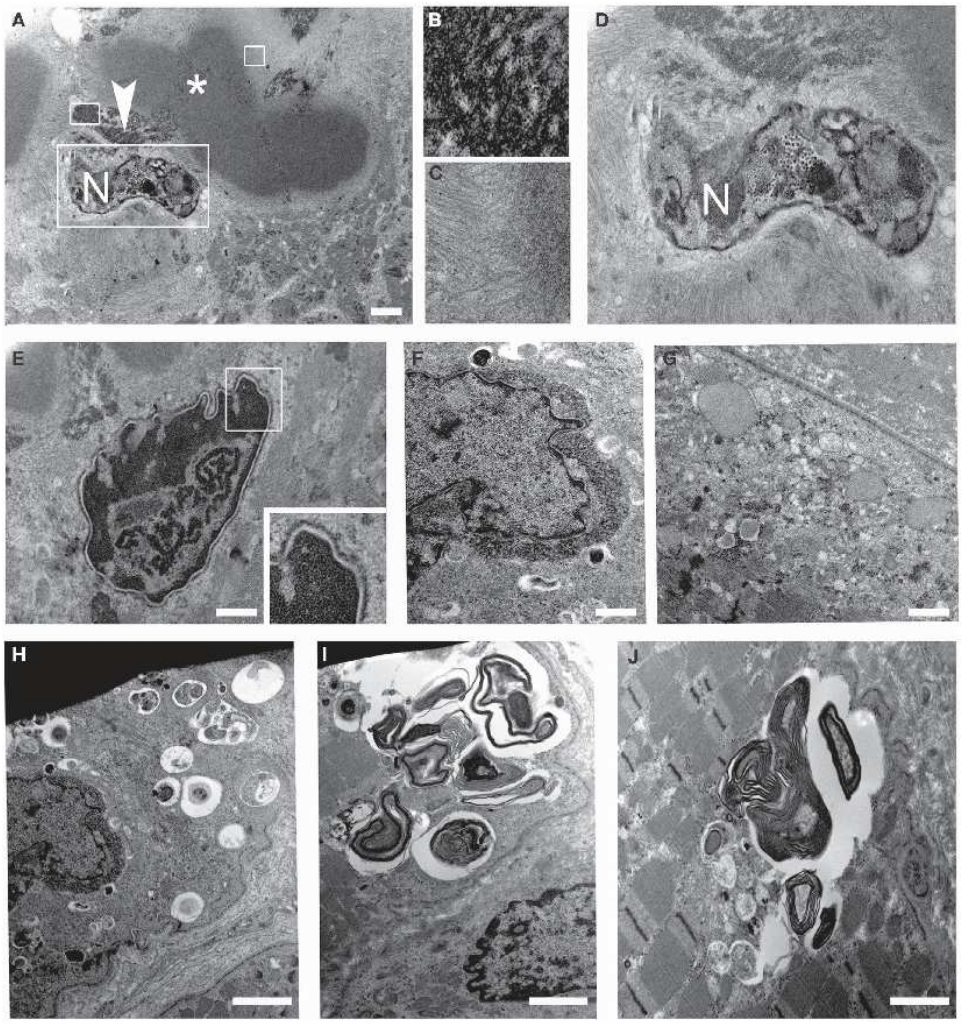

FIGURE 5 | Transmission electron microscopy of patient muscle biopsy. **(A–D)** Images showing cytoplasmic body (asterisk) and tubulofilamentous aggregates (arrowhead) close to degenerated nuclei (N). Higher magnification of the areas defined by boxes in **(A)** is shown in **(B–D)**. **(E,F)** Images showing altered nuclei with granular material accumulated at the nuclear rim. **(G)** Images showing dilated sarcoplasmic reticulum filled with amorphous material in a myofiber. **(H–J)** Images showing autophagic vacuoles and myelin figures close to nuclei and throughout some sarcomeres of muscle fibers. Scale bar, 500 nm.

(Selcen et al., 2011) presented extensor pollicis weakness, which was the first symptom noticed by our index case. Our patient had an atrophic phenotype. Underweight by body mass index, she was recognized to be sarcopenic-obese as determined by DXA given the marked reduction of lean body mass with relative increase of fat mass (Baumgartner et al., 2004). The sarcopenic condition was also reflected in the muscle CT that showed diffuse end stage degeneration. The brother of the index case had a severe progressive course; he lost ambulation at age 18, and underwent tracheostomy at age 28. In previously reported families, male patients were the most affected, while female carriers showed varying manifestations usually mild and some were asymptomatic (Schessl et al., 2010; Selcen et al., 2011). In our family, the two female patients had a very different course: severe and progressive in the index case and mild in her mother who was ambulant and without spine rigidity at age 58. Because of X chromosome inactivation, heterozygous women are mosaic for X-linked gene expression. This may explain the much milder phenotype in the mother compared with that of her daughter (Schessl et al., 2010; Selcen et al., 2011). The less affected mother was also much less atrophic, pointing to a possible differential activation of muscle atrophy pathways. However, no muscle biopsy of the mother was available, and X-inactivation studies were not performed in this family.

Muscle findings included menadione-NBT-positive aggregates, consistent with RBs, which also contained FHL1. The same *FHL1* mutation was previously reported in a family with RBM phenotype (Schessl et al., 2010) and in two patients with RBs and myofibrillar myopathy (Selcen et al., 2011). Also in those patients, the mutated FHL1 protein accumulated in RBs, pointing to a causative effect of this mutation in RB formation. The mutated cysteine residue localizes in the second LIM domain of the protein and it is expected to affect all FHL1 isoforms, i.e., full-length FHL1A and the shorter FHL1B and FHL1C polypeptides. Cys150 is a crucial coordinating residue in the second LIM domain (Michelsen et al., 1994) and mutations occurring at this site are predicted to induce protein misfolding. It has been proposed that the accumulation of misfolded FHL1 polypeptides results in the characteristic RB aggregates observed in muscle of RBM patients as well as in C2C12 myoblasts transfected with the mutant FHL1 protein (Schessl et al., 2008).

Aggresomes are structures proposed to facilitate the sequestration and degradation of toxic misfolded proteins. In agreement with previous reports (Bertrand et al., 2014), the RBs of the proband displayed characteristics of aggresomes, as indicated by the increase of proteins involved in aggresome formation and by the accumulation of ubiquitin, Grp78, p62, and cytoskeletal components, such as desmin and α-B-crystallin. Moreover, the FHL1-containing aggresomes were mainly accumulated around nuclei. It is well known that aggresome formation is mediated by the dynein/dynactin-mediated transport of misfolded proteins to the centrosome, as confirmed by the presence of aggresomes in the perinuclear region and matching with centrosome markers (Olzmann et al., 2008). In muscle cells, the centrosome undergoes redistribution at the nuclear rim during differentiation (Bugnard et al., 2005). This pattern persists in adult muscle (Srsen et al., 2009), as indicated by the localization of centrosome markers on the outer membrane of the nuclear cisterna. This peculiar positioning of the centrosome at the nuclear rim of muscle cells accounts for the recruitment of granular material with aggresome-like features we observed in nuclei of the *FHL1* mutated muscle fibers. In addition, we found that nuclei with perinuclear granular material appeared dysmorphic, with dramatic changes of the nuclear envelope and hypercondensed heterochromatin. These data, in addition to the finding of single-stranded DNA in aggresomes, suggest that the aggresome accumulation at the nuclear rim may induce nuclear degradation. This hypothesis is consistent with the alterations of the nuclear envelope in cells containing inclusion bodies that were described in patients affected by Huntington disease and in transgenic mice expressing mutant huntingtin (Waelter et al., 2001).

We also found that Grp78, an endoplasmic reticulum chaperone up-regulated during the unfolded protein response, was strongly increased and associated to the FHL1 deposits in the proband muscle biopsy. This finding is in agreement with previous work showing increased expression of Grp78 and unfolded protein response in patients with RBM (Liewluck et al., 2007). However, the association of Grp78 with aggresomes may be also due to retrograde transport from the endoplasmic reticulum, as hypothesized by the formation of aggresome-like inclusion bodies induced by mutant huntingtin (Garcia-Mata et al., 2002).

The association of FHL1 with p62 we detected in the proband muscle biopsy indicates that the mutant FHL1 protein is targeted to degradative pathways. p62 is a multifunctional protein containing a number of protein–protein interaction motifs that are involved in protein aggregation and degradation (Moscat and Diaz-Meco, 2009a,b). It has been hypothesized that p62 may act as a critical ubiquitin chain-targeting factor that shuttles substrates for proteasomal degradation (Seibenhener et al., 2004). On the other hand, a role for p62 in aggregate formation for autophagic degradation was also hypothesized (Komatsu et al., 2007; Kirkin et al., 2009; Komatsu and Ichimura, 2010). The strong increase of Beclin 1 and BNIP3 levels we detected in the patient biopsy indicates that autophagy induction is taking place, likely to help the clearance of accumulating aggregates. This is further confirmed by the slight increase of LC3 lipidation and by the accumulation of LC3 deposits in proximity to aggresomes in the proband muscle. The presence of autophagic vacuoles and myelin figures further confirms the involvement of the autophagic pathway in the pathophysiological alterations of this patient. Interestingly, the presence of autophagosomes and autophagic vacuoles was also reported in muscle biopsies of RBM patients (Bertrand et al., 2014). It is also interesting to consider that FHL1 null mice, lacking global FHL1 expression and without aggregates accumulation, display susceptibility to autophagy, as indicated by increased LC3 lipidation in skeletal muscle (Domenighetti et al., 2014). These findings point to a causative role of FHL1 deficiency in autophagy activation, and indicate that activation of the autophagic pathway in FHL1-related myopathies may be a common pathophysiological mechanism, independent from the accumulation of protein aggregates. Although future studies of the autophagic flux in muscle cells from patients and animal models for FHL1 deficiency are needed in order to understand in detail how and to which extent deregulation of autophagy contributes to the pathogenesis of FHL1-related myopathies, our data demonstrate for the first time the coexistence of aggresomes and autophagy in the muscle biopsy of a patient with severe sarcopenia caused by p.C150R mutation in *FHL1*. These findings add new insights in delineating the altered mechanisms involved in the pathogenesis of *FHL1*-associated diseases.

ACKNOWLEDGMENTS

This work was supported by the Italian Ministry of Education, University and Research (FIRB RBAP10KCNS to Patrizia Sabatelli, and FIRB RBAP11Z3YA_003 to Paolo Bonaldo), and by "5 per mille" 2010 Rizzoli Orthopaedic Institute.

REFERENCES

Baumgartner, R. N., Wayne, S. J., Waters, D. L., Janssen, I., Gallagher, D., and Morley, J. E. (2004). Sarcopenic obesity predicts instrumental activities of daily living disability in the elderly. *Obes. Res.* 12, 1995–2004. doi:10.1038/oby.2004.250

Bertrand, A. T., Bonnemann, C. G., and Bonne, G. (2014). 199th ENMC international workshop: FHL1 related myopathies, June 7-9, 2013, Naarden, the Netherlands. *Neuromuscul. Disord.* 24, 453–462. doi:10.1016/j.nmd.2014.02.002

Bjorkoy, G., Lamark, T., Brech, A., Outzen, H., Perander, M., Overvatn, A., et al. (2005). p62/SQSTM1 forms protein aggregates degraded by autophagy and has a protective effect on huntingtin-induced cell death. *J. Cell Biol.* 171, 603–614. doi:10.1083/jcb.200507002

Bjorkoy, G., Lamark, T., and Johansen, T. (2006). p62/SQSTM1: a missing link between protein aggregates and the autophagy machinery. *Autophagy* 2, 138–139. doi:10.4161/auto.2.2.2405

Brooke, M. H., and Neville, H. E. (1972). Reducing body myopathy. *Neurology* 22, 829–840. doi:10.1212/WNL.22.8.829

Brown, S., Mcgrath, M. J., Ooms, L. M., Gurung, R., Maimone, M. M., and Mitchell, C. A. (1999). Characterization of two isoforms of the skeletal muscle LIM protein 1, SLIM1. Localization of SLIM1 at focal adhesions and the isoform slimmer in the nucleus of myoblasts and cytoplasm of myotubes suggests distinct roles in the cytoskeleton and in nuclear-cytoplasmic communication. *J. Biol. Chem.* 274, 27083–27091.

Bugnard, E., Zaal, K. J., and Ralston, E. (2005). Reorganization of microtubule nucleation during muscle differentiation. *Cell Motil. Cytoskeleton* 60, 1–13. doi:10.1002/cm.20042

Chen, D. H., Raskind, W. H., Parson, W. W., Sonnen, J. A., Vu, T., Zheng, Y., et al. (2010). A novel mutation in FHL1 in a family with X-linked scapuloperoneal myopathy: phenotypic spectrum and structural study of FHL1 mutations. *J. Neurol. Sci.* 296, 22–29. doi:10.1016/j.jns.2010.06.017

Chen, P., Cescon, M., Megighian, A., and Bonaldo, P. (2014). Collagen VI regulates peripheral nerve myelination and function. *FASEB J.* 28, 1145–1156. doi:10.1096/fj.13-239533

Cowling, B. S., Mcgrath, M. J., Nguyen, M. A., Cottle, D. L., Kee, A. J., Brown, S., et al. (2008). Identification of FHL1 as a regulator of skeletal muscle mass: implications for human myopathy. *J. Cell Biol.* 183, 1033–1048. doi:10.1083/jcb.200804077

Darzynkiewicz, Z. (1994). Simultaneous analysis of cellular RNA and DNA content. *Methods Cell Biol.* 41, 401–420. doi:10.1016/S0091-679X(08)61731-8

Dawid, I. B., Toyama, R., and Taira, M. (1995). LIM domain proteins. *C. R. Acad. Sci. III, Sci. Vie* 318, 295–306.

Domenighetti, A. A., Chu, P. H., Wu, T., Sheikh, F., Gokhin, D. S., Guo, L. T., et al. (2014). Loss of FHL1 induces an age-dependent skeletal muscle myopathy associated with myofibrillar and intermyofibrillar disorganization in mice. *Hum. Mol. Genet.* 23, 209–225. doi:10.1093/hmg/ddt412

Feldkirchner, S., Walter, M. C., Muller, S., Kubny, C., Krause, S., Kress, W., et al. (2013). Proteomic characterization of aggregate components in an intrafamilial variable FHL1-associated myopathy. *Neuromuscul. Disord.* 23, 418–426. doi:10.1016/j.nmd.2013.02.006

Friedrich, F. W., Wilding, B. R., Reischmann, S., Crocini, C., Lang, P., Charron, P., et al. (2012). Evidence for FHL1 as a novel disease gene for isolated hypertrophic cardiomyopathy. *Hum. Mol. Genet.* 21, 3237–3254. doi:10.1093/hmg/dds157

Garcia-Mata, R., Bebok, Z., Sorscher, E. J., and Sztul, E. S. (1999). Characterization and dynamics of aggresome formation by a cytosolic GFP-chimera. *J. Cell Biol.* 146, 1239–1254. doi:10.1083/jcb.146.6.1239

Garcia-Mata, R., Gao, Y. S., and Sztul, E. (2002). Hassles with taking out the garbage: aggravating aggresomes. *Traffic* 3, 388–396. doi:10.1034/j.1600-0854.2002.30602.x

Goldberg, A. L. (2003). Protein degradation and protection against misfolded or damaged proteins. *Nature* 426, 895–899. doi:10.1038/nature02263

Greene, W. K., Baker, E., Rabbitts, T. H., and Kees, U. R. (1999). Genomic structure, tissue expression and chromosomal location of the LIM-only gene, SLIM1. *Gene* 232, 203–207. doi:10.1016/S0378-1119(99)00125-0

Gueneau, L., Bertrand, A. T., Jais, J. P., Salih, M. A., Stojkovic, T., Wehnert, M., et al. (2009). Mutations of the FHL1 gene cause Emery-Dreifuss muscular dystrophy. *Am. J. Hum. Genet.* 85, 338–353. doi:10.1016/j.ajhg.2009.07.015

Iwata, A., Riley, B. E., Johnston, J. A., and Kopito, R. R. (2005). HDAC6 and microtubules are required for autophagic degradation of aggregated huntingtin. *J. Biol. Chem.* 280, 40282–40292. doi:10.1074/jbc.M508786200

Johannessen, M., Moller, S., Hansen, T., Moens, U., and Van Ghelue, M. (2006). The multifunctional roles of the four-and-a-half-LIM only protein FHL2. *Cell. Mol. Life Sci.* 63, 268–284. doi:10.1007/s00018-005-5438-z

Kadrmas, J. L., and Beckerle, M. C. (2004). The LIM domain: from the cytoskeleton to the nucleus. *Nat. Rev. Mol. Cell Biol.* 5, 920–931. doi:10.1038/nrm1499

Kawaguchi, Y., Kovacs, J. J., Mclaurin, A., Vance, J. M., Ito, A., and Yao, T. P. (2003). The deacetylase HDAC6 regulates aggresome formation and cell viability in response to misfolded protein stress. *Cell* 115, 727–738. doi:10.1016/S0092-8674(03)00939-5

Kirkin, V., Lamark, T., Sou, Y. S., Bjorkoy, G., Nunn, J. L., Bruun, J. A., et al. (2009). A role for NBR1 in autophagosomal degradation of ubiquitinated substrates. *Mol. Cell* 33, 505–516. doi:10.1016/j.molcel.2009.01.020

Knoblauch, H., Geier, C., Adams, S., Budde, B., Rudolph, A., Zacharias, U., et al. (2010). Contractures and hypertrophic cardiomyopathy in a novel FHL1 mutation. *Ann. Neurol.* 67, 136–140. doi:10.1002/ana.21839

Komatsu, M., and Ichimura, Y. (2010). Physiological significance of selective degradation of p62 by autophagy. *FEBS Lett.* 584, 1374–1378. doi:10.1016/j.febslet.2010.02.017

Komatsu, M., Waguri, S., Koike, M., Sou, Y. S., Ueno, T., Hara, T., et al. (2007). Homeostatic levels of p62 control cytoplasmic inclusion body formation in autophagy-deficient mice. *Cell* 131, 1149–1163. doi:10.1016/j.cell.2007.10.035

Lee, J. Y., Chien, I. C., Lin, W. Y., Wu, S. M., Wei, B. H., Lee, Y. E., et al. (2012). Fhl1 as a downstream target of Wnt signaling to promote myogenesis of C2C12 cells. *Mol. Cell. Biochem.* 365, 251–262. doi:10.1007/s11010-012-1266-2

Lee, S. M., Tsui, S. K., Chan, K. K., Garcia-Barcelo, M., Waye, M. M., Fung, K. P., et al. (1998). Chromosomal mapping, tissue distribution and cDNA sequence of four-and-a-half LIM domain protein 1 (FHL1). *Gene* 216, 163–170. doi:10.1016/S0378-1119(98)00302-3

Liewluck, T., Hayashi, Y. K., Ohsawa, M., Kurokawa, R., Fujita, M., Noguchi, S., et al. (2007). Unfolded protein response and aggresome formation in hereditary reducing-body myopathy. *Muscle Nerve* 35, 322–326. doi:10.1002/mus.20691

McGrath, M. J., Cottle, D. L., Nguyen, M. A., Dyson, J. M., Coghill, I. D., Robinson, P. A., et al. (2006). Four and a half LIM protein 1 binds myosin-binding protein C and regulates myosin filament formation and sarcomere assembly. *J. Biol. Chem.* 281, 7666–7683. doi:10.1074/jbc.M512552200

McGrath, M. J., Mitchell, C. A., Coghill, I. D., Robinson, P. A., and Brown, S. (2003). Skeletal muscle LIM protein 1 (SLIM1/FHL1) induces alpha 5 beta 1-integrin-dependent myocyte elongation. *Am. J. Physiol. Cell Physiol.* 285, C1513–C1526. doi:10.1152/ajpcell.00207.2003

Michelsen, J. W., Sewell, A. K., Louis, H. A., Olsen, J. I., Davis, D. R., Winge, D. R., et al. (1994). Mutational analysis of the metal sites in an LIM domain. *J. Biol. Chem.* 269, 11108–11113.

Moghadaszadeh, B., Petit, N., Jaillard, C., Brockington, M., Roy, S. Q., Merlini, L., et al. (2001). Mutations in SEPN1 cause congenital muscular dystrophy with spinal rigidity and restrictive respiratory syndrome. *Nat. Genet.* 29, 17–18. doi:10.1038/ng713

Morgan, M. J., and Madgwick, A. J. (1999). The LIM proteins FHL1 and FHL3 are expressed differently in skeletal muscle. *Biochem. Biophys. Res. Commun.* 255, 245–250. doi:10.1006/bbrc.1999.0179

Moscat, J., and Diaz-Meco, M. T. (2009a). p62 at the crossroads of autophagy, apoptosis, and cancer. *Cell* 137, 1001–1004. doi:10.1016/j.cell.2009.05.023

Moscat, J., and Diaz-Meco, M. T. (2009b). To aggregate or not to aggregate? A new role for p62. *EMBO Rep.* 10, 804. doi:10.1038/embor.2009.172

Ng, E. K., Lee, S. M., Li, H. Y., Ngai, S. M., Tsui, S. K., Waye, M. M., et al. (2001). Characterization of tissue-specific LIM domain protein (FHL1C) which is an alternatively spliced isoform of a human LIM-only protein (FHL1). *J. Cell. Biochem.* 82, 1–10. doi:10.1002/jcb.1110

Olzmann, J. A., Li, L., and Chin, L. S. (2008). Aggresome formation and neurodegenerative diseases: therapeutic implications. *Curr. Med. Chem.* 15, 47–60. doi:10.2174/092986708783330692

Purcell, N. H., Darwis, D., Bueno, O. F., Muller, J. M., Schule, R., and Molkentin, J. D. (2004). Extracellular signal-regulated kinase 2 interacts with and is negatively regulated by the LIM-only protein FHL2 in cardiomyocytes. *Mol. Cell. Biol.* 24, 1081–1095. doi:10.1128/MCB.24.3.1081-1095.2004

Quinzii, C. M., Vu, T. H., Min, K. C., Tanji, K., Barral, S., Grewal, R. P., et al. (2008). X-linked dominant scapuloperoneal myopathy is due to a mutation in the gene encoding four-and-a-half-LIM protein 1. *Am. J. Hum. Genet.* 82, 208–213. doi:10.1016/j.ajhg.2007.09.013

Schessl, J., Columbus, A., Hu, Y., Zou, Y., Voit, T., Goebel, H. H., et al. (2010). Familial reducing body myopathy with cytoplasmic bodies and rigid spine revisited: identification of a second LIM domain mutation in FHL1. *Neuropediatrics* 41, 43–46. doi:10.1055/s-0030-1254101

Schessl, J., Taratuto, A. L., Sewry, C., Battini, R., Chin, S. S., Maiti, B., et al. (2009). Clinical, histological and genetic characterization of reducing body myopathy caused by mutations in FHL1. *Brain* 132, 452–464. doi:10.1093/brain/awn325

Schessl, J., Zou, Y., Mcgrath, M. J., Cowling, B. S., Maiti, B., Chin, S. S., et al. (2008). Proteomic identification of FHL1 as the protein mutated in human reducing body myopathy. *J. Clin. Invest.* 118, 904–912. doi:10.1172/JCI34450

Schreckenbach, T., Henn, W., Kress, W., Roos, A., Maschke, M., Feiden, W., et al. (2013). Novel FHL1 mutation in a family with reducing body myopathy. *Muscle Nerve* 47, 127–134. doi:10.1002/mus.23500

Seibenhener, M. L., Babu, J. R., Geetha, T., Wong, H. C., Krishna, N. R., and Wooten, M. W. (2004). Sequestosome 1/p62 is a polyubiquitin chain binding protein

involved in ubiquitin proteasome degradation. *Mol. Cell. Biol.* 24, 8055–8068. doi:10.1128/MCB.24.18.8055-8068.2004

Selcen, D., Bromberg, M. B., Chin, S. S., and Engel, A. G. (2011). Reducing bodies and myofibrillar myopathy features in FHL1 muscular dystrophy. *Neurology* 77, 1951–1959. doi:10.1212/WNL.0b013e31823a0ebe

Shalaby, S., Hayashi, Y. K., Goto, K., Ogawa, M., Nonaka, I., Noguchi, S., et al. (2008). Rigid spine syndrome caused by a novel mutation in four-and-a-half LIM domain 1 gene (FHL1). *Neuromuscul. Disord.* 18, 959–961. doi:10.1016/j.nmd.2008.09.012

Shalaby, S., Hayashi, Y. K., Nonaka, I., Noguchi, S., and Nishino, I. (2009). Novel FHL1 mutations in fatal and benign reducing body myopathy. *Neurology* 72, 375–376. doi:10.1212/01.wnl.0000341311.84347.a0

Sheikh, F., Raskin, A., Chu, P. H., Lange, S., Domenighetti, A. A., Zheng, M., et al. (2008). An FHL1-containing complex within the cardiomyocyte sarcomere mediates hypertrophic biomechanical stress responses in mice. *J. Clin. Invest.* 118, 3870–3880. doi:10.1172/JCI34472

Srsen, V., Fant, X., Heald, R., Rabouille, C., and Merdes, A. (2009). Centrosome proteins form an insoluble perinuclear matrix during muscle cell differentiation. *BMC Cell Biol.* 10:28. doi:10.1186/1471-2121-10-28

Taniguchi, Y., Furukawa, T., Tun, T., Han, H., and Honjo, T. (1998). LIM protein KyoT2 negatively regulates transcription by association with the RBP-J DNA-binding protein. *Mol. Cell. Biol.* 18, 644–654.

Waelter, S., Boeddrich, A., Lurz, R., Scherzinger, E., Lueder, G., Lehrach, H., et al. (2001). Accumulation of mutant huntingtin fragments in aggresome-like inclusion bodies as a result of insufficient protein degradation. *Mol. Biol. Cell* 12, 1393–1407. doi:10.1091/mbc.12.5.1393

Wang, J., Qin, H., Liang, J., Zhu, Y., Liang, L., Zheng, M., et al. (2007). The transcriptional repression activity of KyoT2 on the Notch/RBP-J pathway is regulated by PIAS1-catalyzed SUMOylation. *J. Mol. Biol.* 370, 27–38. doi:10.1016/j.jmb.2007.04.010

Wilding, B. R., Mcgrath, M. J., Bonne, G., and Mitchell, C. A. (2014). FHL1 mutants that cause clinically distinct human myopathies form protein aggregates and impair myoblast differentiation. *J. Cell. Sci.* 127, 2269–2281. doi:10.1242/jcs.140905

Windpassinger, C., Schoser, B., Straub, V., Hochmeister, S., Noor, A., Lohberger, B., et al. (2008). An X-linked myopathy with postural muscle atrophy and generalized hypertrophy, termed XMPMA, is caused by mutations in FHL1. *Am. J. Hum. Genet.* 82, 88–99. doi:10.1016/j.ajhg.2007.09.004

Yao, T. P. (2010). The role of ubiquitin in autophagy-dependent protein aggregate processing. *Genes Cancer* 1, 779–786. doi:10.1177/1947601910383277

Conflict of Interest Statement: The authors declare that the research was conducted in the absence of any commercial or financial relationships that could be construed as a potential conflict of interest.

Received: 26 June 2014; paper pending published: 23 July 2014; accepted: 04 August 2014; published online: 19 August 2014.

*Citation: Sabatelli P, Castagnaro S, Tagliavini F, Chrisam M, Sardone F, Demay L, Richard P, Santi S, Maraldi NM, Merlini L, Sandri M and Bonaldo P (2014) Aggresome–autophagy involvement in a sarcopenic patient with rigid spine syndrome and a p.C150R mutation in FHL1 gene. Front. Aging Neurosci. **6**:215. doi: 10.3389/fnagi.2014.00215*

This article was submitted to the journal Frontiers in Aging Neuroscience.

References

Alexopoulos, L.G. et al., 2009. Developmental and osteoarthritic changes in Col6a1-knockout mice: biomechanics of type VI collagen in the cartilage pericellular matrix. *Arthritis and rheumatism*, 60(3), pp.771–9.

Allamand, V. et al., 2011. ColVI myopathies: where do we stand, where do we go? *Skeletal muscle*, 1(1), p.30.

Angelin, A. et al., 2007. Mitochondrial dysfunction in the pathogenesis of Ullrich congenital muscular dystrophy and prospective therapy with cyclosporins. *Proceedings of the National Academy of Sciences of the United States of America*, 104(3), pp.991–6.

Avivar-Valderas, A. et al., 2011. PERK integrates autophagy and oxidative stress responses to promote survival during extracellular matrix detachment. *Molecular and Cellular Biology*, 31(17), pp.3616–29.

Di Bartolomeo, S. et al., 2010. The dynamic interaction of AMBRA1 with the dynein motor complex regulates mammalian autophagy. *The Journal of cell biology*, 191(1), pp.155–68.

Benato, F. et al., 2013. Ambra1 knockdown in zebrafish leads to incomplete development due to severe defects in organogenesis. *Autophagy*, 9(4), pp.476–95.

Bernardi, P. & Bonaldo, P., 2008. Dysfunction of mitochondria and sarcoplasmic reticulum in the pathogenesis of collagen VI muscular dystrophies. *Annals of the New York Academy of Sciences*, 1147, pp.303–11.

Bertrand, A.T. et al., 2014. 199th ENMC international workshop: FHL1 related myopathies, June 7-9, 2013, Naarden, The Netherlands. *Neuromuscular Disorders*, 24(5), pp.453–462.

Bjørkøy, G., Lamark, T. & Johansen, T., 2006. p62/SQSTM1: A missing link between protein aggregates and the autophagy machinery. *Autophagy*, 2(2), pp.138–139.

Bonaldo, P. et al., 1998. Collagen VI deficiency induces early onset myopathy in the mouse: an animal model for Bethlem myopathy. *Human Molecular Genetics*, 7(13), pp.2135–40.

Bonaldo, P. et al., 1990. Structural and functional features of the alpha 3 chain indicate a bridging role for chicken collagen VI in connective tissues. *Biochemistry*, 29(5), pp.1245–54.

Bonaldo, P. & Sandri, M., 2013. Cellular and molecular mechanisms of muscle atrophy. *Disease Models & Mechanisms*, 6(1), pp.25–39.

Bönnemann, C.G., 2011. The collagen VI-related myopathies: muscle meets its matrix. Nature reviews. *Neurology*, 7(7), pp.379–90.

Booth, L. a. et al., 2014. The role of cell signaling in the crosstalk between autophagy and apoptosis. *Cellular Signaling*, 26(3), pp.549–555.

Boya, P., Reggiori, F. & Codogno, P., 2013. Emerging regulation and functions of autophagy. *Nature Cell Biology*, 15(7), pp.713–20.

Braghetta, P. et al., 2008. An enhancer required for transcription of the Col6a1 gene in muscle connective tissue is induced by signals released from muscle cells. *Experimental Cell Research*, 314(19), pp.3508–18.

Braghetta, P. et al., 1996. Distinct regions control transcriptional activation of the alpha1(VI) collagen promoter in different tissues of transgenic mice. *The Journal of cell biology*, 135(4), pp.1163–77.

Briñas, L. et al., 2010. Early onset collagen VI myopathies: Genetic and clinical correlations. *Annals of neurology*, 68(4), pp.511–20.

Brodsky, B. & Persikov, A. V, 2005. Molecular structure of the collagen triple helix. *Advances in protein chemistry*, 70, pp.301–39.

Brown, S. et al., 1999. The cardiac expression of striated muscle LIM protein 1 (SLIM1) is restricted to the outflow tract of the developing heart. *Journal of molecular and cellular cardiology*, 31(4), pp.837–43.

Buraschi, S. et al., 2013. Decorin causes autophagy in endothelial cells via Peg3. *Proceedings of the National Academy of Sciences of the United States of America*, 110(28), pp.E2582–91.

Burg, M. a et al., 1996. Binding of the NG2 proteoglycan to type VI collagen and other extracellular matrix molecules. *The Journal of biological chemistry*, 271(42), pp.26110–6.

Carmignac, V. et al., 2011. Autophagy is increased in laminin α2 chain-deficient muscle and its inhibition improves muscle morphology in a mouse model of MDC1A. *Human Molecular Genetics*, 20(24), pp.4891–902.

Castello-Cros, R. et al., 2011. Matrix remodeling stimulates stromal autophagy, “fueling” cancer cell mitochondrial metabolism and metastasis. *Cell Cycle*, 10(12), pp.2021–2034.

Chen, P., Cescon, M., Megighian, A., et al., 2014. Collagen VI regulates peripheral nerve myelination and function. *FASEB journal*, 28(3), pp.1145–56.

Chen, P., Cescon, M., Zuccolotto, G., et al., 2014. Collagen VI regulates peripheral nerve regeneration by modulating macrophage recruitment and polarization. *Acta neuropathologica*, 129, pp.97–113.

Chen, P.M., Gombart, Z.J. & Chen, J.W., 2011. Chloroquine treatment of ARPE-19 cells leads to lysosome dilation and intracellular lipid accumulation: possible implications of lysosomal dysfunction in macular degeneration. *Cell & bioscience*, 1(1), p.10.

Cheng, I.H. et al., 2011. Collagen VI protects against neuronal apoptosis elicited by ultraviolet irradiation via an Akt/phosphatidylinositol 3-kinase signaling pathway. *Neuroscience*, 183, pp.178–88.

Cheng, J.S. et al., 2009. Collagen VI protects neurons against Abeta toxicity. *Nature Neuroscience*, 12(2), pp.119–21.

Colombatti, A. et al., 1987. Biosynthesis of chick type VI collagen. I. Intracellular assembly and molecular structure. *The Journal of biological chemistry*, 262(30), pp.14454–60.

Colombatti, A. & Bonaldo, P., 1987. Biosynthesis of chick type VI collagen. II. Processing and secretion in fibroblasts and smooth muscle cells. *The Journal of biological chemistry*, 262(30), pp.14461–6.

Colombatti, A., Mucignat, M.T. & Bonaldo, P., 1995. Secretion and matrix assembly of recombinant type VI collagen. *Journal of Biological Chemistry*, 270, pp.13105–13111.

Corcelle, E. et al., 2007. Control of the Autophagy Maturation Step by the MAPK ERK and p38: Lessons from Environmental Carcinogens. *Autophagy*, 3(1), pp.57–59.

Cowling, B.S. et al., 2008. Identification of FHL1 as a regulator of skeletal muscle mass: implications for human myopathy. *The Journal of cell biology*, 183(6), pp.1033–48.

Cullup, T. et al., 2013. Recessive mutations in EPG5 cause Vici syndrome, a multisystem disorder with defective autophagy. *Nature Genetics*, 45(1), pp.83–7.

Doliana, R. et al., 1998. Alternative splicing of VWFA modules generates variants of type VI collagen alpha 3 chain with a distinctive expression pattern in embryonic chicken tissues and potentially different adhesive function. *Matrix biology*, 16(7), pp.427–42.

Duan, L. et al., 2014. Critical roles for nitric oxide and ERK in the completion of prosurvival autophagy in 4OHTAM-treated estrogen receptor-positive breast cancer cells. *Cancer letters*, 353(2), pp.290–300.

Egan, D.F. et al., 2010. Phosphorylation of ULK1 (hATG1) by AMP-activated protein kinase connects energy sensing to mitophagy. *Science*, 331(6016), pp.456–461.

Eskelinen, E.-L. et al., 2002. Role of LAMP-2 in lysosome biogenesis and autophagy. *Molecular biology of the cell*, 13(9), pp.3355–3368.

Feng, Y. et al., 2014. The machinery of macroautophagy. *Cell research*, 24(1), pp.24–41.

Ferraro, E. & Cecconi, F., 2007. Autophagic and apoptotic response to stress signals in mammalian cells. *Archives of biochemistry and biophysics*, 462(2), pp.210–9.

Fimia, G.M. et al., 2007. Ambra1 regulates autophagy and development of the nervous system. *Nature*, 447(7148), pp.1121–5.

Fimia, G.M. & Piacentini, M., 2010. Regulation of autophagy in mammals and its interplay with apoptosis. *Cellular and molecular life sciences*, 67(10), pp.1581–8.

Fortunato, F. et al., 2009. Impaired autolysosome formation correlates with Lamp-2 depletion: role of apoptosis, autophagy, and necrosis in pancreatitis. *Gastroenterology*, 137(1), pp.350–60, 360.e1–5.

Fujita, N. et al., 2008. The Atg16L complex specifies the site of LC3 lipidation for membrane biogenesis in autophagy. *Molecular biology of the cell*, 19(5), pp.2092–100.

Fung, C. et al., 2008. Induction of autophagy during extracellular matrix detachment promotes cell survival. *Molecular biology of the cell*, 19(3), pp.797–806.

Galluzzi, L. et al., 2015. Essential versus accessory aspects of cell death : recommendations of the NCCD 2015. *Cell Death and Differentiation*, 22, pp.58–73.

Gattazzo, F., Urciuolo, A. & Bonaldo, P., 2014. Extracellular matrix: a dynamic microenvironment for stem cell niche. *Biochimica et biophysica acta*, 1840(8), pp.2506–19.

Gomes, L.C. & Scorrano, L., 2008. High levels of Fis1, a pro-fission mitochondrial protein, trigger autophagy. *Biochimica et Biophysica Acta - Bioenergetics*, 1777(7-8), pp.860–866.

Gomes, L.C. & Scorrano, L., 2011. Mitochondrial elongation during autophagy: a stereotypical response to survive in difficult times. *Autophagy*, 7(10), pp.1251–3.

González-Polo, R.-A. et al., 2005. The apoptosis/autophagy paradox: autophagic vacuolization before apoptotic death. *Journal of cell science*, 118(Pt 14), pp.3091–102.

Goyal, A. et al., 2014. Decorin activates AMPK, an energy sensor kinase, to induce autophagy in endothelial cells. *Matrix Biology*, 35, pp.42–50.

Grumati, P. et al., 2010. Autophagy is defective in collagen VI muscular dystrophies, and its reactivation rescues myofiber degeneration. *Nature Medicine*, 16(11), pp.1313–20.

Grumati, P. et al., 2011. Physical exercise stimulates autophagy in normal skeletal muscles but is detrimental for collagen VI-deficient muscles. *Autophagy*, 7(12), pp.1415–1423.

Guo, X. et al., 2007. Morphologic characterization of organized extracellular matrix deposition by ascorbic acid-stimulated human corneal fibroblasts. *Investigative ophthalmology & visual science*, 48(9), pp.4050–60.

Hatamochi, A. et al., 1989. Regulation of collagen VI expression in fibroblasts. Effects of cell density, cell-matrix interactions, and chemical transformation. *Journal of Biological Chemistry*, 264(6), pp.3494–3499.

He, C. & Levine, B., 2010. The Beclin 1 interactome. *Current opinion in cell biology*, 22(2), pp.140–9.

Howell, S.J. & Doane, K.J., 1998. Type VI collagen increases cell survival and prevents anti-beta 1 integrin-mediated apoptosis. *Experimental Cell Research*, 241(1), pp.230–41.

Hubmacher, D. & Apte, S.S., 2013. The biology of the extracellular matrix: novel insights. *Current opinion in rheumatology*, 25(1), pp.65–70.

Huynh, K.K. et al., 2007. LAMP proteins are required for fusion of lysosomes with phagosomes. *The EMBO journal*, 26(2), pp.313–24.

Hynes, R.O., 2009. The extracellular matrix: not just pretty fibrils. *Science*, 326(5957), pp.1216–9.

Ichimura, Y. et al., 2000. A ubiquitin-like system mediates protein lipidation. *Nature*, 408(6811), pp.488–92.

Ichimura, Y. et al., 2008. Selective turnover of p62/A170/SQSTM1 by autophagy. *Autophagy*, 4(8), pp.1063–6.

Irwin, W. a et al., 2003. Mitochondrial dysfunction and apoptosis in myopathic mice with collagen VI deficiency. *Nature Genetics*, 35(4), pp.367–71.

Iyengar, P. et al., 2005. Adipocyte-derived collagen VI affects early mammary tumor progression in vivo, demonstrating a critical interaction in the tumor/stroma microenvironment. *Journal of Clinical Investigation*, 115(5), pp.1163–1176.

Jiang, P. & Mizushima, N., 2014. LC3- and p62-based biochemical methods for the analysis of autophagy progression in mammalian cells. *Methods*, pp.18–22.

Jimenez-Mallebrera, C. et al., 2006. A comparative analysis of collagen VI production in muscle, skin and fibroblasts from 14 Ullrich congenital muscular dystrophy patients with dominant and recessive COL6A mutations. *Neuromuscular Disorders*, 16(9-10), pp.571–82.

Kabeya, Y. et al., 2004. LC3, GABARAP and GATE16 localize to autophagosomal membrane depending on form-II formation. *Journal of cell science*, 117(Pt 13), pp.2805–12.

Kasahara, A. & Scorrano, L., 2014. Mitochondria: from cell death executioners to regulators of cell differentiation. *Trends in cell biology*, 24(12), pp.761–770.

Keene, D.R., Engvall, E. & Glanville, R.W., 1988. Ultrastructure of type VI collagen in human skin and cartilage suggests an anchoring function for this filamentous network. *The Journal of cell biology*, 107(5), pp.1995–2006.

Khan, T. et al., 2009. Metabolic dysregulation and adipose tissue fibrosis: role of collagen VI. *Molecular and Cellular Biology*, 29(6), pp.1575–91.

Kim, J. et al., 2011. AMPK and mTOR regulate autophagy through direct phosphorylation of Ulk1. *Nature Cell Biology*, 13(2), pp.132–41.

Kim, J.H. et al., 2014. Raf/MEK/ERK can regulate cellular levels of LC3B and SQSTM1/p62 at expression levels. *Experimental Cell Research*, 327(2), pp.340–52.

Klionsky, D.J. et al., 2012. Guidelines for the use and interpretation of assays for monitoring autophagy. *Autophagy*, 8(4), pp.445–544.

Komatsu, M. et al., 2007. Homeostatic Levels of p62 Control Cytoplasmic Inclusion Body Formation in Autophagy-Deficient Mice. *Cell*, 131(6), pp.1149–1163.

Kroemer, G., Mariño, G. & Levine, B., 2010. Autophagy and the integrated stress response. *Molecular cell*, 40(2), pp.280–93.

Kuo, H.-J.J. et al., 1997. Type VI collagen anchors endothelial basement membranes by interacting with type IV collagen. *Journal of Biological Chemistry*, 272(42), pp.26522–26529.

Kuo, J.-C., 2013. Mechanotransduction at focal adhesions: integrating cytoskeletal mechanics in migrating cells. *Journal of cellular and molecular medicine*, 17(6), pp.704–12.

Lampe, A.K. & Bushby, K.M.D., 2005. Collagen VI related muscle disorders. *Journal of medical genetics*, 42(9), pp.673–685.

Lee, J.Y. et al., 2012. Fhl1 as a downstream target of Wnt signaling to promote myogenesis of C2C12 cells. *Molecular and Cellular Biochemistry*, 365(1-2), pp.251–262.

Lee, S.J. et al., 2010. A functional role for the p62-ERK1 axis in the control of energy homeostasis and adipogenesis. *EMBO reports*, 11(3), pp.226–32.

Levine, B. & Kroemer, G., 2008. Autophagy in the pathogenesis of disease. *Cell*, 132(1), pp.27–42.

Liesa, M. & Shirihai, O.S., 2013. Mitochondrial dynamics in the regulation of nutrient utilization and energy expenditure. *Cell Metabolism*, 17(4), pp.491–506.

Lock, R. & Debnath, J., 2008. Extracellular matrix regulation of autophagy. *Current opinion in cell biology*, 20(5), pp.583–8.

Malicdan, M.C. V & Nishino, I., 2012. Autophagy in lysosomal myopathies. *Brain pathology*, 22(1), pp.82–8.

Mammucari, C. et al., 2007. FoxO3 controls autophagy in skeletal muscle in vivo. *Cell metabolism*, 6(6), pp.458–71.

Manning, B.D. & Cantley, L.C., 2007. AKT/PKB Signaling: Navigating Downstream. *Cell*, 129, pp.1261–1274.

Mariño, G. et al., 2014. Self-consumption: the interplay of autophagy and apoptosis. *Molecular Cell Biology*, 15(2), pp.81–94.

Martina, J.A. et al., 2012. MTORC1 functions as a transcriptional regulator of autophagy by preventing nuclear transport of TFEB. *Autophagy*, 8(6), pp.903–14.

Masiero, E. et al., 2009. Autophagy is required to maintain muscle mass. *Cell metabolism*, 10(6), pp.507–15.

Menazza, S. et al., 2010. Oxidative stress by monoamine oxidases is causally involved in myofiber damage in muscular dystrophy. *Human Molecular Genetics*, 19(21), pp.4207–15.

Mercuri, E. & Longman, C., 2005. Congenital muscular dystrophy. *Pediatric annals*, 34(7), pp.560–2, 564–8.

Merlini, L. et al., 2008. Autosomal recessive myosclerosis myopathy is a collagen VI disorder. *Neurology*, 71(16), pp.1245–53.

Merlini, L. & Nishino, I., 2014. 201st ENMC International Workshop: Autophagy in muscular dystrophies--translational approach, 1-3 November 2013, Bussum, The Netherlands. *Neuromuscular Disorders*, 24(6), pp.546–61.

Mizushima, N. et al., 2008. Autophagy fights disease through cellular self-digestion. *Nature*, 451(7182), pp.1069–75.

Mizushima, N. et al., 2004. In vivo analysis of autophagy in response to nutrient starvation using transgenic mice expressing a fluorescent autophagosome marker. *Molecular biology of the cell*, 15(3), pp.1101–11.

Mizushima, N. et al., 2003. Mouse Apg16L, a novel WD-repeat protein, targets to the autophagic isolation membrane with the Apg12-Apg5 conjugate. *Journal of cell science*, 116(Pt 9), pp.1679–88.

Mizushima, N., 2010. The role of the Atg1/ULK1 complex in autophagy regulation. *Current opinion in cell biology*, 22(2), pp.132–9.

Mizushima, N. & Komatsu, M., 2011. Autophagy: renovation of cells and tissues. *Cell*, 147(4), pp.728–41.

Mizushima, N. & Kuma, A., 2008. Autophagosomes in GFP-LC3 Transgenic Mice. *Methods in molecular biology*, 445, pp.119–24.

Mizushima, N. & Levine, B., 2010. Autophagy in mammalian development and differentiation. *Nature Cell Biology*, 12(9), pp.823–30.

Mizushima, N. & Yoshimori, T., 2007. How to Interpret LC3 Immunoblotting. *Autophagy*, 3(12), pp.542–545.

Morgan, M.J. & Madgwick, A.J., 1999. The LIM proteins FHL1 and FHL3 are expressed differently in skeletal muscle. *Biochemical and biophysical research communications*, 255(2), pp.245–250.

Murphy, M.M. et al., 2011. Satellite cells, connective tissue fibroblasts and their interactions are crucial for muscle regeneration. *Development*, 138(17), pp.3625–37.

Nair, U. & Klionsky, D.J., 2011. Activation of autophagy is required for muscle homeostasis during physical exercise. *Autophagy*, 7(12), pp.1405–6.

Narendra, D. et al., 2008. Parkin is recruited selectively to impaired mitochondria and promotes their autophagy. *The Journal of cell biology*, 183(5), pp.795–803.

Nazio, F. et al., 2013. mTOR inhibits autophagy by controlling ULK1 ubiquitylation, self-association and function through AMBRA1 and TRAF6. *Nature Cell Biology*, 15(4), pp.406–16.

Neill, T., Schaefer, L. & Iozzo, R. V, 2012. Decorin: a guardian from the matrix. *The American journal of pathology*, 181(2), pp.380–7.

Neill, T., Schaefer, L. & Iozzo, R. V, 2014. Instructive Roles of Extracellular Matrix on Autophagy. *The American journal of pathology*, 184(6), pp.2146–53.

Nemoto, T. et al., 2003. The Mouse APG10 Homologue, an E2-like Enzyme for Apg12p Conjugation, Facilitates MAP-LC3 Modification. *Journal of Biological Chemistry*, 278(41), pp.39517–39526.

Nguyen, T.M.B. et al., 2009. Endostatin induces autophagy in endothelial cells by modulating Beclin 1 and beta-catenin levels. *Journal of cellular and molecular medicine*, 13(9B), pp.3687–98.

Nguyen, T.M.B. et al., 2007. Kringle 5 of human plasminogen, an angiogenesis inhibitor, induces both autophagy and apoptotic death in endothelial cells. *Blood*, 109(11), pp.4793–802.

Ohsumi, Y., 2001. Molecular dissection of autophagy: two ubiquitin-like systems. Nature reviews. *Molecular Cell Biology*, 2(3), pp.211–6.

Olsen, D.R. et al., 1989. Collagen gene expression by cultured human skin fibroblasts. Abundant steady-state levels of type VI procollagen messenger RNAs. *The Journal of clinical investigation*, 83(3), pp.791–5.

De Palma, C. et al., 2012. Autophagy as a new therapeutic target in Duchenne muscular dystrophy. *Cell Death & Disease*, 3(11), p.e418.

Pan, T.-C. et al., 2003. New molecular mechanism for Ullrich congenital muscular dystrophy: a heterozygous in-frame deletion in the COL6A1 gene causes a severe phenotype. *American journal of human genetics*, 73(2), pp.355–69.

Pepe, G. et al., 2002. Bethlem myopathy (BETHLEM) and Ullrich scleroatonic muscular dystrophy: 100th ENMC international workshop, 23-24 November 2001, Naarden, The Netherlands. *Neuromuscular Disorders*, 12(10), pp.984–93.

Poluzzi, C. et al., 2014. Endorepellin evokes autophagy in endothelial cells. *The Journal of biological chemistry*, 289(23), pp.16114–28.

Raben, N. et al., 2008. Suppression of autophagy in skeletal muscle uncovers the accumulation of ubiquitinated proteins and their potential role in muscle damage in Pompe disease. *Human Molecular Genetics*, 17(24), pp.3897–908.

Ricard-Blum, S., 2011. The Collagen Family. *Cold Spring Harbor Perspectives in Biology*, 3, pp.1–19.

Rühl, M. et al., 1999. Soluble collagen VI drives serum-starved fibroblasts through S phase and prevents apoptosis via down-regulation of Bax. *The Journal of biological chemistry*, 274(48), pp.34361–8.

Russell, R.C., Yuan, H.-X. & Guan, K.-L., 2014. Autophagy regulation by nutrient signaling. *Cell research*, 24(1), pp.42–57.

Sabatelli, P. et al., 2001. Collagen VI deficiency affects the organization of fibronectin in the extracellular matrix of cultured fibroblasts. *Matrix Biology*, 20(7), pp.475–86.

Sabatelli, P. et al., 2012. Critical evaluation of the use of cell cultures for inclusion in clinical trials of patients affected by collagen VI myopathies. *Journal of cellular physiology*, 227(7), pp.2927–35.

Saitta, B. et al., 1990. Alternative splicing of the human alpha 2(VI) collagen gene generates multiple mRNA transcripts which predict three protein variants with distinct carboxyl termini. *The Journal of biological chemistry*, 265(11), pp.6473–80.

Sandri, M. et al., 2013. Misregulation of autophagy and protein degradation systems in myopathies and muscular dystrophies. *Journal of cell science*, 126(Pt 23), pp.5325–33.

Sardiello, M. et al., 2009. A gene network regulating lysosomal biogenesis and function. *Science*, 325(5939), pp.473–7.

Schiaffino, S. et al., 2013. Mechanisms regulating skeletal muscle growth and atrophy. *The FEBS journal*, 280(17), pp.4294–314.

Schneider, J.L. & Cuervo, A.M., 2014. Autophagy and human disease: emerging themes. *Current opinion in genetics & development*, 26C, pp.16–23.

Scorrano, L., 2005. Proteins that fuse and fragment mitochondria in apoptosis: Con-fissing a deadly con-fusion? *Journal of Bioenergetics and Biomembranes*, 37(3), pp.165–170.

Settembre, C. et al., 2012. A lysosome-to-nucleus signaling mechanism senses and regulates the lysosome via mTOR and TFEB. *The EMBO Journal*, 31(5), pp.1095–1108.

Settembre, C. et al., 2011. TFEB links autophagy to lysosomal biogenesis. *Science*, 332(6036), pp.1429–33.

Settembre, C. & Ballabio, A., 2011. TFEB regulates autophagy. An integrated coordination of cellular degradation and recycling processes. *Autophagy*, 7(11), pp.1379–1381.

Shalini, S. et al., 2014. Old , new and emerging functions of caspases. *Cell Death and Differentiation*, pp.1–14.

Shang, L. & Wang, X., 2011. AMPK and mTOR coordinate the regulation of Ulk1 and mammalian autophagy initiation. *Autophagy*, 7(8), pp.924–926.

Shen, H. & Codogno, P., 2011. Autophagic cell death: Loch Ness monster or endangered species? *Autophagy*, 7(5), pp.457–465.

Shen, H. & Mizushima, N., 2014. At the end of the autophagic road: an emerging understanding of lysosomal functions in autophagy. *Trends in biochemical sciences*, 39(2), pp.61–71.

Spitali, P. et al., 2013. Autophagy is Impaired in the Tibialis Anterior of Dystrophin Null Mice. *PLoS currents*, 5, pp.1–12.

Stallcup, W.B., 2002. The NG2 proteoglycan: past insights and future prospects. *Journal of neurocytology*, 31(6-7), pp.423–35.

Stolz, A., Ernst, A. & Dikic, I., 2014. Cargo recognition and trafficking in selective autophagy. *Nature Cell Biology*, 16(6), pp.495–501.

Tanaka, Y. et al., 2000. Accumulation of autophagic vacuoles and cardiomyopathy in LAMP-2-deficient mice. *Nature*, 406(8), pp.902–906.

Tillet, E. et al., 1994. Recombinant expression and structural and binding properties of alpha 1(VI) and alpha 2(VI) chains of human collagen type VI. *European journal of biochemistry / FEBS*, 221(1), pp.177–85.

Tsang, K.Y. et al., 2010. The developmental roles of the extracellular matrix: beyond structure to regulation. *Cell and tissue research*, 339(1), pp.93–110.

Tuloup-Minguez, V. et al., 2013. Autophagy modulates cell migration and β1 integrin membrane recycling. *Cell Cycle*, 12(20), pp.3317–28.

Tuloup-Minguez, V. et al., 2011. Regulation of autophagy by extracellular matrix glycoproteins in HeLa cells. *Autophagy*, 7(1), pp.27–39.

Turrina, A., Martínez-González, M.A. & Stecco, C., 2013. The muscular force transmission system: Role of the intramuscular connective tissue. *Journal of Bodywork and Movement Therapies*, 17(1), pp.95–102.

Twig, G. et al., 2008. Fission and selective fusion govern mitochondrial segregation and elimination by autophagy. *The EMBO journal*, 27(2), pp.433–46.

Urciuolo, A. et al., 2013. Collagen VI regulates satellite cell self-renewal and muscle regeneration. *Nature Communications*, 4(5), p.1964.

Vainshtein, A. et al., 2014. Skeletal muscle, autophagy, and physical activity: the ménage à trois of metabolic regulation in health and disease. *Journal of molecular medicine*, 92(2), pp.127–37.

Wirawan, E. et al., 2012. Autophagy: for better or for worse. *Cell research*, 22(1), pp.43–61.

Wooten, M.W. et al., 2008. Essential role of sequestosome 1/p62 in regulating accumulation of Lys63-ubiquitinated proteins. *The Journal of biological chemistry*, 283(11), pp.6783–9.

Yoon, Y.H. et al., 2010. Induction of lysosomal dilatation, arrested autophagy, and cell death by chloroquine in cultured ARPE-19 cells. *Investigative ophthalmology & visual science*, 51(11), pp.6030–7.

Youle, R.J. & Narendra, D.P., 2011. Mechanisms of mitophagy. *Molecular Cell Biology*, 12(1), pp.9–14.

Yu, L. et al., 2004. Regulation of an ATG7-beclin 1 program of autophagic cell death by caspase-8. *Science*, 304(5676), pp.1500–2.

Zanotti, S. et al., 2011. Fibroblasts from the muscles of Duchenne muscular dystrophy patients are resistant to cell detachment apoptosis. *Experimental Cell Research*, 317(17), pp.2536–47.

Zhang, Y. et al., 2010. Myofibroblasts protect myoblasts from intrinsic apoptosis associated with differentiation via β1 integrin-PI3K/Akt pathway. *Development, growth & differentiation*, 52(8), pp.725–33.

Zhou, L. et al., 2013. Bcl-2-dependent upregulation of autophagy by sequestosome 1/p62 in vitro. *Acta pharmacologica Sinica*, 34(5), pp.651–6.

Zou, Y. et al., 2008. Muscle interstitial fibroblasts are the main source of collagen VI synthesis in skeletal muscle: implications for congenital muscular dystrophy types Ullrich and Bethlem. *Journal of neuropathology and experimental neurology*, 67(2), pp.144–54.